Organisation for Economic Co-operation and Development

ENV/CBC/MONO(2021)35

Unclassified English - Or. English

27 October 2021

ENVIRONMENT DIRECTORATE
CHEMICALS AND BIOTECHNOLOGY COMMITTEE

Case Study on use of an Integrated Approach for Testing and Assessment (IATA) for Systemic Toxicity of Phenoxyethanol when included at 1% in a body lotion

Series on Testing and Assessment,
No. 349

JT03483903

SERIES ON TESTING AND ASSESSMENT

NO. 349

Case Study on use of an Integrated Approach for Testing and Assessment (IATA) for Systemic Toxicity of Phenoxyethanol when included at 1% in a body lotion

INTER-ORGANIZATION PROGRAMME FOR THE SOUND MANAGEMENT OF CHEMICALS

A cooperative agreement among FAO, ILO, UNDP, UNEP, UNIDO, UNITAR, WHO, World Bank and OECD

Environment Directorate
ORGANISATION FOR ECONOMIC COOPERATION AND DEVELOPMENT
Paris 2021

About the OECD

The Organisation for Economic Co-operation and Development (OECD) is an intergovernmental organisation in which representatives of 38 industrialised countries in North and South America, Europe and the Asia and Pacific region, as well as the European Commission, meet to co-ordinate and harmonise policies, discuss issues of mutual concern, and work together to respond to international problems. Most of the OECD's work is carried out by more than 200 specialised committees and working groups composed of member country delegates. Observers from several countries with special status at the OECD, and from interested international organisations, attend many of the OECD's workshops and other meetings. Committees and working groups are served by the OECD Secretariat, located in Paris, France, which is organised into directorates and divisions.

The Environment, Health and Safety Division publishes free-of-charge documents in eleven different series: **Testing and Assessment**; **Good Laboratory Practice and Compliance Monitoring**; **Pesticides**; **Biocides**; **Risk Management**; **Harmonisation of Regulatory Oversight in Biotechnology**; **Safety of Novel Foods and Feeds; Chemical Accidents; Pollutant Release and Transfer Registers; Emission Scenario Documents;** and **Safety of Manufactured Nanomaterials.** More information about the Environment, Health and Safety Programme and EHS publications is available on the OECD's World Wide Web site (www.oecd.org/chemicalsafety/).

This publication was developed in the IOMC context. The contents do not necessarily reflect the views or stated policies of individual IOMC Participating Organizations.

The Inter-Organisation Programme for the Sound Management of Chemicals (IOMC) was established in 1995 following recommendations made by the 1992 UN Conference on Environment and Development to strengthen co-operation and increase international co-ordination in the field of chemical safety. The Participating Organisations are FAO, ILO, UNDP, UNEP, UNIDO, UNITAR, WHO, World Bank and OECD. The purpose of the IOMC is to promote co-ordination of the policies and activities pursued by the Participating Organisations, jointly or separately, to achieve the sound management of chemicals in relation to human health and the environment.

This publication is available electronically, at no charge.

Also published in the Testing and Assessment link

For this and many other Environment, Health and Safety publications, consult the OECD's World Wide Web site (www.oecd.org/chemicalsafety/)

or contact:

OECD Environment Directorate,
Environment, Health and Safety Division
2 rue André-Pascal
75775 Paris Cedex 16
France

Fax: (33-1) 44 30 61 80

E-mail: ehscont@oecd.org

This case study was developed by Cosmetics Europe (BIAC) for illustrating practical use of IATA and submitted to the 2020 review cycle of the IATA Case Studies Project. This case study was reviewed by the project team and revised to consider the comments from reviewers. The final version of the case study has been accepted by the project team to be published.

The learnings and lessons obtained from the review experience of the case study were summarised in a considerations document [ENV/CBC/HA(2021)3].

Foreword

OECD member countries have been making efforts to expand the use of alternative methods in assessing chemicals. The OECD has been developing guidance documents and tools for the use of alternative methods such as (Q)SAR, chemical categories and Adverse Outcome Pathways (AOPs) as a part of Integrated Approaches for Testing and Assessment (IATA). There is a need for the investigation of the practical applicability of these methods/tools for different aspects of regulatory decision-making, and to build upon case studies and assessment experience across jurisdictions.

The objective of the IATA Case Studies Project is to increase experience with the use of IATA by developing case studies, which constitute examples of predictions that are fit for regulatory use. The aim is to create common understanding of using novel methodologies and the generation of considerations/guidance stemming from these case studies.

This case study was developed by Cosmetics Europe (BIAC) for illustrating practical use of IATA and submitted to the 2020 review cycle of the IATA Case Studies Project. This case study was reviewed by the project team.

The case study is illustrative examples, and their publication as OECD monographs does not translate into direct acceptance of the methodologies for regulatory purposes across OECD countries. In addition, the cases study should not be interpreted as official regulatory decisions made by the authoring member countries.

In addition, a considerations document summarising the learnings and lessons of the review experience of the case studies is published with the case studies:

REPORT ON CONSIDERATIONS FROM CASE STUDIES ON INTEGRATED APPROACHES FOR TESTING AND ASSESSMENT (IATA) Sixth Review Cycle (2020), ENV/CBC/HA(2021)3.

Abstract

The present work is an exposure-based next generation risk assessment (NGRA) case study for the preservative ingredient phenoxyethanol. The case study was guided by the SEURAT-1 assessment workflow (Berggren *et al*., (2017) and the International Cooperation on Cosmetics Regulation NGRA principles (Dent *et al*., 2018), with the aim of using only non-animal approaches to assure the systemic safety of this ingredient when present at an active level (1%) in a product with a high level of consumer use (body lotion). This strategy is aligned with the US EPA's next generation blueprint for computational toxicology, which seeks to characterize whether a chemical acts via defined biological pathways/targets or if it may induce cellular changes by a non-specific mechanism (Thomas *et al*., 2019). The overall strategy of the case study is one where *in vitro*/*in silico* approaches instead of animal-based approaches for hazard identification are used in the risk assessment. No animal data were therefore used in the assessment. Instead, the approach involved the generation of new approach methodology (NAM) data on biokinetics and biodynamics. *In silico* and *in vitro* approaches showed the major metabolite of phenoxyethanol to be phenoxyacetic acid (PAA), and PBK modelling was used to predict the 95th percentile population exposures of both phenoxyethanol and PAA in blood and tissues. These internal exposures were compared with points of departure (PoDs) derived from *in vitro* bioactivity assays. These included published non-animal data and new *in vitro* pharmacological profiling, cell stress, and transcriptomics data. The PoDs exceeded the predicted internal exposure levels for both phenoxyethanol and PAA. This provided some assurance that *in vitro* bioactivity does not occur at consumer-relevant exposure levels. However, the margins of internal exposure for PAA were small (2 and 3 for C_{max} and AUC_{24} respectively), meaning that confidence in the risk assessment was low. This case study illustrates one possible approach to safety assess both a parent chemical and its major stable metabolite in non-animal systemic toxicity risk assessment.

Table of Contents

Table

Figure

Abbreviations and acronyms

ADH	Alcohol dehydrogenase
ALDH	Aldehyde dehydrogenase
BMD	BenchMark Dose
BMDL	BenchMark Dose Level
BMR	BenchMark Response
CAS	Chemical Abstracts Service
IATA	Integrated approaches to testing and assessment
ICCR	International Cooperation on Cosmetics Regulation
LRSS	Long Range Science Strategy
MIE	Molecular initiating event
MoIE	Margin of internal exposure
MoA	Mode of action
MoS	Margin of safety
NAM	New approach methodology
NGRA	Next generation risk assessment
NOTEL	No-observed-transcriptional-effect level
PAA	Phenoxyacetic acid
PBK	Physiologically based kinetic
PHH	Primary human hepatocytes
PoD	Point of departure
SCCS	Scientific Committee on Consumer Safety
SMILES	Simplified molecular-input line-entry system
SEURAT-1	Safety Evaluation Ultimately Replacing Animal Testing-1
TTC	Threshold of toxicological concern
US EPA	United States Environment Protection Agency

Introduction

Non-animal approaches have been applied in the human health risk assessment of cosmetics for many years, chiefly in the assessment of genetic toxicity and local effects such as skin and eye irritation. Fully addressing more complex health effects associated with systemic exposures is more challenging (Adler *et al*., 2011). Cosmetics Europe's Long Range Science Strategy (LRSS) is working to address this challenge (Desprez *et al*., 2018).

The present case study is a next generation risk assessment (NGRA). NGRA is an exposure-led and hypothesis-driven assessment approach to enable robust decision making (US EPA, 2014). The current case study was structured according to the SEURAT-1 assessment workflow (Figure 2) and the International Cooperation on Cosmetics Regulation NGRA principles (Dent *et al*., 2018). The aim was to use new approach methodologies (NAMs) to illustrate a systemic risk assessment for a cosmetic ingredient (phenoxyethanol) present at 1% in a product with a high level of consumer use (body lotion). Phenoxyethanol is a broadly acting anti-microbial and is safely used in both rinse-off and leave-on cosmetics at up to 1%. However, as the purpose of this case study was to test the current ability to make a safety decision without using any *in vivo* data, any pre-existing animal data on the case study ingredient were discounted. Furthermore, any existing human data was only considered at the higher tiers of the workflow, because in real life human studies would only be performed once a risk assessment is in place.

The overall strategy was one where *in vitro*/*in silico* approaches instead of animal-based approaches for hazard identification are used in the risk assessment. In other words, it was not the intention to predict what adverse effects may occur following high doses of phenoxyethanol. Instead, the strategy was to generate a broad suite of human-relevant bioactivity data and, by comparison to data from physiologically based kinetic (PBK) modelling (WHO, 2010), ensure that human exposures remain below the level that results in *in vitro* bioactivity. With relevant bioactivity data providing sufficient biological coverage, this approach is intended to be protective of human health rather than predictive of apical endpoints. To do this, a margin of internal exposure (MoIE) approach was used. A MoIE is calculated using a measure of internal exposure, such as blood concentration or target-tissue dose, rather than comparing the externally applied dose or ingested dose (Bessems *et al*., 2017). It is acknowledged that this strategy will likely result in a very conservative risk assessment (Paul Friedman *et al*., 2020). Therefore, where this approach is insufficient to arrive at a safety decision, it is necessary to use higher-tier approaches that can differentiate between exposures that cause *in vitro* bioactivity and those that can cause an adverse health effect. Such higher-tier approaches were not used in this case study.

The overall strategy is aligned with the US EPA's next generation blueprint for computational toxicology, which seeks to characterize whether a chemical acts via defined biological pathways/targets or if it may induce cellular changes by a non-specific mechanism (Thomas *et al*., 2019). The latter may prove to be particularly relevant to cosmetic ingredients.

1. Purpose

1.1. Purpose of use

Cosmetic products are required to be assessed for safety, and systemic toxicity is an important part of the assessment. However, in the EU the 7th Amendment to the Cosmetics Regulation bans the generation of animal test data for cosmetic ingredients. In addition to this regulatory action in the EU and across the world, consumers are increasingly demanding cosmetics that do not contain ingredients that have been tested on animals.

It is widely acknowledged that a one-for-one replacement of animal studies for systemic effects is not appropriate. Therefore, in-line with the work of the US EPA (Thomas *et al*., 2019) this case study is an exploration of whether, comparing *in vitro* bioactivity with estimated consumer exposures, is a workable solution for cosmetic ingredients to ensure a high level of consumer protection whilst also ensuring the risk assessment is animal-free. Any pre-existing animal data on this case study ingredient were discounted.

1.2. Target chemical

The target is the single chemical phenoxyethanol for which descriptors and structure (Figure 1) are provided below. This substance was selected because it is a common ingredient within consumer products, and has a favourable safety profile. In addition, the amount of this ingredient applied in certain consumer products is appreciable (up to 1% in a body lotion), therefore it represents a significant challenge to safety assess using only NAMs.

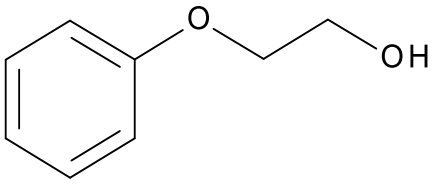

Figure 1 Chemical structure of phenoxyethanol

CAS: 122-99-6
SMILES: c1ccc(cc1)OCCO
Molecular Weight: 138.16
Purity: >99%

1.3. Endpoint(s)

The IATA is applied for the risk assessment of systemic toxicity. The risk assessment has been carried out using *in vitro/in silico* approaches instead of animal-based approaches for hazard identification.

1.4. Exposure information

The exposure considered in this case study is dermal application to consumers when 1% of phenoxyethanol is included in a body lotion that is marketed in Europe. For the product use applied dose exposure assessment, worst-case (conservative) assumptions were made regarding product use. Consumer use and physiological data for females were used as a conservative approach (lower body weight, greater use levels).

In silico predictions and *in vitro* data were used to characterize the metabolism of the parent molecule. A PBK model was developed to calculate the internal concentration of both phenoxyethanol and its major metabolite, phenoxyacetic acid (PAA). For the *in vitro* to *in vivo* extrapolation, the nominal (total) concentration was considered, because free concentration *in vivo* was predicted to be lower than the free concentration *in vitro*. Therefore, for the purpose of the risk assessment, using the nominal *in vitro* dose was considered to be conservative.

2. Hypothesis for performing IATA and Approaches used (Potential Blocks for Inclusion)

The case study's overarching hypothesis is that "Systemic exposure to phenoxyethanol present at 1% in body lotion will not cause any adverse health effects in consumers". Adverse effects were defined as any biochemical, morphological or physiological change that either singly or in combination adversely affects the consumer or reduces their ability to respond to an additional environmental challenge (Lewis *et al*., 2002).

The hypothesis for risk assessment was formulated stepwise following the SEURAT-1 workflow (Figure 2), bearing in mind the context of the given scenario, systemic effects and the 'absence' of animal data. The SEURAT-1 workflow was selected as the basis for the case study because it was the only published OECD IATA dealing with *ab initio* NGRA. This workflow includes the provision to use tools such as read across or the threshold of toxicological concern (TTC). The TTC is a pragmatic tool allowing exposures to an untested chemical to be placed into context against a database of points of departure (PoDs) from toxicology data on other substances (Yang et *al*., 2017). Exiting the workflow at Tier 0 was not possible due to the high consumer exposure (above TTC) and lack of read across candidates with systemic toxicity data. Because this case study focussed on the *ab initio* approach, TTC and read across are not discussed in this document.

The risk assessment hypothesis formed at conclusion of Tier 1 of the SEURAT-1 workflow was that, given the lack of compelling evidence that phenoxyethanol was active in humans by any particular mechanism, it is considered to fit into the 'no defined biological target or pathway' category as described in the US EPAs blueprint for computational toxicology (Thomas *et al*., 2019). These two workflows are different, for example the SEURAT-1 workflow has a more explicit emphasis on exposure, whereas the US EPA blueprint is more explicit about data needs and how a specific decision on mode of action (MoA) may be reached. Taken together were seen as complementary and able to support robust decision making. Along with these workflows, the case study was also guided by the ICCR principles for NGRA (Dent *et al*., 2018).

An underlying assumption is that the biological coverage provided by the high throughput transcriptomics assessment, coupled with the specific assays evaluating cellular stress, a search for possible MIEs and the ToxCast data provides at least the same breadth of protection as would a package of rodent toxicity studies (including repeat-dose, developmental and reproductive studies). This assumption is supported by work ongoing as part of the Accelerating Pace of Chemical Risk Assessment (APCRA) initiative (Paul Friedman *et al.*, 2020) and was tested by comparing the MoIE derived in the NGRA with the margin of safety (MoS) derived from the traditional (animal-based) risk assessment for the same product.

2.1. Mode of Action (MoA)

In Tier 1 the existing (non-animal) data were interrogated to try and elucidate the MoA of phenoxyethanol. *In silico* tools were also applied at this tier.

In Tier 2 several types of bioactivity data were generated. High throughput transcriptomics, SafetyScreen44™, and data on cellular stress. These data confirmed that there was not a defined target of concern for phenoxyethanol, and the risk assessment was based on the

most conservative no-observed-transcriptional effect level (NOTEL) derived from the transcriptomics data. Biokinetic refinement included generating information describing AUC_{24} for both phenoxyethanol and its major metabolite phenoxyacetic acid and the C_{max} for phenoxyacetic acid at the NOTEL.

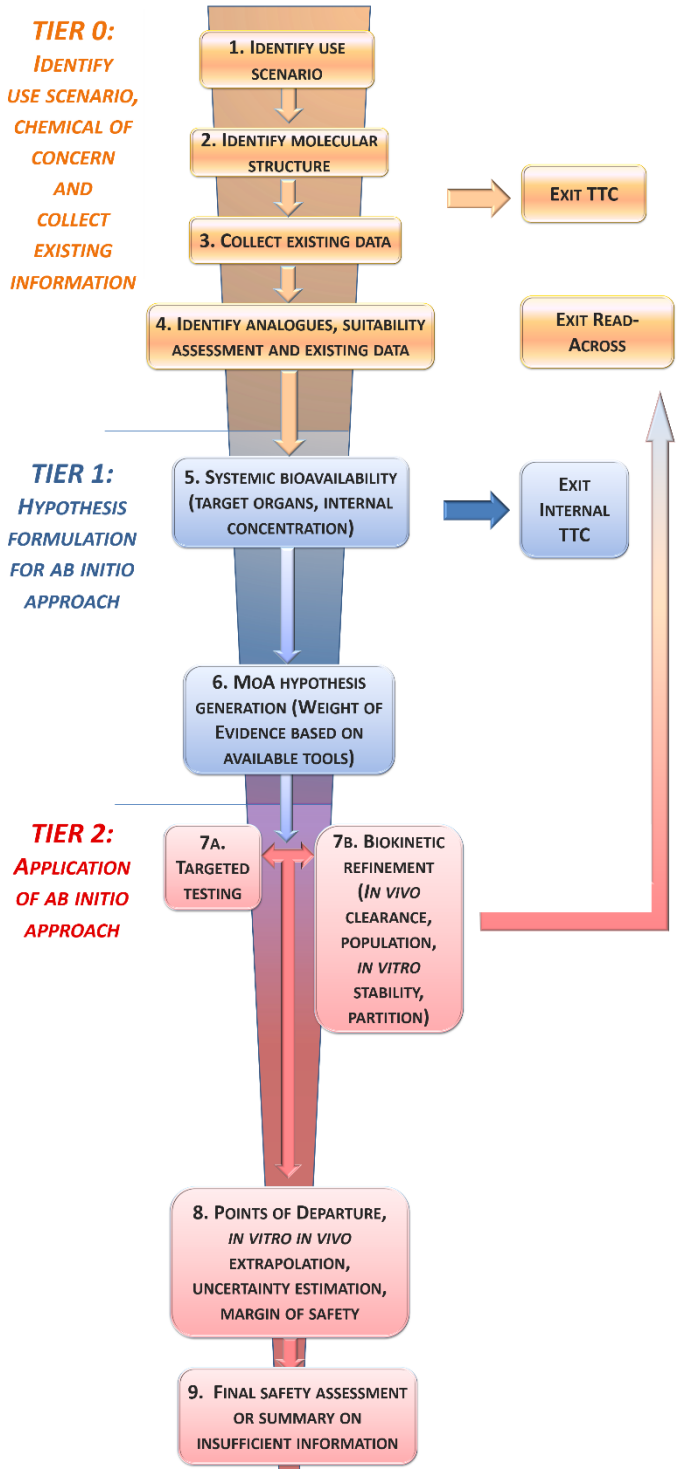

SCCS Notes of Guidance 90th percentile exposure to body lotion, ingredient present at 1%

Existing data harvested from PubChem and ToxCast, no animal data considered in the evaluation

TTC or read across was not a focus for this case study

PBK model developed using literature inputs: no *in vitro* data were generated in Tier 1.

Possible metabolic products predicted *in silico* using Meteor

In silico tools used to supplement existing *in vitro* data to try to identify any modes of action of concern: OECD QSAR Toolbox, Derek Nexus, COSMOS nuclear Receptors Binding profilers, MIE Atlas, CERAPP and CoMPARA. See text for full names and URL/reference.

Targeted testing: High throughput transcriptomics in HepG2, HepaRG and MCF-7 cells; cell stress panel in HepG2 cells; *in vitro* pharmacological profiling.

Biokinetic refinement including population modelling, confirmatory *in vitro* clearance data, confirmatory *in vitro* metabolite characterization in primary hepatocytes and in cells used in targeted testing.

Margins of internal exposure based on C_{max} and AUC_{24} of both phenoxyethanol and the stable acid metabolite phenoxyacetic acid

Figure 2 How the data used in this case study map to the Next Generation Risk Assessment workflow for systemic effects (Berggren *et al.*, 2017), and the order in which the case study was performed

3. Data/Information gathering

3.1. Exposure Characterisation:

3.1.1. Tier 0

For the applied dose exposure assessment, worst-case (conservative) assumptions were made regarding product use. Female body weight and use levels were used as a conservative approach. Consumer use data for body lotion and mean consumer bodyweight were taken from the Scientific Committee on Consumer Safety (SCCS) Notes of Guidance for the Testing of Cosmetic Ingredients and their Safety Evaluation, 10th Revision (SCCS, 2018). This exposure scenario assumes all the applied body lotion is left in contact with skin until the next application. In Tier 0 the dermal absorption was assumed to be 100%.

3.1.2. Tier 1

The PBK model parameters for exposure to phenoxyethanol through consumer product use, skin penetration, evaporation and hepatic clearance, which were taken from the literature, are summarised in Table 1. Other parameter values required for PBK simulation (e.g., tissue volumes and blood flows, blood to tissue partition coefficients) have been provided in Annex I.

Table 1 Key input parameters for PBK modelling

	Value	Units	Source
Consumer use of body lotion	123	mg/kg/day	SCCS Notes of Guidance, 10th Edition (SCCS, 2018)
Applied dose of phenoxyethanol	1.23	mg/kg/day	Assumed that ingredient present at 1%
Dermal Penetration (K_p)	0.0025	cm/hour	Human skin *in vitro* (Roper *et al.*, 1997).
Dermal Evaporation (K_{loss})	0.0025	cm/hour	
Hepatic Clearance	20	µL/min/million cells	Primary human hepatocytes (Wetmore *et al.*, 2012)
Fraction Unbound (Fup)	0.56	no units	Average of 3 QSAR estimates (ChemSilico v1.6.1 (fup=0.71), ACD/Percepta v14.0.0 (fup=0.37), ADMET Predictor v6.5.0013 (fup=0.59))

Dermal Dose	0.616	mg/kg/application	Troutman *et al*, 2015
Body Surface Area	15760	cm^2	
Dosing interval	12	Hours	

The model output was verified using measured legacy human urinary excretion data (Howes, 1991). Sensitivity analysis and human population variability analysis was also performed. Variability in metabolism of phenoxyethanol was considered using reported prevalence of polymorphisms in the enzyme responsible for its metabolism. Full details of the model structure, parameterizations, verification, sensitivity analysis and population modelling are provided in Annex Ix.

To better understand the metabolic transformations that may occur following exposure to phenoxyethanol, predictions of *in vivo* metabolism were made. In Tier 1 these were *in silico* predictions performed using Meteor Nexus version 3.1.0 (Lhasa Ltd.) using "Site of Metabolism Scoring (with Molecular Mass Variance)" with relative threshold of 70 as reasoning methodology (default setting).

3.1.3. Tier 2

Additional *in vitro* experiments in primary human hepatocytes (PHH) were performed to confirm or refute the *in silico* metabolism predictions and to provide further quantitative data on the clearance of phenoxyethanol. This also provided clearance data showing that the clearance values used in the Tier 1 PBK model (Wetmore *et al*., 2012) were reproducible. The metabolic capacity of PHH was demonstrated using reference controls for low, medium and high clearance compounds (tolbutamide, midazolam and naloxone, respectively). In addition, appropriate control samples were included to exclude non-enzymic metabolism or chemical instability e.g., incubations with heat-inactivated hepatocytes and incubations without hepatocytes.

Short-term (3 h) incubations with PHH suspensions were used to determine the metabolite profile in a test system that is closer to *in vivo* than other hepatic models, such as liver subcellular fractions. It gives an idea of the types of metabolites formed, including conjugates (glucuronides, sulfates), allowing the *in silico* predictions from Tier 1 to be confirmed or refuted. Intrinsic clearance data from these studies were used in the PBK model to help predict the *in vivo* clearance. The hepatocyte assay was carried out at 3 concentrations (10, 30 and 100 µM) with multiple sampling time points across a 3 h period. None of the doses were cytotoxic and all were used to generate quantitative clearance data by measuring the depletion of parent chemical with time.

Following identification of the major metabolite of phenoxyethanol, further *in vitro* experiments were performed to assess the formation of this metabolite over time following exposure to the cell lines used to generate the critical *in vitro* bioactivity data (HepG2, HepaRG and MCF-7 cells, see 'Bioactivity Data' below). The purpose of this additional *in vitro* kinetics work was to determine if the data generated in those cell lines following

incubation with phenoxyethanol were also relevant to the evaluation of the major metabolite.

To achieve this, HepG2, HepaRG and MCF-7 cells were incubated at approximately the same seeding density and under the same conditions used in the cell stress and whole genome transcriptomics assays, and dosed with phenoxyethanol at concentrations of 0 (control), 10, 30, 100, 300 or 1000 µM for 0, 1, 3, 6 or 24-h. At each concentration and timepoint the total amount of phenoxyethanol and its major metabolite PAA were analyzed in both the medium and cell lysate by LC-(HR)MS. Three replicates were conducted.

To calculate the concentration of PAA in the cellular compartment, the total amount detected in the cell lysate was divided by the average volume of the cells used which was assumed to be 3375 μm^3, 3000 μm^3, and 850 μm^3 per cell for MCF-7, HepaRG, HepG2 and cells respectively (Geltmeier *et al*., 2015; Wiśniewski *et al*., 2016), multiplied by the approximate number of cells present. Both the maximum concentration detected in the cellular compartment (C_{max}) and the area under the curve (AUC_{24}) were calculated for PAA for each replicate. The AUC_{24} of phenoxyethanol in assay media was also calculated.

Exposure Summary:

- Conservative assumptions were made in calculating the applied dose of phenoxyethanol
- A PBK was developed to characterise the internal exposure to phenoxyethanol. The model was verified using human urinary data
- *In vitro* metabolite identification in PHH was carried out to confirm/refute *in silico* predictions. These data were used to develop a sub-PBK model so that internal exposure to the major metabolite can also be characterised
- Additional *in vitro* biokinetic refinements included measuring the concentration of phenoxyethanol and its major metabolite in cells and media under the same conditions as the bioactivity assays described below. This allows a quantitative *in vitro* to *in vivo* extrapolation to be performed for both the parent and the major metabolite.

3.2. Bioactivity Characterisation

3.2.1. Tier 0

Following the initial exposure calculation, the next step of the SEURAT-1 framework was to gather and review the information that is already available on phenoxyethanol, starting with characterisation of the chemical structure and any existing *in chemico/in vitro* data. The literature search was conducted in the PubChem database (https://pubchem.ncbi.nlm.nih.gov) and using the US EPA's Computational Toxicology Dashboard (https://comptox.epa.gov/dashboard). Any *in vitro* data reported in the most recent SCCS opinion on the safety of phenoxyethanol in cosmetics was also considered, with the exception of *in vitro* data generated as a result of effects in animals.

3.2.2. Tier 1

The preservative action of phenoxyethanol and its relevance to human safety was also considered. Phenoxyethanol can inhibit malate dehydrogenase in bacteria, which is part of the citric acid cycle and therefore conserved across most, if not all, species including humans. Sequence homology was used to determine the level of sequence identity and similarity between the bacterial and human enzymes. To further understand whether the human isoforms of the bacterial target enzyme could be a target for phenoxyethanol the docking of phenoxyethanol inside the active site of the relevant enzymes in the presence of NAD+/NADH was simulated using CDOCKER module in Discovery Studio 2018 (Gagnon, Law and Brooks, 2016). Re-docking of endogenous substrates (malate and oxaloacetate) in the same active site was used as a positive control.

In silico tools that were used to identify potential MoA of phenoxyethanol were: OECD QSAR Toolbox v. 4.1 (https://www.oecd.org/chemicalsafety/risk-assessment/oecd-qsar-toolbox.htm), Derek Nexus v 5.0.2 Lhasa Ltd.), COSMOS nuclear Receptors Binding profilers (https://knimewebportal.cosmostox.eu/com.knime.enterprise.server/#login /), MIE (Molecular initiating event) Atlas (Allen *et al*., 2018), models of the Collaborative Estrogen Receptor Activity Prediction Project (CERAPP) (Mansouri *et al*., 2016) and the Collaborative Modeling Project of Androgen Receptor Activity (CoMPARA) (Grisoni, Consonni and Ballabio, 2019). Only alerts relevant to systemic toxicity (including genetic toxicity) were considered. Each of these tools has been developed to give insights on the possible mechanisms by which a chemical might exhibit toxicity based on associations observed between the chemical structures contained within a training set and known biological effects. However, some tools (e.g. Derek Nexus and some profilers in the OECD QSAR Toolbox) are informed by effects in animals, which may have limited relevance in developing a human-relevant NGRA. Tools more focussed upon MIEs such as receptor interactions may have more relevance to this case study. For example, the MIE Atlas is based on association between chemical structure and ChEMBL protein binding data for several common off target effects associated with pharmaceutical drug attrition, including; enzymes, GPCRs, ion channels, and a limited number of nuclear receptors and transporters (Bowes *et al*., 2012).

3.2.3. Tier 2

In an attempt to provide a broad biological coverage within the risk assessment, the data described in Table 2 were generated.

Table 2 Summary of Tier 2 data generated

Assay	Cell types	Rationale for generation
SafetyScreen44™ pharmacological profiling	N/A (initial profiling is cell-free, with positive responses followed-up *in vitro*)	Panel of 44 targets recommended by 4 major pharmaceutical companies as significant liabilities in drug development (Bowes *et al.*, 2012)
Cell stress panel*	HepG2	Cellular stress underlies many adverse health effects and is likely to be especially relevant for cosmetic ingredients with a low affinity for specific biological targets.
Transcriptomics (TempO-Seq) (dose response)	MCF7, HepG2, HepaRG	Transcriptional activity across the entire genome provides wide biological coverage;

		adverse cellular changes will result in changes to gene transcription

* Cell stress panel data were generated independently of this case study (Hatherell *et al.*, 2020). Because they were not available for the Tier 1 evaluation, for the purposes of this case study they were considered Tier 2 (newly generated) rather than Tier 1 (existing) data.

The SafetyScreen44™ panel included 44 targets associated with *in vivo* adverse drug reactions, and interested readers are pointed to the original article for full details of the 44 targets, and their implications for safety (Bowes *et al*., 2012). The panel consists of 24 G-protein-coupled receptors (GPCRs), 7 enzymes, 2 nuclear receptors, 8 ion channels and 3 transporters. The experiments were carried out at Eurofins Cerep SA using phenoxyethanol sourced from Sigma-Aldrich (99699, purity >99%) at a typical drug-screening concentration of 10 µM using 2 replicates. Compound binding from the assay was calculated as a percentage inhibition of the binding of a radioactively labelled ligand specific for each target. Compound enzyme inhibition effect was calculated as a percentage inhibition of control enzyme activity. Results showing an inhibition or stimulation higher than 50% were considered to represent significant effects of the test compound.

Saturation of cellular stress pathways can lead to adverse health effects and can result in several target organ toxicities. A panel has therefore been developed to identify whether substances cause cellular stress, and if so at what concentrations (Hatherell *et al*., 2020). This panel, performed in HepG2 cells, included biomarkers that address key cellular stress pathways, including oxidative stress, DNA damage, inflammation, endoplasmic reticulum stress, metal stress, heat shock and hypoxia (Simmons, Fan and Ramabhadran, 2009) as well as mitochondrial toxicity and general cellular health. Phenoxyethanol was tested in this panel at concentrations of 0.0128, 0.064, 0.32, 1.6, 8, 40, 200 or 1000 µM (Hatherell *et al*., 2020).

Transcriptomics dose response analysis was performed to derive a no-observed-transcriptional-effect level (NOTEL) (Lobenhofer *et al*., 2004) for phenoxyethanol to use in the risk assessment. HepG2 (human hepatoblastoma) MCF-7 (human Caucasian breast adenocarcinoma) and HepaRG cells (cryopreserved differentiated) were used. Briefly, phenoxyethanol (Sigma Aldrich Catalogue Number 77699, ≥99% purity) was prepared in DMSO as serial dilutions, resulting in concentrations in media of 1000, 100, 10, 0.1, or 0.01 µM with 0.5% DMSO used as a vehicle control. Three biological replicates were treated with the appropriate dose of compound for 24-h prior to cell lysis. TempO-Seq analysis was performed as described previously (Yeakley *et al*., 2017) using the human whole genome panel version 1 (BioSpyder, Carlsbad, CA). For concentration response analysis samples were filtered in BMDexpress2 (Phillips *et al.*, 2019) using a Williams t-test with a threshold of $p<0.05$ and a minimum required fold change of 1.5. The prefiltered data were fitted to the following 6 models Poly2, Exp 3, Exp 4, Exp5, Power and Hill to determine the best fit model. A BMR factor of 1.349 was used, which represents a 10% increase over the assumed background rate of response (Yang, Allen and Thomas, 2007). This is a standard increase in response used in safety evaluation by regulatory authorities (Haber *et al.*, 2018). At a pathway level a functional classification was performed using Reactome with minimal acceptance criteria of Fishers Exact test of $p<0.1$ with at least 3 input genes and a BMDU/BMDL ratio of <40.

Bioactivity Characterisation Summary:

- Literature searches were carried out to evaluate existing data by searching ToxCast and PubChem.
- *In silico* tools were applied for phenoxyethanol and PAA including OECD QSAR Toolbox v. 4.1, COSMOS nuclear Receptors Binding profilers, MIE Atlas, CERAPP CoMPARA and CDOCKER.
- *In vitro* and *in chemico* data were generated including SafetyScreen44™, Cell Stress and transcriptomics data to provide broad coverage of phenoxyethanol's bioactivity *in vitro*.

3.3. Risk Assessment

All available *in vitro* data were evaluated, and PoDs were selected for the risk assessment considering the biological relevance of the effects observed. The lowest relevant PoD was used to determine the MoIE.

To inform whether to base the in-vitro-to-in-vivo extrapolation (IVIVE) on free or nominal phenoxyethanol concentrations, the free fraction of the dose of phenoxyethanol in the *in vitro* test system was estimated and compared to the free fraction in the *in vivo* (human) system i.e. plasma. The partitioning of a chemical in a static *in vitro* assay system is a function of two primary processes, passive diffusion/equilibrium distribution between the aqueous phase of the culture media and other test system components and active transport into and out of the cells. Active cellular transport in *in vitro* cell systems is currently not well understood and was therefore assumed to be equivalent to active transport in *in vivo* tissues. Equilibrium distribution is driven by the chemical's physico-chemical properties and can be predicted from these and test system specific parameters. The predictions for phenoxyethanol were made using a model similar to the ones described by (Kramer *et al*., 2012; Armitage, Wania and Arnot, 2014; Fischer *et al*., 2017).

The model is based on mass balance equations describing the partitioning between the following 5 compartments of an *in vitro* test system: 1: headspace, 2: serum components (proteins + lipids), 3: cells (protein + lipids + water), 4: water phase (free), 5: plastic.

The fraction of the initial amount of chemical that is free in the aqueous phase of the medium is calculated as follows:

$$F_{free} = \frac{1}{1 + K_{serum} \times \frac{V_{serum}}{V_{water}} + K_{cell} \times \frac{V_{cell}}{V_{water}} + K_{plastic} \times \frac{A_{plastic}}{V_{water}} + K_{air} \times \frac{V_{air}}{V_{water}}}$$

F_{free}: Free fraction in media

K_{serum}: distribution coefficient between serum matrix (lipids, proteins) and water expressed as [L/L serum albumin]

V_{serum}/V_{water}: Volume ratio serum matrix to media water

K_{cell}: distribution coefficient between cells and water expressed as [L/L cells]

V_{cell}/V_{water}: Volume ratio cells to media water

$K_{plastic}$: Distribution coefficient between plastic and water [expressed as L/m^2]

$A_{plastic}/V_{water}$: Ratio between exposed area of plastic [m^2] and media water

K_{air}: Distribution coefficient between air and water [L/L]

V_{air}/V_{water}: Volume ratio between headspace in well and media water

K_{serum}, and K_{cell} were calculated based on the respective fraction of proteins and lipids in serum and cells and the partition coefficients K_{BSA} and K_{lipid}, which were derived from log P (1.16) as described in Armitage, Wania and Arnot, 2014; $K_{plastic}$ was calculated from log P based on a published QSAR (Kramer *et al*., 2012). System volumes and the exposed area of plastic were calculated based on well plate dimensions, media volume and seeded cell numbers.

In a traditional risk assessment, the *in vivo* PoD is compared with the applied consumer dose to describe the level of risk. In NGRA a calculation of MoIE is possible using quantitative IVIVE (QIVIVE). In addition to a comparison between predicted blood C_{max} values incorporating population variability and the *in vitro* PoD, the QIVIVE also included a comparison of the predicted *in vivo* area under the curve over 24-h (AUC_{24}) with the *in vitro* AUC_{24} at the PoD. Comparison of both these metrics ensures that the risk assessment covers acute (C_{max}) driven effects as well as chronic (AUC-driven) effects. Internationally accepted rationale for the choice of an acceptable *in vitro*-based MoIE are not yet available. Each uncertainty in the risk assessment was therefore assessed, and a decision taken regarding whether it would affect the overall assessment, and if so whether it would result in over- or under-conservatism.

Risk assessment:

- A MOIE is calculated using QIVIVE
- The uncertainties in the risk assessment will be assessed and quantified
- It is necessary to ensure the assessment covers the main acid metabolite (PAA)

4. Application of IATA

4.1. Summary of data

4.1.1. Exposure:

Tier 0

The exposure values taken from the SCCS Notes of Guidance, 10th Edition (SCCS, 2018) indicate that consumers use 7.82 g body lotion per day, which normalized to the body weight of the participants in that use survey results in an applied dose of body lotion of 123 mg/kg/day. Since the case study subject was phenoxyethanol at up to 1% in this product type the applied dose of the case study ingredient is 1.23 mg/kg/day.

Tier 1

An example output of the Tier 1 PBK model is shown in Figure 3. The C_{max} in plasma predicted by the model was 3.4 µM, and the AUC_{24} in plasma was 5.4 µM/h.

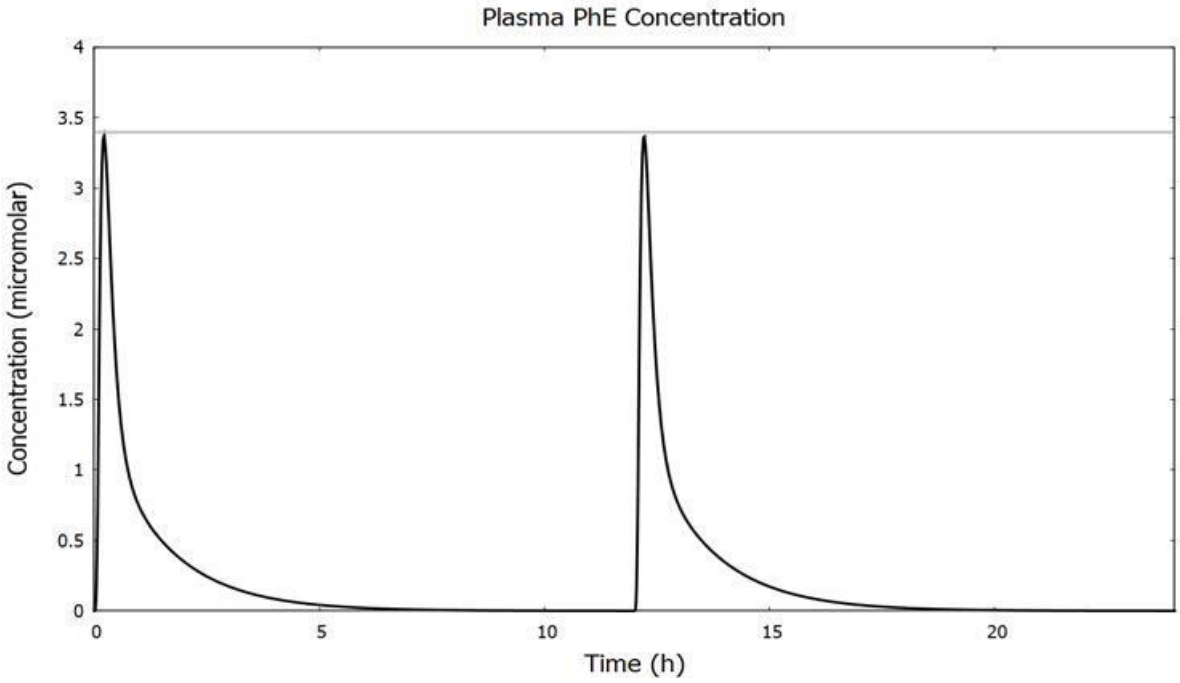

Note:
Source:

Figure 3 Tier 1 simulation of plasma exposure to phenoxyethanol following use of a body lotion containing 1% of the ingredient applied to whole body (minus head) of a 60 kg human, twice daily. Black line = predicted plasma concentration with time, grey line C_{max}

The major routes of metabolism predicted by the software (Meteor Nexus v. 3.1.0 v, Lhasa Ltd.) are summarised in Figure 4 and comprised: aromatic hydroxylation, oxidative dealkylation, glucuronidation, oxidation of primary alcohols and O-sulphonation. Meteor Nexus predicted 19 unique metabolites (30 in total). Eight of these metabolites were predicted to be formed directly from the parent compound (level 1 metabolism).

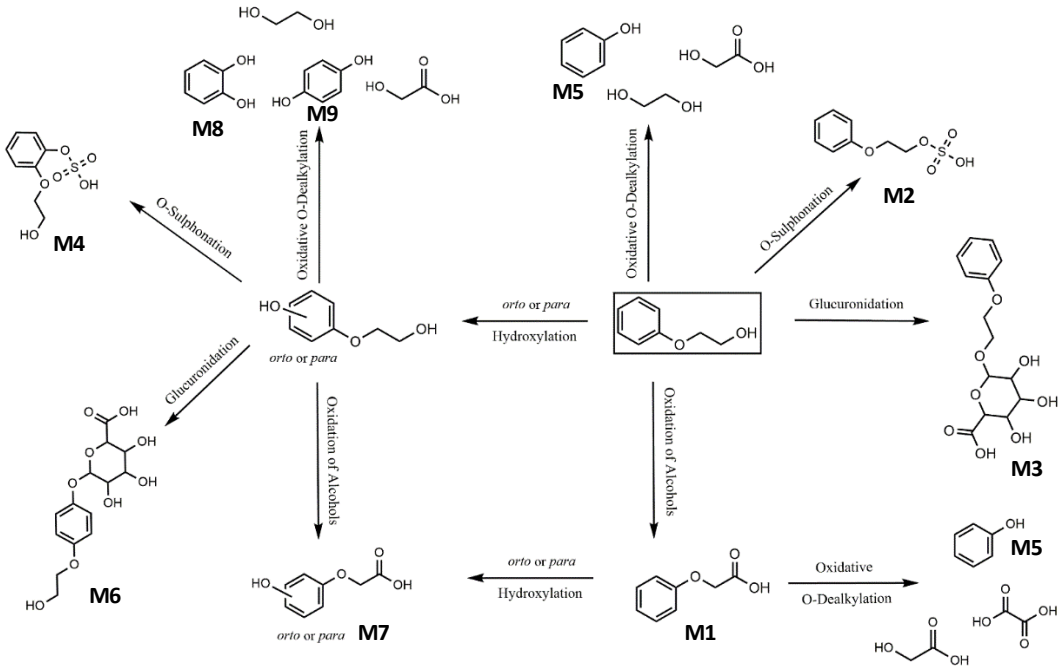

Figure 4 The major *in silico* predicted routes of metabolism (Meteor Nexus). The labels, M1-M9 denote different metabolites.

Tier 2

Metabolism and metabolite identification experiments with PHH assays were carried out to refine the exposure assessment. A half-life consistent between the 2 lowest doses (10 and 30 µM) gave reassurance that concentrations were low enough that individual pathways were not saturated. The hepatic clearance value of 20 µL/min/million cells from the literature (Wetmore *et al*., 2012) using cryopreserved PHH was confirmed in these incubations (22.3 – 25.3 µL/min/million cells). The *in vitro* metabolite identification confirmed that phenoxyacetic acid (PAA, metabolite M1 in Figure 4) was the major metabolite, and rapidly formed as phenoxyethanol depleted (Figure 5). PAA formation and phenoxyethanol depletion were used to estimate apparent K_m and V_{max} by various methods (Table 3).

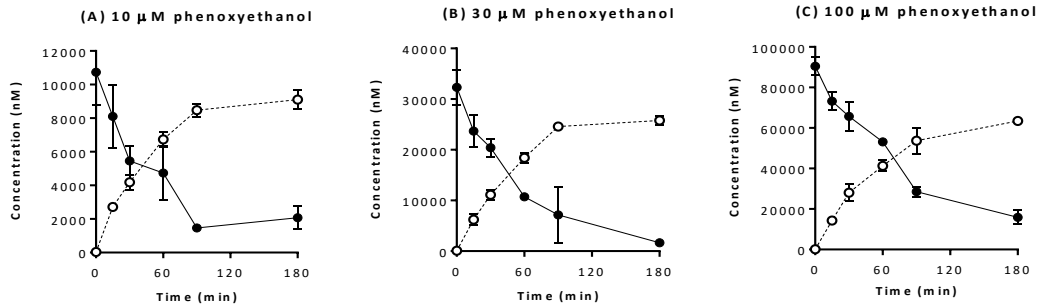

Figure 5 Depletion of phenoxyethanol (closed circles) and appearance of PAA (open circles) in primary human hepatocytes with (A) 10 µM, (B) 30 µM and (C) 100 µM phenoxyethanol (pooled donor n=5).

Table 3 phenoxyethanol kinetics data derived from primary human hepatocyte suspension incubations. V_{max} = maximum velocity; K_m = Michaelis constant; CL_{int} = intrinsic clearance

Parameter	Unit	PAA formation data			Phenoxyethanol depletion data
		Lineweaver-Burke	Eadie-Hofstee	Michaelis-Menten	Obach (ke method)
V_{max}	pmoL/min/10^6 cells	2000	2187	2541	3010
K_m	µM	79.4	89.4	114	119
CL_{int}	µL/min/10^6 cells	25.2	24.5	22.3	25.3

The fraction of phenoxyethanol metabolized to PAA was estimated, based on the CL_{int} ratio PAA /phenoxyethanol, and was calculated to be 0.88. This indicated that 88% of phenoxyethanol metabolism is converted to the PAA metabolite and 12% is metabolized to other metabolites. Four other metabolites were identified in PHH, which were also predicted by the *in silico* model, Meteor Nexus. These were M2 (direct sulfate conjugate), M3 (direct glucuronide conjugate), M4 (oxidized sulfate) and M5 (dealkylated metabolite, present as a sulfate conjugate).

In the presence of a selective aldehyde dehydrogenase (ALDH) inhibitor, 1 mM cyanamide, formation of PAA after incubation with 10, 30 and 100 µM phenoxyethanol was decreased by ~70% compared to solvent control, indicating that ALDH was involved in the metabolism.

Additional incubations of PAA with PHH suspensions in short-term (3 h) and longer-term cultures (24 h) were conducted to determine whether further metabolism of the acid was likely to occur or whether the acid could be confirmed as the likely main renally excreted metabolite. While PAA was metabolized to methylated, sulfated and oxidized products, these were considered negligible given that there was no observable depletion of the parent compound in either incubation (3 h or 24 h). Chemical degradation of phenoxyethanol and PAA was shown not to occur, based on incubations with heat-inactivated human

hepatocytes. These *in vitro* incubations of phenoxyethanol with PHH suspensions also included biokinetics measurements of both the parent and the main metabolite, PAA. Phenoxyethanol did not accumulate in the cells and was undetectable in cell lysates (Figure 6). By contrast, PAA was detected in the cells even at the first time point (1 minute after adding phenoxyethanol) (Figure 6).

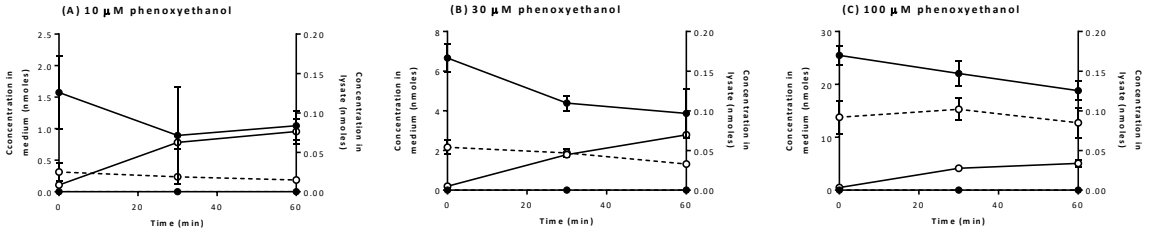

Figure 6 Amount in nmoles of phenoxyethanol (closed circles) and PAA (open circles) in the medium (solid lines) and cell lysates (dotted lines) of primary human hepatocyte suspensions incubated with (A) 10, (B) 30 and (C) 100 µM phenoxyethanol

In conclusion from PHH experiments, phenoxyethanol was shown to be taken up by PHH and very efficiently metabolised, since the metabolic conversion rate was at least the same as the uptake rate and therefore no/very little phenoxyethanol was detected in the lysate. The acid metabolite accounted for the majority of the metabolites formed, with 88% of phenoxyethanol metabolism giving rise to PAA. The acid was presumably formed through conversion of the alcohol to aldehyde by alcohol dehydrogenase (ADH) followed by conversation of the aldehyde to the acid via ALDH (which was inhibited by cyanamide). Approximately 12% of phenoxyethanol was metabolised to other metabolites. These data were in accordance with previous values measured using primary human hepatocytes (Wetmore *et al*., 2012).

Following identification of PAA as the major metabolite of phenoxyethanol, a sub-model was added to the PBK model for phenoxyethanol (model structure and parameterization in Appendix). A major refinement at Tier 2 was the inclusion of population modelling. Although ALDH was shown to be important for PAA production from the intermediate aldehyde, it was assumed that reaction with alcohol dehydrogenase 3 (ADH3) is the rate limiting step for phenoxyethanol removal (Lockley, Howes and Williams, 2005). Human ADH3 is polymorphic, with ADH3*2 being associated with reduced enzyme activity toward ethanol than the wild type ADH3*1. The prevalence of ADH3*1 (55.6%) is slightly greater than that of ADH3*2 (44.4%) in the European population (Borras *et al*., 2000). Activity of the two isoforms toward ethanol spans roughly a factor of 2 (Bosron and Li, 1986; Poupon *et al*., 1992). A normal distribution was defined for each isozyme (CL_h_invitro*1 and CL_H_invitro*2), with means that were 2-fold apart, and with each distribution spanning an order of magnitude. One clearance distribution was selected for each iteration of the Monte Carlo simulation based on the prevalence in the European population. The mean, 5^{th} percentile and 95^{th} percentile AUC and C_{max} values for phenoxyethanol and PAA are shown in Table 4.

Table 4 Results of variability analysis for the C_{max} and AUC of phenoxyethanol and PAA.

	Blood Phenoxyethanol		Blood PAA		Kidney PAA	
	C_{max}	AUC_{24}	C_{max}	AUC_{24}	C_{max}	AUC_{24}
	µM	µmol*h/L	µM	µmol*h/L	µM	µmol*h/L
Mean	3.7	7.3	10.5	230	36	789
SD	1.4	4.2	4.9	115	17	401
5th %ile	1.8	3.3	4.5	93	15	312
95th %ile	6.2	15	20	453	69	1569

Further analytical work was also performed to measure levels of phenoxyethanol and PAA in the media following culture of HepG2, MCF-7 and HepaRG cells for 0, 1, 3, 6 and 24-hours, analogous to the assay conditions of the cell stress panel (Hatherell *et al*., 2020) and the whole genome transcriptomics dose-response assays which were used to derive the *in vitro* PoD for the eventual risk assessment. This was important information because the majority of phenoxyethanol absorbed following product use is converted to PAA, therefore it is important to understand whether this was also the case in the critical dose-response assays performed on phenoxyethanol. This further analytical work allowed the cellular C_{max} and AUC_{24} values in the 24-h dose-response studies in HepG2, HepaRG and MCF-7 cells to be predicted. These experiments showed that phenoxyethanol concentrations in the medium were stable over 24-h, and that following uptake by the cells, levels of PAA detected in the lysate increased over time as phenoxyethanol was converted to PAA (Figure 7). The reason the medium concentration of phenoxyethanol did not fall as PAA was formed was the very large reserve of phenoxyethanol available to cells in the medium and the comparatively small volume of the cellular compartment. As expected, based on their enzymatic profile, MCF-7 cells showed the least metabolism followed by HepG2 cells, and HepaRG cells produced the greatest amount of PAA. Data generated on HepG2 cells are presented in Figure 7 because this cell line provided the lowest PoD.

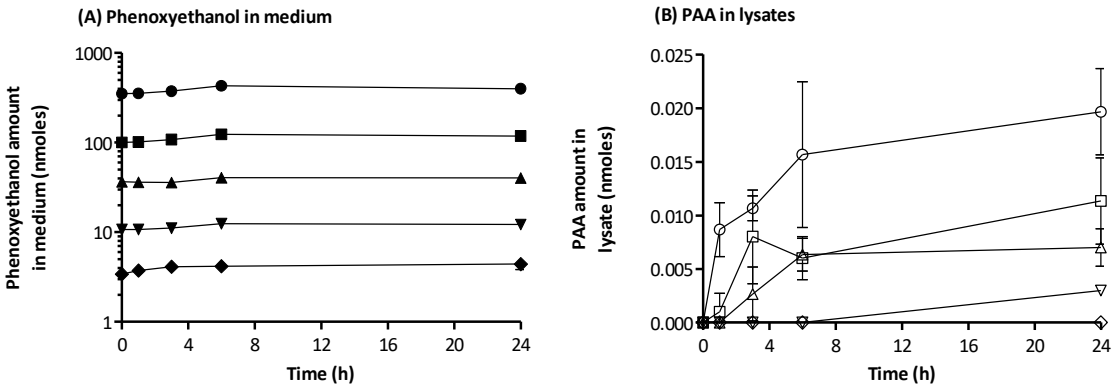

Figure 7 Concentration of phenoxyethanol in medium (A) and PAA in cell lysate (B) over time following treatment of HepG2 cells with phenoxyethanol for up to 24-h. Circles = treatment at 1000 µM, squares = 300 µM, up-pointing triangles 100 µM, down-pointing triangles 30, diamonds = 10 µM (data for 3 replicates).

The cellular C_{max} and AUC_{24} values of PAA in HepG2 and HepaRG cells were calculated for each concentration of phenoxyethanol dosed (Figure 8). As stated above, formation of PAA in MCF-7 cells was negligible.

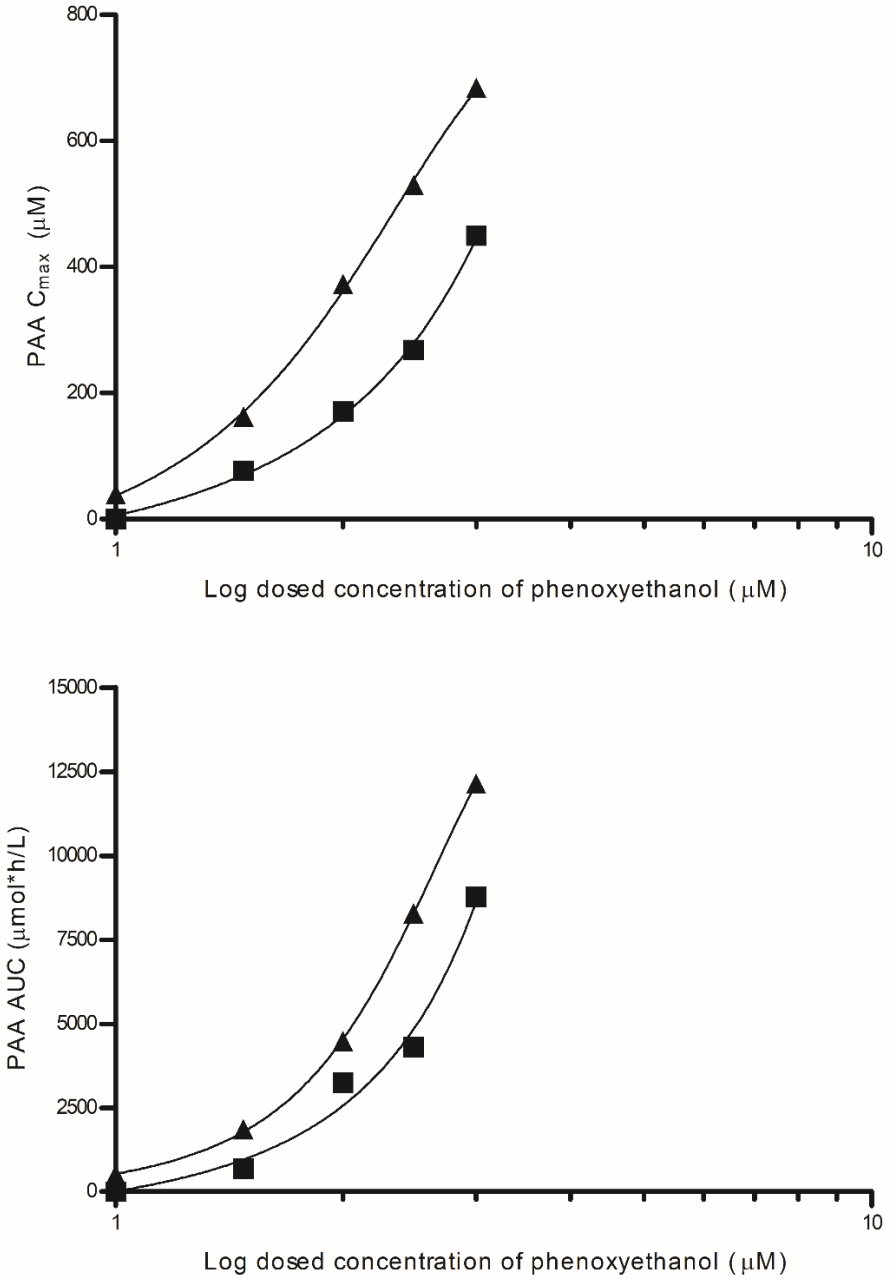

Figure 8 Non-linear regression of cellular PAA (C_{max} and AUC_{24}) against the log10 concentration of phenoxyethanol dosed to HepaRG cells (triangles) and HepG2 cells (squares).

Exposure characterisation:

- The worst-case applied dose of phenoxyethanol was calculated to be 1.23 mg/kg/day
- The PBK model developed for internal exposure predicted a 95th percentile plasma C_{max} of 6.2 µM and AUC_{24} of 15 µM/h for phenoxyethanol
- *In vitro* metabolism identification in PHH showed the major metabolites of phenoxyethanol is PAA. The PBK sub-model for the internal exposure of PAA predicted a 95th percentile kidney C_{max} of 69 µM and AUC_{24} of 1569 µM. This indicated the importance of including a NGRA for PAA at levels predicted in kidney tissue.
- C_{max} and AUC_{24} for PAA and AUC_{24} for phenoxyethanol was calculated in the cell systems used to generate the bioactivity data so the relevance of the bioactivity data to PAA could be assessed

4.1.2. Bioactivity Characterisation:

Tier 0

Phenoxyethanol

From the literature search for phenoxyethanol data, 785 ToxCast/Tox21 assays were identified, and the hit rate (proportion of positive results) was extremely low (8 hits). The hits found and their interpretation are described in Table 5.

Table 5 ToxCast/Tox21 hits for phenoxyethanol

ToxCast assay name	Expert interpretation of hit
BSK_CASM3C_SAA_up	Only top concentration above the cut-off (the threshold indicating a positive response); hit potentially confounded by overfitting. The curve fit and resultant AC_{50} (16.6 µM) are reasonable.
ATG_AP_1_CIS_dn	Disregarded as a borderline hit with a single replicate; single concentration just above the cut-off (the threshold indicating a response) at 100 µM.
NVS_ADME_hCYP2C19_Activator	Disregarded as a borderline hit at a single dose at the cut-off and predicts an AC_{50} at a concentration where the activity was not seen above the cut-off. Further, the NVS_ assays in the Activator direction are not likely to be biologically meaningful (increased activity in an enzyme inhibition assay).
ACEA_AR_agonist_80hr	Disregarded. Of the 4 replicates at each concentration, 2 replicates were completely negative and 2 were positive. Since the overall AR model score was negative (Kleinstreuer *et al.*, 2017), phenoxyethanol was considered to not exhibit any meaningful AR-related activity.

TOX21_RT_HEPG2_FLO_08hr_viability	Disregarded. These data represent a single replicate at each concentration, and only one concentration in the middle of the range is marginally higher than the cut-off. It does not make biological sense for a viability assay, so this result was considered to be due to biological variation.
TOX21_p53_BLA_p5_ch2	Disregarded because a single point drives a gain-loss fit. This is likely assay interference because it does not make biological sense for p53 activity to increase and decrease precipitously for one point in the curve.
TOX21_p53_BLA_p5_ratio	Disregarded because a single point drives a gain-loss fit. This is likely assay interference because it does not make biological sense for p53 activity to increase and decrease precipitously for one point in the curve.
TOX21_ERR_Antagonist	Disregarded because there was a lot of variability within the data and divergence between replicates.

As described in Table 5, most ToxCast hits were disregarded because the dose-response or variability in the data were not suggestive of a true effect of treatment. The only hit that was not disregarded on this basis was an increase in serum amyloid A1 in vascular smooth muscle cells in assay BSK_CASM3C_SAA_up, which gave an AC_{50} value of 16.6 µM. This hit was from one assay in the BioMap set of assays, which consists of 8 different cell types chosen to identify and characterize perturbations relevant to human inflammatory disease (Houck *et al*., 2009). Because this was a single hit on one protein target with no clearly mechanistically related hits in other cell types or inflammatory markers, this was deemed low priority for follow up.

A total of 1,646 bioassay results for phenoxyethanol were found in the PubChem database, of which 4 were marked as active. It should be noted that some of these assays were ToxCast/Tox21 assays and therefore there was some overlap between databased. One of the positive PubChem assays was from an *in vivo* test (fathead minnow acute toxicity – AID 1188) so was not used. The remaining 3 assays indicate the potential for human retinoid X receptor (RXR) agonism with an AC_{50} of 15.8 µM, human SUMO peptidase NEDD8 specific (SENP8) inhibition, and aryl hydrocarbon receptor (AhR) activation. The AhR activation data were from a Tox21 assay (TOX21+HhR_LUC_Agonist). The PubChem record notes that the activity call from these assay results were based on different analysis methods from those used by the EPA, which concluded that this assay result was negative. This is further substantiated by an additional ToxCast assay which was negative (ATG-Ahr_CIS). ToxCast provides extensive coverage of retinoic acid signalling, using 6 reporter gene assays for trans-activation of retinoic acid receptors (RARa, RARb, RARg, RXRa, RXRb and RXRg) and cis-activation of DR5 response elements by RAR/RXR (Baker *et al*., 2017). Phenoxyethanol did not trigger hits in any of these assays. The PubChem RXR and AhR results are therefore considered to be of no significance. The SENP8 enzyme inhibition result was from a fluorescent assay using NEDD8 protein substrate, and was very close to the cut-off value. SENP8 is a critical enzyme in the NEDD8 pathway, and loss of function results in defective cell cycle progression (Tateishi *et al*., 2001; Coleman *et al*., 2017). This *in chemico* assay result may therefore be considered significant if phenoxyethanol could affect the cell cycle *in vitro*.

Phenoxyethanol has been shown to act as both a bacteriostatic and bactericidal agent by various mechanisms. At bacteriostatic concentrations phenoxyethanol has been shown to inhibit the growth of *Escherichia coli* through uncoupling of oxidative phosphorylation and inhibition of malate dehydrogenase (MDH) by competing for the active site of the enzyme (Gilbert, Beveridge and Crone, 1977a, 1977b). There is also evidence that phenoxyethanol inhibits DNA and RNA biosynthesis (Gilbert, Beveridge and Crone, 1980) and causes gross membrane damage (Langsrud *et al*., 2016). Phenoxyethanol therefore acts on several targets in the cell depending on the concentrations and most likely cell death is a result of a combination of these mechanisms leading to non-reversible injuries to the cell.

In addition to the available data mentioned above, there is a significant body of literature showing that phenoxyethanol is not genotoxic *in vitro* as summarised in the SCCS Opinion on Phenoxyethanol. As the focus of this case study is systemic effects these data will not be discussed further.

Tier 1

To supplement the existing literature data found in Tier 1, the *in silico* tools provided the following results:

- Derek Nexus: inactive (negative) in the Ames assay
- OECD Toolbox: *in vivo* mutagenicity (micronucleus) in rodents: alert for H-acceptor-path3-H-acceptor
- MIE Atlas: no alerts
- CERAPP and CoMPARA: no binding predicted
- COSMOS profilers: potential binding to Thyroid Hormone Receptor (THR).

Knowing that phenoxyethanol is a well characterised chemical, it is plausible that data on this substance are present in the training set for the tools used, which may result in some bias in many of these predictions. Overall, the *in silico* alerts that warranted consideration related to *in vivo* mutagenicity and the potential to bind to the THR. However, the *in vivo* mutagenicity (micronucleus) alert is known to give a high number of false positives, and because the available *in vitro* data included a robust dataset which showed that phenoxyethanol does not damage DNA as described in the SCCS Opinion on Phenoxyethanol, this was considered to be of no biological relevance. Similarly, because there were no alerts for THR alpha or beta interactions in the ToxCast data, THR binding was considered adequately addressed.

Literature data describing the preservative MoA of phenoxyethanol were evaluated to assess whether they could have implications for human safety. Any direct effects on cell membranes, nucleic acid synthesis or cellular respiration that are relevant for eukaryotic cells are likely to result in observable changes in *in vitro* cell systems. Therefore, any point of departure derived from the relevant cell-based systems would likely be protective for these effects, and it was determined that specific tests to assess these some of these modes of action were not needed. However, as a potentially highly specific enzyme-mediated effect, the potential for disruption of MDH activity was further considered *in silico*. As a key part of the citric acid cycle, MDH is conserved across most, if not all, species. MDH is found in all eukaryotic cells as two isozymes: mitochondrial (mMDH) and cytoplasmic

(soluble, sMDH) (Bleile *et al*., 1975). By contrast, prokaryotes contain only a single form of MDH. Sequence alignment shows that mMDH is more closely related to the prokaryotic MDH than is sMDH. In particular, the sequences of human mMDH (UniProt ID: P40926) and *Escherichia coli* MDH (UniProt ID: P61889) share 53.8% of sequence identity and 69.8% of sequence similarity. On the other hand, the sequences of the human sMDH (UniProt ID: P40925) and *Escherichia coli* MDH (UniProt ID: P61889) share 21.7% of sequence identity and 40.7% of sequence similarity.

The active site residues in *E. coli* MDH and both human MDHs are preserved, hence, confirming the identical catalytic mechanism. The crystal structures of *E. coli* MDH and human mMDH are essentially identical (Goward & Nicholls, 1994) and display a backbone root-mean-square deviation of 0.97 Å. By contrast, the structure of human sMDH deviates from the *E. coli* MDH mainly in the loop regions and displays a backbone root-mean-square deviation of 1.85 Å. Therefore, assuming that phenoxyethanol inhibits *E. coli* MDH, it is more likely that phenoxyethanol also inhibits mMDH rather than sMDH. Based on these analyses there appears to be too much similarity between bacterial and human MDH to be able to disregard mMDH or sMDH as targets of phenoxyethanol.

To understand further whether either of the human isoforms of MDH could be a target for phenoxyethanol, molecular docking was carried out using the CDOCKER module in Discovery Studio 2018 (Gagnon, Law and Brooks, 2016). The structure of phenoxyethanol was docked inside the active site of mMDH and sMDH in the presence of NAD+/NADH. Re-docking of malate and oxcaloacetate in the same active site was used as a positive control. The results obtained show that phenoxyethanol is very unlikely to competitively inhibit mMDH or sMDH (Figure 9). Since molecular docking cannot rule out non-competitive and allosteric inhibition of MDH, it is important that any disruption of cellular respiration is examined *in vitro*. This was done by evaluating the data from the cell stress panel (see below).

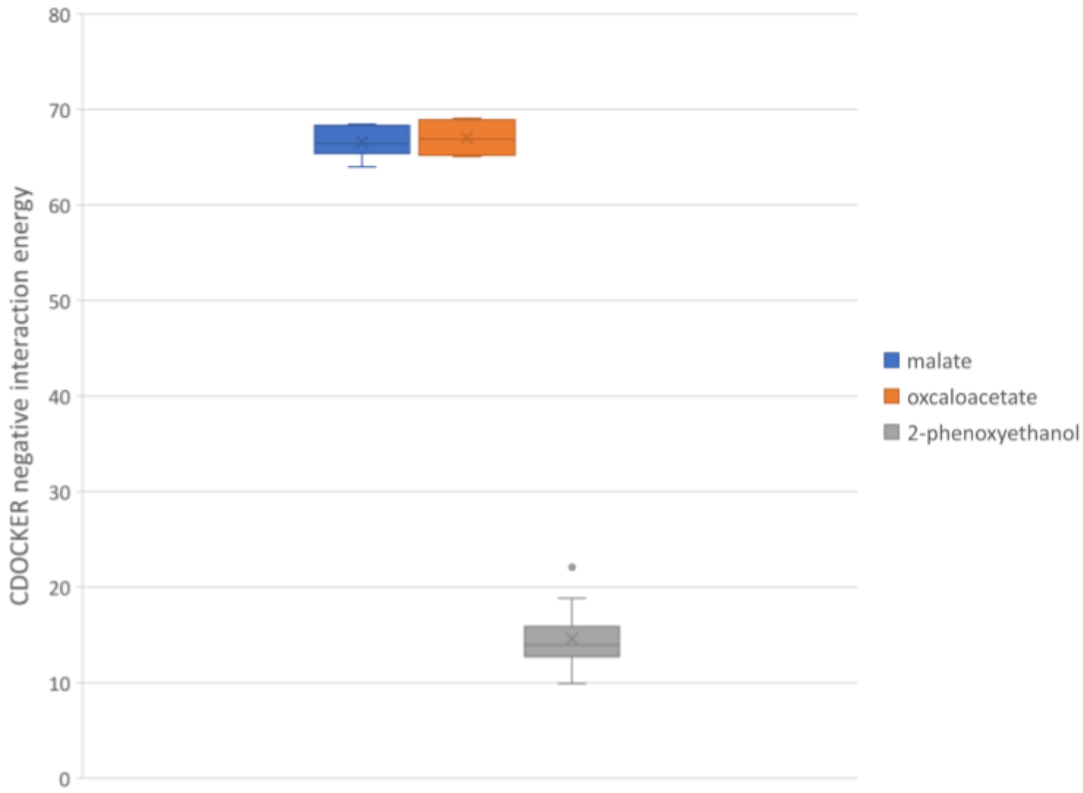

Figure 9 Interaction energies obtained from CDOCKER. Docking was carried out using 10 lowest energy models of MDH. Corresponding energies are represented as distributions: malate (blue), oxcaloacetate (orange) and 2-phenoxyethanol (grey). Interaction energies o

Phenoxyacetic acid (PAA)

As NGRA is a tiered and iterative approach (Dent *et al.*, 2018), following identification of PAA as a major metabolite of phenoxyethanol, the bioactivity of PAA was further characterised as for any substance health effects may be driven by a metabolite rather than the parent chemical. PAA was therefore profiled using the same *in silico* tools as phenoxyethanol in Tier 1. The decision was taken not to specifically evaluate the minor metabolites (M2, M3, M4 and M5 in Figure 4). This is because the minor metabolites were formed in hepatocyte experiments at much lower levels than PAA as sulfate or glucuronide conjugates which would likely be rapidly excreted, resulting in markedly lower potential consumer exposure when compared with exposure to phenoxyethanol and PAA. The results for PAA were the same as for phenoxyethanol with the following additional alerts:

- Derek Nexus: alert for plausible hepatotoxicity,

- OECD Toolbox: binding to the oestrogen receptor (ER), binding to proteins, hepatoxicity.
- COSMOS profilers: potential binding to both ER and THR.

Additionally, PAA has also been tested in 400 ToxCast assays, including the endocrine-related assays, and produced no hits. The *in silico* alerts for ER and THR binding were therefore considered to be adequately addressed. The Derek Nexus alert "phenoxyacetic acid or derivatives" for hepatotoxicity was identified for PAA. This alert describes the hepatotoxicity of phenoxyacetic acid or derivatives including the fibrates. These compounds have been reported to cause liver toxicity in humans with various outcomes including cholestasis, necrosis and cirrhosis (Pierce and Chesler, 1978; Leonard *et al*., 1997). Formation of protein adducts were observed in animals exposed to fibrates (Sallustio *et al*., 1991). The proposed mechanism of toxicity involves metabolic activation of these compounds and subsequent formation of acyl glucuronides and acyl CoA thioesters as reactive intermediates (Shore *et al.*, 1995; Grillo and Benet, 2002) which are not formed by PAA in *in vitro* incubations with PHH or predicted to be formed using Meteor Nexus. This alert was therefore considered to be of no toxicological relevance.

Tier 2

Assay	Summary results for phenoxyethanol
SafetyScreen44™ pharmacological profiling	Inactive
Cell stress panel	Inactive
Transcriptomics (TempO-Seq)	$BMDL_{10}$ of 171 µM in HepG2 cells

The SafetyScreen44™ assays showed no significant effect for phenoxyethanol in any of the binding and enzymatic assays at the 10 µM concentration. The highest reported inhibition was 12.1% and was attributed to variability of the signal around the control level. The results showing the percentage inhibition of the binding of a radioactively labelled ligand and percentage inhibition of control enzyme activity are shown in Table 6.

In a panel of biomarkers to identify PoDs in HepG2 cells for risk assessment based on several key cellular stress pathways, mitochondrial function and general cellular health, phenoxyethanol did not show any activity at concentrations up to 1000 µM (Hatherell *et al*., 2020). This panel, consisting mostly of high content imaging assays, assessed several biomarkers of cellular respiration including cellular ATP levels, oxygen consumption rate, and mitochondrial reserve capacity) showed that even at a high concentration phenoxyethanol did not cause any effects. This contrasted with substances known to cause cellular stress that were shown to perturb these pathways (Figure 10), and therefore alleviated concern that phenoxyethanol could cause adverse effects by interfering with human MDH.

Table 6 Results of the binding and enzymatic assays using the Safety Screen 44 panel.

ASSAY NAME	**radioligand/positive control**	**RESPONSE/ READOUT**	**VALUE [Mean % inhibition]**
mu (MOP) human opioid GPCR binding (agonist radioligand)	DAMGO	Specific binding	12.10
D2S human dopamine GPCR binding (agonist radioligand)	7-OH-DPAT	Specific binding	10.33
5-HT3 human serotonin ion channel binding (antagonist radioligand)	MDL 72222	Specific binding	9.45
5-HT1A human serotonin GPCR binding (agonist radioligand)	8-OH-DPAT	Specific binding	9.36
D1 human dopamine GPCR binding (antagonist radioligand)	SCH 23390	Specific binding	8.27
M2 human acetylcholine (muscarinic) GPCR binding (antagonist radioligand)	methoctramine	Specific binding	7.47
beta 2 human adrenoreceptor GPCR binding (antagonist radioligand)	ICI 118551	Specific binding	6.55
kappa (KOP) human opioid GPCR binding (agonist radioligand)	U 50488	Specific binding	6.49
CB2 human cannabinoid GPCR binding (agonist radioligand)	WIN 55212-2	Specific binding	5.73
Human androgen receptor (AR) nuclear hormone receptor binding (agonist radioligand)	testosterone	Specific binding	5.56
H1 human histamine GPCR binding (antagonist radioligand)	pyrilamine	Specific binding	5.17
H2 human histamine GPCR binding (antagonist radioligand)	cimetidine	Specific binding	4.94
DAT human dopamine transporter (antagonist radioligand)	BTCP	Specific binding	4.55
Monoamine oxidase A (MAO-A) rat binding (antagonist radioligand)	clorgyline	Specific binding	3.84
M1 human acetylcholine (muscarinic) GPCR binding (antagonist radioligand)	pirenzepine	Specific binding	3.83

M3 human acetylcholine (muscarinic) (antagonist radioligand)	4-DAMP	Specific binding	3.54
beta 1 human adrenoreceptor GPCR binding (agonist radioligand)	atenolol	Specific binding	3.53
A2A human adenosine GPCR binding (agonist radioligand)	NECA	Specific binding	3.46
alpha 1A human adrenoreceptor GPCR binding (antagonist radioligand)	WB 4101	Specific binding	2.44
V1a human vasopressin/oxytocin GPCR binding (agonist radioligand)	[d(CH2)5 1,Tyr(Me)2]-AVP	Specific binding	1.19
Lck human TK kinase enzymatic lanthanide chelate excite (LANCE)	staurosporine	Enzymatic activity	0.75
alpha 2A human adrenoreceptor GPCR binding (antagonist radioligand)	yohimbine	Specific binding	0.56
norepinephrine transporter (h) (antagonist radioligand)	protriptyline	Specific binding	0.51
COX1 Human cyclooxygenase enzymatic	diclofenac	Enzymatic activity	-0.279
Human acetylcholinesterase enzymatic	galanthamine	Enzymatic activity	-0.403
delta (DOP) human opioid GPCR binding (agonist radioligand)	DPDPE	Specific binding	-0.412
BZD (central) (agonist radioligand)	diazepam	Specific binding	-0.522
5-HT1B human serotonin GPCR binding (antagonist radioligand)	serotonin	Specific binding	-0.585
PDE4D2 human phosphodiesterase enzymatic	Ro 20-1724	Enzymatic activity	-1.57
Potassium Channel hERG (human)- [3H] Dofetilide	terfenadine	Specific binding	-1.61
GR human glucocorticoid nuclear hormone receptor binding (agonist radioligand)	dexamethasone	Specific binding	-2.08
5-HT transporter (h) (antagonist radioligand)	imipramine	Specific binding	-2.31
Cav1.2 (L-type) rat calcium ion channel binding (dihydropyridine site)	nitrendipine	Specific binding	-3.57
5-HT2A human serotonin GPCR (agonist radioligand)	±)DOI	Specific binding	-3.88

COX2 human cyclooxygenase enzymatic	NS398	Enzymatic activity	-4.47
Non-selective rat sodium ion channel [3H] batrachotoxinin binding (Site 2) (antagonist radioligand)	veratridine	Specific binding	-5.23
CB1 human cannabinoid GPCR binding (agonist radioligand)	CP 55940	Specific binding	-6.85
5-HT2B human serotonin GPCR (agonist radioligand)	(±)DOI	Specific binding	-8.87
Glutamate (NMDA, non-selective) rat ion channel binding (antagonist radioligand)	CGS 19755	Specific binding	-9.52
PDE3A human phosphodiesterase enzymatic	milrinone	Enzymatic activity	-9.70
KV (non-selective) rat potassium ion channel [125I] alpha-dendrotoxin binding (antagonist radioligand)	α-dendrotoxin	Specific binding	-11.4
nAChR (alpha4/beta2) human ion channel binding (agonist radioligand)	nicotine	Specific binding	-18.2
ETA human endothelin GPCR binding (agonist radioligand)	endothelin-1	Specific binding	-21.6
CCK1 (CCKA) human cholecystokinin GPCR binding (agonist radioligand)	CCK-8s	Specific binding	-21.8

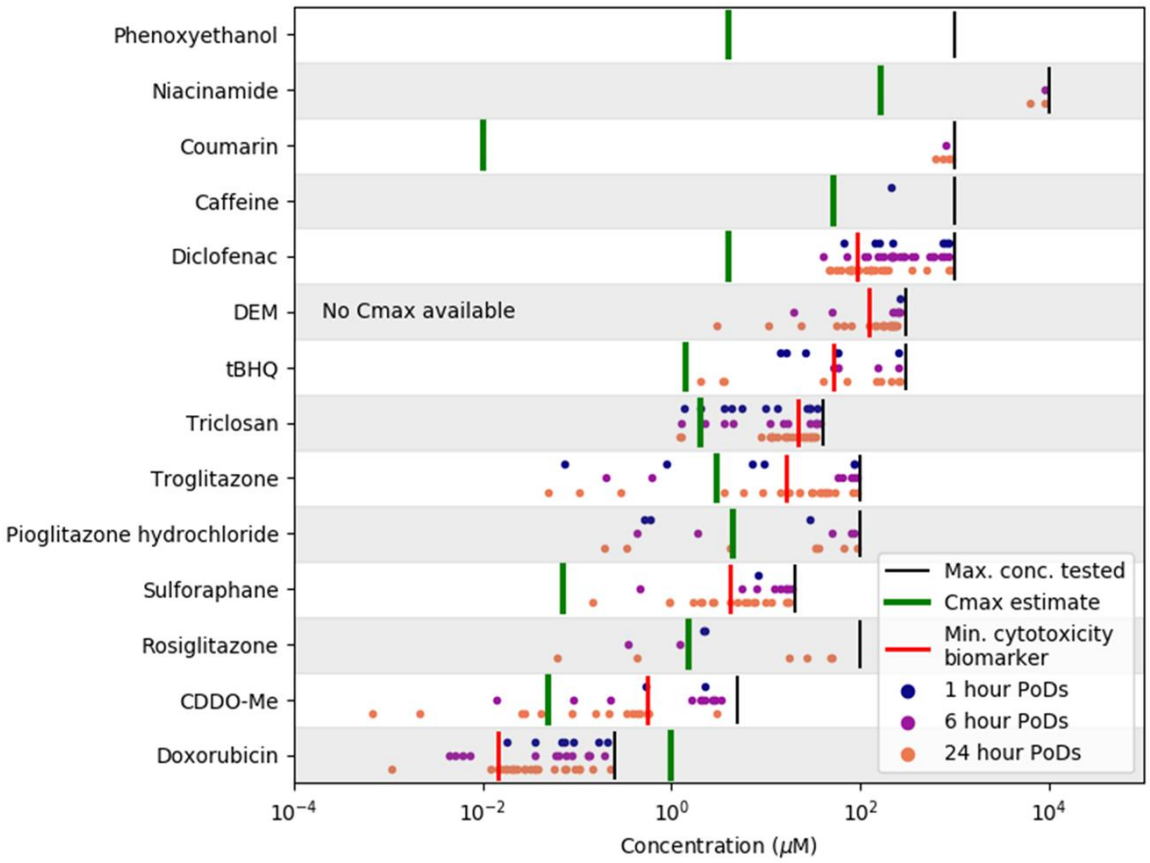

Figure 10 Overview of PoDs and associated C_{max} for several substances used in the development of a cell stress panel. Phenoxyethanol was inactive in all assays, in contrast to other test items known to cause adverse health effects and cellular stress (Hatherell *et al.*, 2020) reproduced under Creative Commons CC-BY-NC license.

Dose-response modelling was performed on the Biospyder data. This applied filtering criteria to BMD modelling as previously described (Farmahin *et al*., 2017) which resulted in fewer than the recommended 20 pathways for NOTEL calculations for each cell line. As a result, all pathways BMDs were included in pathway NOTEL calculations. For all cell lines at 24-h, pathway level NOTELs ranged from 232 µM to 920 µM. In HepaRG cells, cytochrome p450 genes CYP2B6 and CYP2A6 showed the greatest fold changes. Along with presence of cytochrome p450 genes, the Reactome (Fabregat *et al.*, 2018) pathways 'Metabolism (R-HSA-1430728)' and 'Metabolism of proteins' (R-HSA-392499) were identified at the pathway level for HepaRG cells. There was, however, little evidence to suggest a mechanistic response. The pathways identified were large, top-level pathways and no lower level, specific pathways were significantly altered. A similar case was also seen in the MCF-7 cells, which showed a very narrow BMD range across the 18 pathways meeting the significance criteria set, ranging from 760.33 – 866.48 µM. None of these were specific pathways indicating a mechanistic effect. Two differentially expressed genes (ANO6 and RAB36), associated with the 'Neutrophil Degranulation' (R-HSA-6798695) pathway, were observed for MCF7 cells, but these genes were not well represented within the total number of genes in this pathway (477). This was therefore considered to be not biologically significant.

HepG2 cells had fewest number of genes that were affected and only one pathway showing significant response to treatment, 'signal transduction', which showed the lowest calculated $BMDL_{10}$ of 171µM. NOTELs for all 3 cell types are presented in Table 7.

Table 7 NOTEL values for phenoxyethanol across 3 cell lines calculated using BMD modelling.

Gene Tests	HepaRG	MCF-7	HepG2
BMD_{10} of pathway with the lowest BMD_{10} (µM)	552.90	760.33	232.00
$BMDL_{10}$	220.92	512.84	171.25
$BMDU_{10}$	911.72	1648.51	557.20

Bioactivity characterisation:

- Literature searches in the ToxCast and PubChem databases indicated some hits for phenoxyethanol. However, most of these hits were considered to be not biologically relevant.
- Phenoxyethanol has several possible preservative MoAs of which the most relevant to humans is inhibition of MDH. CDOCKER analysis reduced concern that phenoxyethanol could competitively inhibit human MDH but cannot rule out allosteric inhibition.
- The *in silico* tools applied for phenoxyethanol and PAA raised some alerts. When these alerts were considered alongside the available *in vitro* data they were determined not be biologically relevant.
- The *In vitro* and *in chemico* data shows that phenoxyethanol is exhibits little bioactivity. The smaller data set generated and available for PAA shows that this major metabolite has a similar low bioactivity.

4.1.3. Additional biokinetic refinements performed in Tier 2

PAA had been shown to be formed in both HepG2 and HepaRG cells, and the cellular C_{max} and AUC_{24} was calculated across a range of doses as shown in Figure 8. It was therefore possible to interpolate the C_{max} and AUC_{24} at the NOTEL for phenoxyethanol in both these cell types (Figure 11). This showed that at the NOTEL for HepG2 and HepaRG cells the cellular C_{max} of PAA was approximately 217 µM and 492 µM respectively, and the AUC_{24} was approximately 3550 µM/L and 7163 µM/L respectively. Note this was only done in the cell lines that showed appreciable formation of PAA (HepG2 and HepaRG). A similar approach was used to calculate the AUC_{24} value for phenoxyethanol in the media at the relevant PoD (Figure 12).

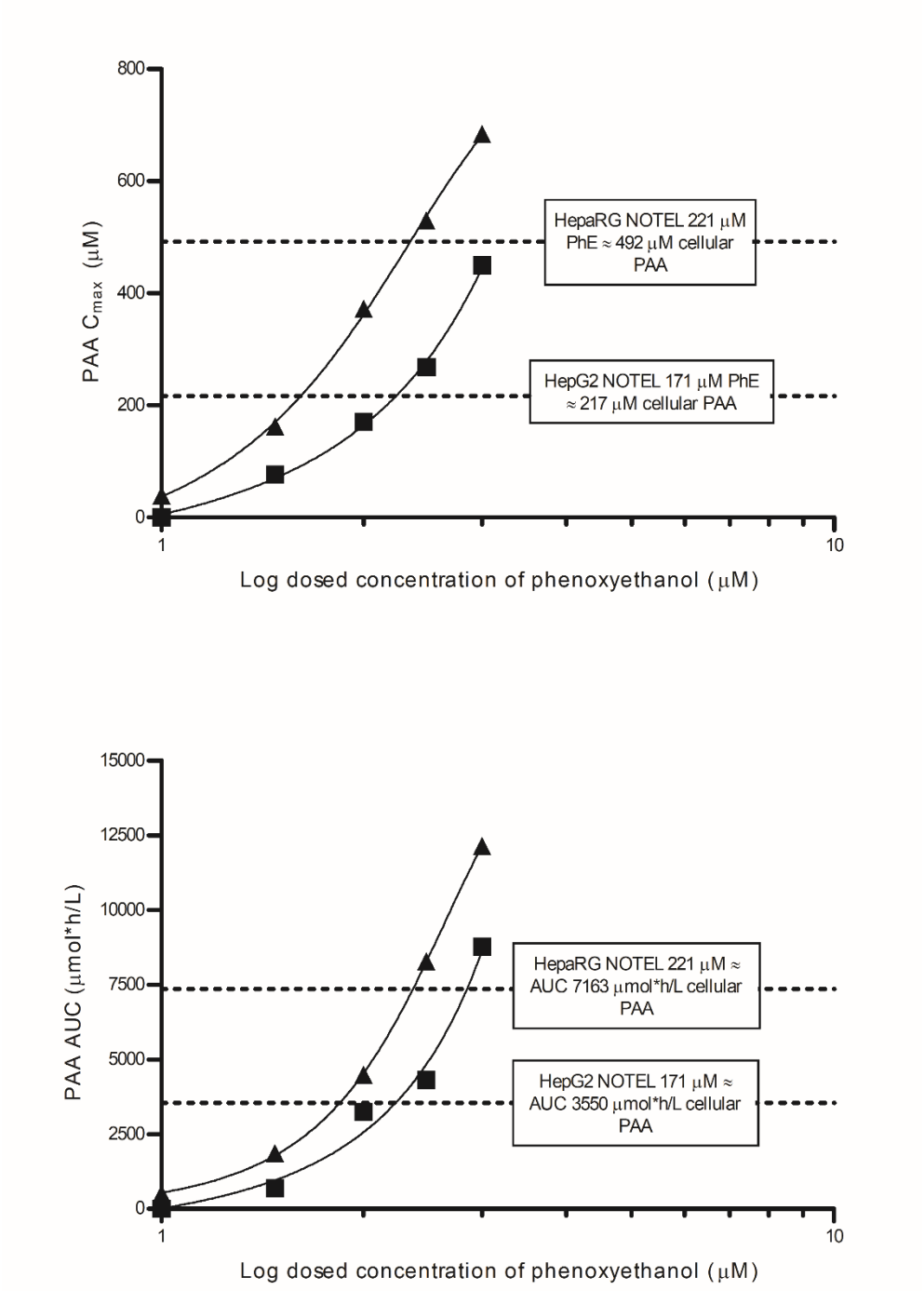

Figure 11 Non-linear regression of cellular PAA (C_{max} and AUC_{24}) against the log10 concentration of phenoxyethanol dosed to HepaRG cells (triangles) and HepG2 cells (squares). This was used to interpolate the approximate C_{max} and AUC_{24} associated with the NOTELs in each cell line (indicated by dotted lines).

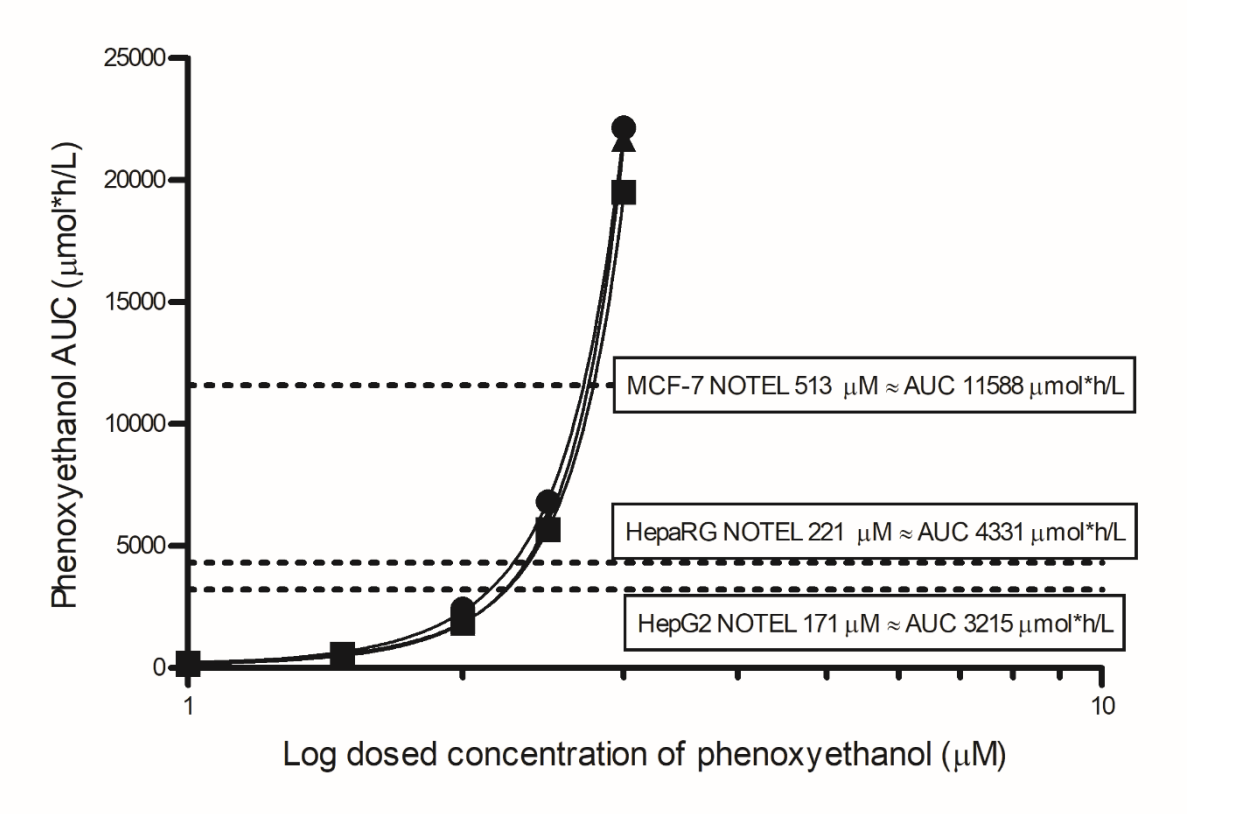

Figure 12 Non-linear regression of AUC_{24} values for phenoxyethanol in culture medium against the log10 concentration of phenoxyethanol dosed to HepaRG (triangles), HepG2 (squares) and MCF-7 cells (circles). This was used to interpolate the approximate AUC_{24} associated with the NOTELs for each cell line (indicated by dotted lines).

4.2. Application of IATA

Given the lack of compelling evidence that phenoxyethanol would be active in humans via a specific mechanism, it was considered to fit into the 'no defined biological target or pathway' category as described in the US EPAs blueprint for computational toxicology (Thomas *et al*., 2019), which provides a hypothesis that can be explored further in Tier 2. The aim of Tier 2 was therefore to build confidence in the exposure and metabolism predictions and to use higher tier tools to ensure broad enough biological coverage of data regarding phenoxyethanol. The latter considered whether MDH and SENP8 were expressed in the cell lines used to help understand if these could be targets of phenoxyethanol, since *in vitro* confirmation that phenoxyethanol can inhibit these enzymes in eukaryotic cells may indicate a more specific toxicity (AOP) that needs to be examined.

Phenoxyethanol showed limited biological activity across all the assays. The only ToxCast hit that showed a credible dose-response was related to SAA1, although this biomarker was only raised at the highest concentration tested, and no pathways relevant to an acute inflammatory response were affected in any of the transcriptomics assays or biomarkers relevant to inflammatory pathways in the cell stress panel. This single hit was therefore considered to be of no biological relevance.

Neither the SafetyScreen44™ nor the cellular stress panel provided sufficient evidence of phenoxyethanol being active to identify a PoD. The PoD from the transcriptomics assessments (the NOTELs) therefore provided important information for the risk assessment.

Phenoxyethanol showed a very low level of transcriptional activity in MCF7, HepaRG and HepG2 cells at 24-hours. The $BMDL_{10}$ of 171 µM in HepG2 cells was taken as the most sensitive PoD for the risk assessment. This PoD is highly conservative because in this cell line only 1 affected pathway (signal transduction) was identified. A full list of the genes affected in the different cell types has been provided in Annex II.

Prediction of the free fraction of the dose in media indicated that differences between binding *in vivo* (fraction unbound in plasma = 0.56) and *in vitro* (fraction free in media = 0.96 for assay containing 10% serum in the media) would be within a factor of 2. The PoD was therefore expressed as total phenoxyethanol present in the culture medium.This PoD was compared with the predicted total blood concentration of phenoxyethanol (95th percentile population C_{max}). In addition, the concentration of phenoxyethanol in medium under the conditions of the *in vitro* bioactivity studies was analysed over time to enable a comparison between the 95th percentile population AUC_{24} values and the AUC_{24} value at the PoD.

The available data on PAA did not highlight a specific mode of action that would drive the risk assessment, although the data on this metabolite were more limited than for phenoxyethanol. To further the risk assessment for the major metabolite PAA, the concentration of PAA present within HepG2 cells over the 24-h transcriptomics experiment was estimated. Although HepaRG cells were more metabolically active and therefore produced more PAA than HepG2 cells, to be conservative the HepG2 PoD was used because it was the lowest PoD in cells that had been exposed to PAA. The cellular concentration was selected for the PAA IVIVE because it more closely reflects the concentration of this metabolite at the putative site of action (the cell/tissue). The predicted C_{max} and AUC_{24}, expressed as total PAA was compared with the 95th percentile population total C_{max} and AUC_{24} within kidney tissue, which was the organ predicted to show the highest level of PAA exposure following product use.

The MoIE values calculated for both phenoxyethanol and PAA acid are shown in Table 8. These have been expressed as a range, considering the worst-case ($BMDL_{10}$/highest exposure) through to the best case (BMDU10/lowest exposure).

Table 8 Margin of internal exposure (MoIE) values

Chemical	Scenario	Human Exposure		PoD		MoIE	
		AUC_{24} µmol*h/L	C_{max} µM	AUC_{24} µmol*h/L	C_{max} µM	AUC_{24}	C_{max}
Phenoxyethanol	Worst case (BMDL/P95 Exposure)	15	6.2	3215	171	214	28
Phenoxyethanol	Mean (BMD/Mean Exposure)	7.3	3.7	4381	232	600	63
Phenoxyethanol	Best case (BMDU/P05 Exposure)	3.3	1.8	10708	557	3245	309
PAA	Worst case (BMDL/P95 Exposure)	1569	69	3550	217	2	3
PAA	Mean (BMD/Mean Exposure)	789	36	4206	249	5	7
PAA	Best case (BMDU/P05 Exposure)	312	15	6573	359	21	24

Risk assessment:

- The 95th percentile population C_{max} and AUC_{24} values were 28 and 214 times lower than the $BMDL_{10}$ NOTELs for phenoxyethanol, whereas the C_{max} and AUC_{24} values for PAA were 2 and 3 times lower than the predicted exposure at the NOTEL. Therefore, although all the MoIE values were above 1, indicating that *in vitro* bioactivity occurred at doses greater than the expected consumer exposures, those for PAA were very close to the expected human exposures.

4.3. Uncertainty

A traditional toxicological risk assessment uses assessment or uncertainty factors to determine whether a margin of exposure is sufficient to assure safety (SCCS, 2018). Instead of applying default assessment factors, the different uncertainties within the case study were described to determine the level of confidence in the MoIE obtained (Table 8). The main areas of uncertainty surrounded the biological coverage of the *in vitro* tests. Although there is increasing evidence that *in vitro* PoDs are likely conservative (Paul Friedman *et al*., 2020), it is unknown whether the cell lines used fully reflected the diversity of all the cells that may be exposed *in vivo*. The range in $BMDL_{10}$ NOTELs from the full genome dose-response analysis in HepG2, HepaRG and MCF-7 cells was 171 µM (HepG2) to 513 µM (MCF-7), a factor of 3. The amount of variability in NOTELs between other cell types is unknown.

The level of certainty in the assessment of the major metabolite, PAA, was lower than the level of certainty associated with the assessment of phenoxyethanol itself. In particular, no transcriptomics data were generated in a kidney cell line. This is a clear limitation, because kidney tissue was predicted to be exposed to the highest levels of PAA, and pathways expressed in renal cells may not be present in the cell lines evaluated. It should also be noted that PAA was not tested in the pharmacological profiling assays (SafetyScreen44™),

and in fewer ToxCast assays than was phenoxyethanol. It is therefore possible that some specific effect related to PAA may have not been addressed in this evaluation.

Other major uncertainties in the PAA assessment relate to the use of PoD values (AUC and C_{max}) calculated using the *in vitro* biokinetic refinement study rather than measured in the same study used to derive the NOTEL. On the one hand, this represents an exposure refinement, because it considered exposure at the cellular/tissue level rather than blood levels. On the other hand, because these values were calculated rather than measured, they provide approximate exposure levels in the transcriptomics experiments at the NOTEL. Nonetheless, basing the risk assessment of the major metabolite on extrapolation rather than directly measured data is a limitation that reduces confidence in the risk assessment.

With the available data it was not possible to confidently quantify these uncertainties. It was therefore determined that these would need to be addressed to confidently assure the safety of phenoxyethanol at 1% using only non-animal approaches.

Table 9 Level of certainty in different areas of the risk assessment

Area	**Level of certainty (rationale)**	**Is value likely an over or under-estimate (rationale)?**	**Impact on risk assessment decision**
Consumer exposure (applied dose)	High (based on consumer habits survey data in relevant population, widely used value)	Considered to be a reasonable worst-case	Increases confidence that assessment is conservative.
Identification of metabolites	High (a tiered approach was used culminating in experiments in PHH, which is a realistic model to identify the metabolite profile in liver. Provides a good indication of quantification of each metabolite. Skin metabolism not considered (due to rapid dermal penetration and low first pass metabolism relative to liver). Given PBK model output showed good correlation with *in vivo* (human) data this did not appear a significant limitation).	Not considered to be over or under-estimated	Increases confidence that assessment is conservative.
Consumer exposure (internal concentration, target organs)	High (PBK predictions verified with human data for PAA, sensitivity analysis, characterization of population variability. Bioaccumulation potential of target substance considered low due to efficient metabolism. See supplementary materials for full details).	Considered to be a reasonable worst-case	Increases confidence that assessment is conservative.

Area	Level of certainty (rationale)	Is value likely an over or under-estimate (rationale)?	Impact on risk assessment decision
Range of biomarkers assessed	**Parent (phenoxyethanol)** Moderate (Addition of SafetyScreen44™, cell stress and transcriptomics to existing ToxCast/Pubchem data for phenoxyethanol covered a wide range of modes of action).	Given the low activity of phenoxyethanol across all available assays, it is considered unlikely a specific MoA exists that would affect the safety assessment.	It is not yet known if additional/different biomarkers would be needed to ensure a robust and relevant assessment. This uncertainty therefore reduces confidence in the safety assessment. Confidence could be increased by assessing how protective the range of biomarkers are for many more compounds and whether different biomarkers are needed to ensure the *in vitro* PoD is protective compared with the *in vivo* PoD.
	Major metabolite (PAA) Low (Testing of PAA more limited than testing of phenoxyethanol with fewer ToxCast assays available. However, it has been shown that PAA would have been formed in HepG2 and HepaRG cells which were used in cell stress (HepG2) and transcriptomics (HepG2 and HepaRG) experiments).	Unknown how significant the lack of SafetyScreen44™ data and limited ToxCast data is. However, given the low biological activity seen in the available data, and the small number of genes affected in cell lines with some metabolic competence, there is a risk that a specific MoA exists that would affect the safety assessment.	Lack of SafetyScreen44™ data and the limited ToxCast data on PAA reduces confidence in the assessment. Generation of additional *in vitro* pharmacological profiling data on PAA could increase confidence.

In vitro biokinetics	Moderate (AUC_{24} and C_{max} values were interpolated rather than measured; cell volume data used in calculations was taken from literature rather than measured in the study, *in vitro* kinetics was performed in a different laboratory to transcriptomics experiments; IVIVE based on total phenoxyethanol and PAA rather than free concentration).	*In silico* predictions suggested that basing the assessment on total rather than free concentration will be conservative. Impact of the use of interpolated PK parameters unknown, therefore need to assume that exposure at NOTEL was over-estimated.	Reduces confidence in the assessment. This could be increased by performing *in vitro* kinetics assessments and measuring cell volume in the same laboratory as bioactivity measurements.
Use of short-term *in vitro* tests to inform risk of long-term human exposure	Moderate (There is increasing evidence showing that for many chemicals use of a short-term *in vitro* PoD, and short-term transcriptomics data in particular are protective for long-term target organ effects (Thomas *et al.*, 2013; Paul Friedman *et al.*, 2020))	Previous analyses show that short term *in vitro* PoDs are protective in most cases	No correction made for duration of exposure from *in vitro* to human exposure.
Point of Departure	**Parent (phenoxyethanol)** Moderate (Full genome NOTEL is only available in 3 cell lines, and other cell lines or cells *in vivo* may provide a lower NOTEL. Changes in gene expression do not necessarily lead to an adverse health effect. Changes in gene expression were only analysed at 24-hours in the full dose-response study. The impact of inter-individual variability in response is not known).	The NOTEL of 171 µM is the $BMDL_{10}$ value from a cell line that showed only 2 genes from one pathway affected with treatment up to 1000 µM. This gives confidence that the PoD is conservative. However, because transcriptomics was performed only 3 cell lines this needs to be	The availability of NOTELs in only 3 cell lines reduces confidence in the assessment because it is likely that if additional cell types were included a lower NOTEL would be found. With the available data it is not possible to quantify this uncertainty. Confidence could be increased by generating data in additional cell lines and at different timepoints. The lack of data in inter-individual variability is

		considered an overestimate of the true NOTEL (i.e. testing in further cells may reduce NOTEL).	also a limitation which reduces confidence in the assessment and therefore needs to be addressed.
	Major Metabolite (PAA) Moderate (Lack of full genome dose-response NOTEL for major metabolite addressed by performing additional *in vitro* kinetics work to characterize exposure to PAA in the phenoxyethanol studies. Lack of transcriptomics data in a kidney cell line is a source of uncertainty. The impact of inter-individual variability in response is not known).	As above, with the addition that testing in a kidney cell line is specifically required for PAA	As above

4.4. Strategy and integrated conclusion

This case study describes the NGRA of an ingredient present in a leave-on cosmetic product at significant concentrations (up to 1%). The SEURAT-1 workflow and the ICCR principles were applied to structure the case study and to carry out a risk assessment. One of these principles is that the assessment should be human relevant (Dent *et al.*, 2018). For this reason, the approach taken was not to use *in vitro* data to replace the *in vivo* animal data types used historically in the assessment of cosmetics. Instead, an exposure-led approach was taken to compare *in vitro* bioactivity assessed using many biomarkers across several human derived cell systems. Using this approach, it is possible to evaluate whether consumer exposures are below those required to elicit biological activity *in vitro*. This move away from identifying hazards or apical endpoints requires safety assessors to adopt a very different mindset. However, with sufficient biological coverage, basing a risk assessment on an *in vitro* PoD is in many cases at least as conservative as using an *in vivo* (animal) PoD (Paul Friedman *et al.*, 2020). Where such a conservative approach does not provide safety assurance, higher tier tools are necessary to differentiate between *in vitro* activity and adversity, in-line with the ICCR Principles of NGRA (Dent *et al.*, 2018)

The strength of this assessment is that it considers specific MoAs that have been demonstrated to represent some of the key safety liabilities of pharmaceuticals (SafetyScreen44™) and industrial chemicals and pesticides (ToxCast). Furthermore, since cosmetic ingredients are not usually associated with highly specific MoAs, it was considered appropriate to also assess the possibility that the ingredient may cause cellular stress (cell stress panel). The cell stress panel was considered critical information for phenoxyethanol, because an 'on target' effect of this preservative is inhibition of bacterial MDH which is critical for normal cellular respiration. Therefore, the lack of an effect on cellular respiration in a human liver cell line (HepG2) formed an important part of the assessment. Finally, in an attempt to provide a breadth of biological coverage, whole genome transcriptomics was performed in 3 cell types to identify a pathways-based

NOTEL, and *in vitro* exposure to both phenoxyethanol and PAA at the NOTEL was characterized. In addition to the breadth and depth of the bioactivity assessments, the exposure characterisation considered the applied dose of body lotion (90th percentile) and used a PBK model to predict the internal exposure to phenoxyethanol taking population variability into account using a robust and well documented workflow. The PBK predictions were verified using *in vivo* human data.

One limitation of this case study is that although the objective of this case study was to ensure breadth of biological coverage, it is not yet apparent whether the measures of bioactivity and cell lines used are protective of all relevant MoAs that could lead to adverse health effects in consumers. This is important because a pre-requisite of any new assessment methodology is that it should perform at least as well as the method it is intended to replace.

An assessment was therefore performed to see how conservative the NGRA presented here is compared with the traditional risk assessment, which used an adjusted PoD of 357 mg phenoxyethanol/kg bodyweight/day, derived from a dermal rabbit 90-day study as described in the SCCS Opinion on Phenoxyethanol. A comparison of the traditional and *in vitro* PoDs, exposure from body lotion and MoS or MoIE values is shown in Table 10.

Table 10 Comparison of the outcome of the 'traditional' risk assessment and the NGRA

	Exposure (following use of ingredient at 1% in body lotion)	PoD	MoS/MoIE
'Traditional' Risk Assessment	1.23 mg/kg/day	357 mg/kg/day	290
NGRA based on C_{max} and NOTEL	6.2 µM	171 µM	28
NGRA based on AUC_{24} and NOTEL	15 µmol*h/L	3215 µmol*h/L	214

The MoIEs derived from this case study are lower than the MoS derived using the animal data. This implies that the NGRA approach presented here is more conservative than the traditional risk assessment. This corroborates other analyses that have shown that NAM-derived PoDs are often more conservative than animal-derived PoDs (Paul Friedman *et al*., 2020). To evaluate whether this holds true for other substances it will be necessary to assess many more substance exposures using these tools, including substances with known and diverse safety liabilities (e.g. cardiotoxicants, developmental and reproductive toxicants, hepatotoxicants) in more cell lines using an extended *in vitro* test battery. The purpose of this evaluation would not necessarily be to ensure that these MoA can be predicted from the NAM data, but rather to ensure that the PoDs obtained for such substances are protective of human health. Until this evaluation is complete it is difficult to know how protective this overall assessment approach is when applied to other substances.

It should be noted that the traditional risk assessment did not explicitly deal with the major metabolite PAA. In the NGRA, PAA gave very small MoIE (2 and 3 for C_{max} and AUC_{24} respectively). This meant that in the absence of the *in vivo* data and history of safe use of phenoxyethanol, confidence in a safety decision based on the NAM data was low.

The current case study has followed the SEURAT-1 framework through from Tier 0 to Tier 2 to complete a risk assessment for the marketing of a body lotion containing 1% phenoxyethanol. This involved forming a hypothesis on the ingredient's MoA and review of and generation of data from NAMs. From start to finish the case study has applied the ICCR principles to underpin the risk assessment to assure that it is human relevant, exposure-led and hypothesis driven, while also well conducted and documented. The US EPA blueprint provided the case study with guidance on how characterise the MoA of our case study ingredient at relevant doses which falls under the category of a chemical with "no defined biological target or pathway".

5. Conclusion

This case study illustrates an *ab initio* risk assessment of a cosmetic ingredient based on the tools and approaches currently available, and provides a possible approach to evaluating major metabolite. Although the calculated MoIEs were above 1, which indicated that *in vitro* bioactivity was not seen at consumer-relevant concentrations, there were several uncertainties in the risk assessment which need to be addressed in future work. More case studies on both high and low risk substance exposures using these tools and approaches will further help to put the MoIE values obtained into context, and further embed the application of NGRA to cosmetics.

6. Acknowledgements

This case study was performed as part of the Cosmetics Europe Long Range Science Strategy (www.lrsscosmeticseurope.eu). The scientists that were involved in many different ways and at different times during the course of the case study in alphabetical order were: Samuel J. Bellfield[1], Harvey J. Clewell III[2], Stella Cochrane[3], Mark T.D. Cronin[1], Matthew P. Dent[3], Bertrand Desprez[5], Alina Efremenko[6], James Firman[1], Joan Fisher[6], C. Eric Hack[6], Nicola J. Hewitt[5], Jade Houghton[3], Richard Judson[7], Gerry Kenna[5], Martina Klaric[5], Predrag Kukic[3], Catherine Mahony[9], Sophie Malcomber[3], Malgorzata Nepelska[3], Yuuko Nukada[4], Beate Nicol[3], Przemyslaw Piechota[3], Katarzyna Przybylak[3], Alexandra Rolaki[5], Andreas Schepky[10], Takahiro Suzuki[4], John A. Troutman[8], Sarah A. Tozer[9], Mustafa Varçin[5], Evita Vandenbossche[3], Andrew White[3]

Affiliation at time of contribution:

[1] Liverpool John Moores University, UK

[2] Ramboll, USA

[3] Unilever, UK

[4] Kao Corporation, Japan

[5] Cosmetics Europe, Belgium

[6] ScitoVation, USA

[7] U.S. Environmental Protection Agency

[8]The Procter & Gamble Company, USA

[9] Procter & Gamble Technical Centres Ltd, UK

[10] Beiersdorf AG, Germany

7. References

Adler, S. *et al*. (2011) 'Alternative (non-animal) methods for cosmetics testing: current status and future prospects—2010', Archives of Toxicology, 85(5), pp. 367–485. doi: 10.1007/s00204-011-0693-2.

Allen, T. E. H. *et al*. (2018) 'Using 2D Structural Alerts to Define Chemical Categories for Molecular Initiating Events', Toxicological Sciences, 165(1), pp. 213–223. doi: 10.1093/toxsci/kfy144.

Armitage, J. M., Wania, F. and Arnot, J. A. (2014) 'Application of mass balance models and the chemical activity concept to facilitate the use of in vitro toxicity data for risk assessment', Environmental Science and Technology. American Chemical Society, 48(16), pp. 9770–9779. doi: 10.1021/es501955g.

Baker, N. *et al.* (2017) 'ToxCast Chemical and Bioactivity Profiles for in vitro Targets in the Retinoid Signaling System. Poster presented at the annual Society of Toxicology Meeting'. doi: 10.23645/EPACOMPTOX.5173810.V1.

Bartels, M., Rick, D., Lowe, E., Loizou, G., Price, P., Spendiff, M., Arnold, S., Cocker, J., Ball, N., 2012. Development of PK- and PBPK-based modeling tools for derivation of biomonitoring guidance values. Comput. Methods Programs Biomed. 108(2):773-788. DOI: 10.1016/j.cmpb.2012.04.014

Barter, ZE., Bayliss, MK., Beaune, PH., Boobis, AR., Carlile, DJ., Edwards, RJ., Houston, JB., Lake, BG., Lipscomb, JC., Pelkonen, OR., Tucker, GT., Rostami-Hodjegan, A. 2007. Scaling factors for the extrapolation of in vivo metabolic drug clearance from in vitro data: reaching a consensus on values of human microsomal protein and hepatocellularity per gram of liver. Curr Drug Metab. 8(1):33-45. DOI: 10.2174/138920007779315053. PMID: 17266522.

Beck, JV., and Arnold, KJ. (1977). Parameter estimation in engineering and science. pp. 17–23. Wiley and Sons, New York.

Berggren, E. *et al*. (2017) 'Ab initio chemical safety assessment: A workflow based on exposure considerations and non-animal methods', Computational Toxicology. Elsevier, 4, pp. 31–44. doi: 10.1016/J.COMTOX.2017.10.001.

Bessems, J. G. M. *et al*. (2017) 'The margin of internal exposure (MOIE) concept for dermal risk assessment based on oral toxicity data - A case study with caffeine.', Toxicology, 392, pp. 119–129. doi: 10.1016/j.tox.2017.03.012.

Bleile, D. M. *et al.* (1975) 'Identification of essential arginyl residues in cytoplasmic malate dehydrogenase with butanedione.', The Journal of biological chemistry, 250(16), pp. 6222–7.

Borras, E. *et al*. (2000) 'Genetic Polymorphism of Alcohol Dehydrogenase in Europeans: The ADH2*2 Allele Decreases the Risk for Alcoholism and Is Associated With ADH3*1'. doi: 10.1053/he.2000.5978.

Bosron, W. F. and Li, T. ‐ K (1986) ′Genetic polymorphism of human liver alcohol and aldehyde dehydrogenases, and their relationship to alcohol metabolism and alcoholism ′, Hepatology, 6(3), pp. 502−510. doi: 10.1002/hep.1840060330.

Bowes, J. *et al*. (2012) 'Reducing safety-related drug attrition: the use of in vitro pharmacological profiling', Nature Reviews Drug Discovery. Nature Publishing Group, 11(12), pp. 909–922. doi: 10.1038/nrd3845.

Brown, RP., Delp, MD., Lindstedt, SL., Rhomberg, LR., Beliles, RP., 1997. Physiological parameter values for physiologically based pharmacokinetic models. Toxicol. Ind. Health 13 (4):407–484. DOI: 10.1177/074823379701300401

Campbell, JL., Yoon, M., Clewell, HJ. 2015. A case study on quantitative in vitro to in vivo extrapolation for environmental esters: Methyl-, propyl- and butylparaben. Toxicology. 332:67-76. DOI: 10.1016/j.tox.2015.03.010

Clewell HJ 3rd and Andersen ME. 1985 Risk assessment extrapolations and physiological modeling. Toxicol Ind Health. 1(4):111-31. DOI: 10.1177/074823378500100408

Clewell, HJ., Gearhart, JM., Gentry, PR., Covington, TR., VanLandingham, CB., Crump, KS., Shipp, AM. 1999 Evaluation of the uncertainty in an oral reference dose for methylmercury due to interindividual variability in pharmacokinetics. Risk Anal. 19(4):547-58. DOI: 10.1023/a:1007017116171

Clewell, HJ 3rd., Andersen, ME., and Barton, HA. 2002. A consistent approach for the application of pharmacokinetic modeling in cancer and noncancer risk assessment. Environ Health Perspect. 110(1):85-93. DOI: 10.1289/ehp.0211085

Clewell, HJ 3rd. 2005. Use of mode of action in risk assessment: past, present, and future. Reg Tox Pharm. 42(1):3-14. DOI: 10.1016/j.yrtph.2005.01.008

Clewell, HJ 3rd., Andersen, ME., Blaauboer, BJ. 2008 On the incorporation of chemical-specific information in risk assessment. Toxicol Lett. 180(2):100-109. DOI: 10.1016/j.toxlet.2008.06.002

Clewell RA and Clewell HJ 3rd. 2008 Development and specification of physiologically based pharmacokinetic models for use in risk assessment. Regul Toxicol Pharmacol. 50(1):129-43. DOI: 10.1016/j.yrtph.2007.10.012

Clewell, HJ., Efremenko, A., Campbell, JL., Dodd, DE., Thomas, RS. 2014. Transcriptional responses in the rat nasal epithelium following subchronic inhalation of naphthalene vapor. Toxicol Appl Pharmacol. 280(1):78-85. DOI: 10.1016/j.taap.2014.06.015

Coleman, K. E. *et al*. (2017) 'SENP8 limits aberrant neddylation of nedd8 pathway components to promote cullin-RING ubiquitin ligase function', eLife. eLife Sciences Publications Ltd, 6. doi: 10.7554/eLife.24325.

Dent, M. P. *et al*. (2018) 'Principles underpinning the use of new methodologies in the risk assessment of cosmetic ingredients', Computational Toxicology, 7, pp. 20–26. doi: 10.1016/J.COMTOX.2018.06.001.

Desprez, B. *et al*. (2018) 'A strategy for systemic toxicity assessment based on non-animal approaches: The Cosmetics Europe Long Range Science Strategy programme', Toxicology in Vitro, 50, pp. 137–146. doi: 10.1016/j.tiv.2018.02.017.

Fabregat, A. *et al*. (2018) 'The Reactome Pathway Knowledgebase', Nucleic Acids Research. Oxford University Press, 46(D1), pp. D649–D655. doi: 10.1093/nar/gkx1132.

Farmahin, R. *et al*. (2017) 'Recommended approaches in the application of toxicogenomics to derive points of departure for chemical risk assessment', Archives of Toxicology. Springer Verlag, 91(5), pp. 2045–2065. doi: 10.1007/s00204-016-1886-5.

Fischer, F. C. *et al*. (2017) 'Modeling Exposure in the Tox21 in Vitro Bioassays', Chemical Research in Toxicology, 30(5), pp. 1197–1208. doi: 10.1021/acs.chemrestox.7b00023.

Gagnon, J. K., Law, S. M. and Brooks, C. L. (2016) 'Flexible CDOCKER: Development and application of a pseudo-explicit structure-based docking method within CHARMM', Journal of Computational Chemistry. John Wiley and Sons Inc., 37(8), pp. 753–762. doi: 10.1002/jcc.24259.

Geltmeier, A. *et al.* (2015) 'Characterization of Dynamic Behaviour of MCF7 and MCF10A Cells in Ultrasonic Field Using Modal and Harmonic Analyses', PLOS ONE. Edited by Y.-J. Chang. Public Library of Science, 10(8), p. e0134999. doi: 10.1371/journal.pone.0134999.

Gerlowski LE and Jain RK. 1983. Physiologically based pharmacokinetic modeling: principles and applications. J Pharm Sci. 72(10):1103-27. DOI: 10.1002/jps.2600721003

Gilbert, P., Beveridge, E. G. and Crone, P. B. (1977a) 'Effect of phenoxyethanol on the permeability of Escherichia coli NCTC 5933 to inorganic ions.', Microbios, 19(75), pp. 17–26.

Gilbert, P., Beveridge, E. G. and Crone, P. B. (1977b) 'The lethal action of 2-phenoxyethanol and its analogues upon Escherichia coli NCTC 5933.', Microbios, 19(76), pp. 125–41.

Gilbert, P., Beveridge, E. G. and Crone, P. B. (1980) 'Effect of 2-phenoxyethanol upon RNA, DNA and protein biosynthesis in Escherichia coli NCTC 5933.', Microbios, 28(111), pp. 7–17.

Goward, C. R., and Nicholls, D. J. (1994) 'Malate dehydrogenase: A model for structure, evolution, and catalysis', Protein Science, 3, pp. 1883-1888.

Grillo, M. P. and Benet, L. Z. (2002) 'Studies on the reactivity of clofibryl-S-acyl-CoA thioester with glutathione in vitro', Drug Metabolism and Disposition, 30(1), pp. 55–62. doi: 10.1124/dmd.30.1.55.

Grisoni, F., Consonni, V. and Ballabio, D. (2019) 'Machine Learning Consensus To Predict the Binding to the Androgen Receptor within the CoMPARA Project', Journal of Chemical Information and Modeling. American Chemical Society, 59(5), pp. 1839–1848. doi: 10.1021/acs.jcim.8b00794.

Haber, L. T. *et al*. (2018) 'Benchmark dose (BMD) modeling: current practice, issues, and challenges', Critical Reviews in Toxicology. Taylor and Francis Ltd, 48(5), pp. 387–415. doi: 10.1080/10408444.2018.1430121.

Hatherell, S. *et al*. (2020) 'Identifying and Characterizing Stress Pathways of Concern for Consumer Safety in Next-Generation Risk Assessment', Toxicological Sciences, 176(1), pp. 11–33. doi: 10.1093/toxsci/kfaa054.

Houck, K. A. *et al*. (2009) 'Profiling Bioactivity of the ToxCast Chemical Library Using BioMAP Primary Human Cell Systems', Journal of Biomolecular Screening. SAGE PublicationsSage CA: Los Angeles, CA, 14(9), pp. 1054–1066. doi: 10.1177/1087057109345525.

Howes, D. (1991) 'Absorption and metabolism of 2-pheoxyethanol in rat and man', 15th IFSCC International Congress on Cosmetic Science, 3, pp. 415–434.

International Commission on Radiological Protection (ICRP). 1975. Report of the Task Group on Reference Man. ICRP Publication 23. Pergamon Press, Oxford, UK.

Ito, Y., Kamijima, M., Hasegawa, C., Tagawa, M., Kawai, T., Miyake, M., Hayashi, Y., Naito, H., Nakajima,T. 2014. Species and inter-individual differences in metabolic capacity of di(2-ethylhexyl)phthalate (DEHP) between human and mouse livers. Environ Health Prev Med, 19(2):117-125. DOI:10.1007/s12199-013-0362-6

Kleinstreuer, N. C. *et al*. (2017) 'Development and Validation of a Computational Model for Androgen Receptor Activity', Chemical Research in Toxicology, 30(4), pp. 946–964. doi: 10.1021/acs.chemrestox.6b00347.

Kramer, N. I. *et al*. (2012) 'Quantifying Processes Determining the Free Concentration of Phenanthrene in Basal Cytotoxicity Assays', Chemical Research in Toxicology. American Chemical Society, 25(2), pp. 436–445. doi: 10.1021/tx200479k.

Langsrud, S. *et al*. (2016) 'Ethylhexylglycerin Impairs Membrane Integrity and Enhances the Lethal Effect of Phenoxyethanol.', PloS one. Public Library of Science, 11(10), p. e0165228. doi: 10.1371/journal.pone.0165228.

Leonard, C. *et al*. (1997) '"Golf ball liver": agent orange hepatitis.', Gut, 40(5), pp. 687–8. doi: 10.1136/gut.40.5.687.

Lewis, R. W. *et al*. (2002) 'Recognition of Adverse and Nonadverse Effects in Toxicity Studies', Toxicologic Pathology. Sage PublicationsSage CA: Los Angeles, CA, 30(1), pp. 66–74. doi: 10.1080/01926230252824725.

Lilienblum, W. (2016) 'Opinion of the Scientific Committee on Consumer Safety (SCCS) – Final version of the opinion on Phenoxyethanol in cosmetic products', Regulatory Toxicology and Pharmacology. Academic Press Inc., p. 156. doi: 10.1016/j.yrtph.2016.11.007.

Lindstedt SL and Schaeffer PJ. 2002. Use of allometry in predicting anatomical and physiological parameters of mammals. Laboratory Animals, 36(1):1-19. DOI: 10.1258/0023677021911731

Livingston EH and Lee S. 2001. Body surface area prediction in normal-weight and obese patients. Am J Physiol Endocrinol Metab 281(3):E586-E591. DOI: 10.1152/ajpendo.2001.281.3.E586

Lobenhofer, E. *et al*. (2004) 'Exploration of low-dose estrogen effects: Identification of No Observed Transcriptional Effect Level (NOTEL)', Toxicologic Pathology, 32(4), pp. 482–492. doi: 10.1080/01926230490483324.

Lockley, D. J., Howes, D. and Williams, F. M. (2005) 'Cutaneous metabolism of glycol ethers', Archives of Toxicology, 79(3), pp. 160–168. doi: 10.1007/s00204-004-0619-3.

Mansouri, K. *et al*. (2016) 'CERAPP: Collaborative Estrogen Receptor Activity Prediction Project.', Environmental health perspectives, 124(7), pp. 1023–33. doi: 10.1289/ehp.1510267.

Paul Friedman, K. *et al*. (2020) 'Utility of In Vitro Bioactivity as a Lower Bound Estimate of In Vivo Adverse Effect Levels and in Risk-Based Prioritization', Toxicological

Sciences. Oxford University Press (OUP), 173(1), pp. 202–225. doi: 10.1093/toxsci/kfz201.

Peyret, T., Poulin, P., Krishnan, K. 2010. A unified algorithm for predicting partition coefficients for PBPK modeling of drugs and environmental chemicals. Tox Appl Pharmacol. 249:197-207. DOI: 10.1016/j.taap.2010.09.010

Phillips, J. R. *et al*. (2019) 'BMDExpress 2: enhanced transcriptomic dose-response analysis workflow', Bioinformatics. Edited by A. Valencia, 35(10), pp. 1780–1782. doi: 10.1093/bioinformatics/bty878.

Pierce, E. H. and Chesler, D. L. (1978) 'Possible Association of Granulomatous Hepatitis with Clofibrate Therapy', New England Journal of Medicine, 299(6), p. 314. doi: 10.1056/NEJM197808102990622.

Poupon, R. E. *et al*. (1992) 'Polymorphism of alcohol dehydrogenase, alcohol and aldehyde dehydrogenase activities: Implication in alcoholic cirrhosis in white patients', Hepatology, 15(6), pp. 1017–1022. doi: 10.1002/hep.1840150608.

Roper, C. S. *et al*. (1997) 'Percutaneous penetration of 2-phenoxyethanol through rat and human skin', Food and Chemical Toxicology. Pergamon, 35(10–11), pp. 1009–1016. doi: 10.1016/S0278-6915(97)00109-9.

Sack, G. H. (2018) 'Serum amyloid A - A review', Molecular Medicine. BioMed Central Ltd., 24(1), pp. 1–27. doi: 10.1186/s10020-018-0047-0.

Sallustio, B. C. *et al*. (1991) 'In vivo covalent binding of clofibric acid to human plasma proteins and rat liver proteins', Biochemical Pharmacology, 42(7), pp. 1421–1425. doi: 10.1016/0006-2952(91)90454-D.

SCCS (2018) 'Scientific Committee on Consumer Safety (SCCS) Notes of Guidance for the Testing of Cosmetic Ingredients and their Safety Evaluation 10th revision, 24-25 October 2018, SCCS/1602/18'.

Shore, L. J. *et al*. (1995) 'Characterization and formation of the glutathione conjugate of clofibric acid.', Drug Metabolism and Disposition, 23(1).

Simmons, S. O., Fan, C. Y. and Ramabhadran, R. (2009) 'Cellular stress response pathway system as a sentinel ensemble in toxicological screening', Toxicological Sciences, pp. 202–225. doi: 10.1093/toxsci/kfp140.

Tateishi, K. *et al*. (2001) 'The NEDD8 system is essential for cell cycle progression and morphogenetic pathway in mice', Journal of Cell Biology, 155(4), pp. 571–579. doi: 10.1083/jcb.200104035.

Thomas, R. S. *et al*. (2013) 'Temporal Concordance Between Apical and Transcriptional Points of Departure for Chemical Risk Assessment', Toxicol. Sci., 134(1), pp. 180–194. doi: https://doi.org/10.1093/toxsci/kft094.

Thomas, R. S. *et al*. (2019) 'The Next Generation Blueprint of Computational Toxicology at the U.S. Environmental Protection Agency', Toxicological Sciences, 169(2), pp. 317–332. doi: 10.1093/toxsci/kfz058.

Troutman, JA., Rick, DL., Stuard, SB., Fisher, J., Bartels, MJ. 2015 Development of a physiologically-based pharmacokinetic model of 2-phenoxyethanol and its metabolite phenoxyacetic acid in rats and humans to address toxicokinetic uncertainty in risk assessment. Regul Toxico Pharmacol. 73(2):530–543. DOI: 10.1016/j.yrtph.2015.07.012.

US EPA (2006) Approaches For the Application of Physiologically Based Pharmacokinetic (PBPK) Models and Supporting Data In Risk Assessment (Final Report). U.S. Environmental Protection Agency, Washington, D.C., EPA/600/R-05/043F

US EPA (2014) 'Next Generation Risk Assessment: Incorporation Of Recent Advances In Molecular, Computational, And Systems Biology (Final Report), EPA/600/R-14/004.' Washington DC: US Environmental Protection Agency.

USFDA (2018) Physiologically Based Pharmacokinetic Analyses—Format and Content. Guidance for Industry. Center for Drug Evaluation and Research, Washington, DC.

Wetmore, B. A. *et al*. (2012) 'Integration of dosimetry, exposure, and high-throughput screening data in chemical toxicity assessment', Toxicological Sciences, 125(1), pp. 157–174. doi: 10.1093/toxsci/kfr254.

WHO (2010) Harmonization Project Document No. 9: Characterization and application of physiologically based pharmacokinetic models in risk assessment. Geneva: World Health Organization.

Wiśniewski, J. R. *et al*. (2016) 'In-depth quantitative analysis and comparison of the human hepatocyte and hepatoma cell line HepG2 proteomes', Journal of Proteomics. Elsevier B.V., 136, pp. 234–247. doi: 10.1016/j.jprot.2016.01.016.

Yang, C. *et al.* (2017) 'Thresholds of Toxicological Concern for cosmetics-related substances: New database, thresholds, and enrichment of chemical space', Food and Chemical Toxicology, 109, pp. 170–193. doi: 10.1016/J.FCT.2017.08.043.

Yang, L., Allen, B. C. and Thomas, R. S. (2007) 'BMDExpress: A software tool for the benchmark dose analyses of genomic data', BMC Genomics. BioMed Central, 8, p. 387. doi: 10.1186/1471-2164-8-387.

Yeakley, J. M. *et al*. (2017) 'A trichostatin A expression signature identified by TempO-Seq targeted whole transcriptome profiling', PLOS ONE. Edited by Y. Xu. Public Library of Science, 12(5), p. e0178302. doi: 10.1371/journal.pone.0178302.

Yoon, M., Campbell, JL., Andersen, ME., Clewell, HJ. 2012. Quantitative in vitro to in vivo extrapolation of cell-based toxicity assay results. Crit Rev Toxicol. 42(8):633-652. DOI: 10.3109/10408444.2012.692115

OECD References

EU-ToxRisk (2018), Recommendations of the EU-ToxRisk Regulatory Advisory Board (RAB) on how to document case studies for regulatory evaluation

OECD (2014a), Guidance on Grouping of Chemicals, Second Edition, Series on Testing & Assessment No. 194, ENV/JM/MONO(2014)4, OECD, Paris.

OECD (2014b), Guidance Document for Describing Non-Guideline In Vitro Test Methods, Series on Testing and Assessment No. 211, ENV/JM/MONO(2014)35, OECD, Paris.

OECD (2016a), Guidance Document on the Reporting of Defined Approaches to Be Used within Integrated Approaches to Testing and Assessment No. 255, ENV/JM/MONO(2016)28, OECD, Paris.

OECD (2016b), Guidance Document on the Reporting of Defined Approaches and Individual Information Sources to Be Used within Integrated Approaches to Testing and Assessment (IATA) for Skin Sensitisation, Series on Testing and Assessment No. 256, ENV/JM/MONO(2016)29, OECD, Paris.

OECD (2016c), "Users' Handbook supplement to the Guidance Document for developing and accessing Adverse Outcome Pathways", OECD Series on Adverse Outcome Pathways, No. 1, OECD Publishing, Paris.

OECD (2017), Chemical Safety Assessment Workflow Based on Exposure Considerations and Non-animal Methods, Series on Testing and Assessment No. 275, ENV/JM/MONO(2017)27, OECD, Paris.

OECD (2018a), Prioritization of chemicals using the Integrated Approaches for Testing and Assessment (IATA)-based Ecological Risk Classification, Series on Testing and Assessment No. 291, ENV/JM/MONO(2018)27, OECD, Paris.

OECD (2018b), Case Study on the use of Integrated Approaches for Testing and Assessment (IATA) for Estrogenicity of the Substituted Phenols, Series on Testing and Assessment No. 290, ENV/JM/MONO(2018)26, OECD, Paris.

OECD (2019a), Case Study on the Use of an Integrated Approach to Testing and Assessment for Identifying Estrogen Receptor Active Chemicals, Series on Testing and Assessment No. 307, ENV/JM/MONO(2019)28, OECD, Paris.

Annex I: PBK report

Physiologically-based kinetic model to support the Next Generation Risk Assessment for a cosmetic ingredient – a case study on phenoxyethanol

1. Executive Summary

In this case study, a Margin of Internal Exposure (MoIE) has been estimated for phenoxyethanol using a physiologically-based kinetic (PBK) model to estimate blood concentrations following exposures to phenoxyethanol in humans that could be compared with concentrations that do not elicit cellular responses *in vitro*. A MoIE differs from a traditional margin of exposure (MoE) in that it is calculated as the ratio of a measure of internal exposure, such as blood concentration or target-tissue dose, rather than comparing external exposure concentration or ingested doses (Bessems *et al*. 2017). The use of a PBK model reduces the uncertainty in the risk assessment by incorporating chemical-specific information on the uptake, distribution, metabolism and excretion of the chemical (Clewell *et al*. 2008).

Tier 2 characterisation of biokinetics provided *in vitro* hepatic clearance estimates and showed that phenoxyacetic acid (PAA) is the major metabolite of phenoxyethanol (PhE). A PBK model of the parent chemical PhE and the PAA metabolite was developed in Berkeley Madonna modelling software to incorporate these data. PhE kinetics are described in arterial and venous blood, the gut, liver, fat, skin, and lumped rapidly and slowly perfused tissues to represent the rest of the body. Metabolism to PAA is simulated in the liver, producing PAA. The PAA metabolite model includes compartments for the liver, kidney, and the rest of the body. Elimination of PAA is simulated as a function of the glomerular filtration rate and concentration of unbound PAA in the plasma. Comparisons of model output to urinary excretion of PAA in humans were performed for model verification. Parameter sensitivity analysis was performed, and variability analysis was conducted with the model to estimate area under the concentration curve (AUC) and the peak plasma concentration (C_{max}) for PhE and PAA in the blood and the kidney for comparison with *in vitro* toxicity values.

The model adequately recapitulated the available human PAA excretion data. Comparison of upper percentile internal dose metric estimates were used to calculate MoIEs. The level of confidence that the application of the PBK modelling is protective was considered to be high, based on agreement with available human kinetic data and the use of upper percentile estimates of the internal dose metrics from the variability analysis.

2. Background Information

PBK models are mathematical models used to quantify the absorption, distribution, metabolism and excretion of a chemical inside the body following exposure. They are constructed as an interconnected system of compartments representing various tissues described by mass balance differential equations that are solved to predict the amount of chemical in each compartment over time (Gerlowski and Jain 1983). The physiological basis of this modelling approach allows internal concentrations resulting from external exposures to be predicted, allowing comparisons including across species and exposure

routes. A number of recent reviews of PBK modelling in environmental risk assessment are available (Clewell and Clewell 2008, Campbell *et al*. 2012, Clewell *et al*. 2014).

PBK models typically rely on three types of parameters; physiological (e.g., tissue volumes, blood flows), physicochemical (e.g., octanol:water partitioning, vapor pressure, water solubility), and biochemical (e.g., absorption rates, metabolism, clearances). The particular parameters needed depend on factors such as the chemical properties and the purpose of the model. Various guidance documents for the application, use, and reporting of PBK models have been published (WHO, 2010; USEPA, 2006; USFDA, 2018).

The physiological structure of PBK models provides a particularly useful framework for conducting cross species extrapolations (Clewell and Andersen 1985). The necessary physiological parameters (tissue weights, blood flows, ventilation rate) for a number of mammals (mouse, rat, dog and human) are available in the literature (Brown *et al*. 1997), and parameters for other species can be estimated allometrically (Lindstedt and Schaeffer 2002). Tissue:blood partition coefficients for a chemical can be estimated using quantitative structure-property relationships (Peyret *et al*. 2010), while the clearance of the chemical in different species can be determined by *in vitro* studies with hepatocytes or cellular fractions and incorporated into the PBK model using *in vitro* to *in vivo* extrapolation (Yoon *et al*. 2012).

The application of PBK models to support interspecies extrapolation depends on the concept of target tissue exposure equivalence; that is, in the absence of pharmacodynamic (susceptibility) differences, the toxicity of a chemical in different species is expected to be associated with similar concentrations of the chemical (or its toxic metabolite) in the tissue where the toxicity is observed (Clewell *et al.* 2002). In cases of general systemic toxicity, or where the target tissue has not been identified, the concentration in the blood can be used to represent the target tissue exposure. While acute effects may depend on the maximum concentration achieved in the tissue, longer-term toxicity is generally associated with the concentration over time, which can be calculated as the area under the curve (AUC). The toxic mode of action determines whether the concentration of interest is that of the parent chemical, a stable metabolite, or a reactive metabolite (Clewell 2005).

Phenoxyethanol is a colourless, oily liquid that is used as an antimicrobial and preservative agent in cosmetics. It is a low molecular weight, neutral organic chemical with a low octanol-water partition, high aqueous solubility, and low volatility. This case study's overarching hypothesis is that "Systemic exposure to phenoxyethanol present at 1% in body lotion will not cause any adverse health effects in consumers". The consumers are defined as any individual who is likely to use a marketed body lotion, including liberal (95th percentile) users. For the applied dose, exposure assessment worst-case (conservative) assumptions were made regarding product use. Consumer use and physiological data for females were used to ensure the safety assessment was conservative. Consumer use data for body lotion and mean consumer bodyweight were taken from the Scientific Committee on Consumer Safety (SCCS) Notes of Guidance for the Testing of Cosmetic Ingredients and their Safety Evaluation, 10th Revision (SCCS, 2018). This exposure scenario assumes all the applied body lotion is left in contact with skin until the next application. In the absence of any skin penetration data identified the dermal absorption was assumed to be 100%.

In vitro experiments were performed to provide quantitative data on the clearance of phenoxyethanol. Experiments with primary human hepatocytes (PHH) were designed to elucidate metabolic stability and metabolism of phenoxyethanol to support the refinement of the PBK model. A half-life consistent between the 2 lowest doses (10 and 30 µM) gave

reassurance that concentrations were low enough that individual pathways were not saturated. The hepatic clearance value of 20 µL/min/million cells from the literature (Wetmore *et al*., 2012) using cryopreserved PHH was similar to the result of these incubations (22.3 – 25.3 µL/min/million cells). The *in vitro* metabolite identification confirmed that phenoxyacetic acid was the major metabolite, and rapidly formed as phenoxyethanol depleted.

A PBK model for PhE and PAA was previously developed and published by Troutman *et al*. (2015). The Troutman model contained compartments for skin, fat, lung, stomach, liver, and lumped rapidly and slowly perfused tissues. The PAA model contained the same compartments minus the stomach, and with an additional kidney compartment for urinary excretion. Dermal penetration through the skin and oral absorption from the stomach are described for PhE. Elimination of PhE is described via metabolism to PAA in the liver, generating PAA, and PAA is metabolized in the liver and excreted in urine. The model was parameterized for rats and humans, and parameter values were calibration through optimization using experimental data across several rat studies and a single human study.

A single human study of the kinetics of PhE was found (Howes, 1991). The study reports urinary excretion profiles of PAA following oral and dermal application of skin cream containing 1.2% PhE. PhE was detected unchanged in the urine. The specifics of the exposures simulated are shown in Table 11.

Table 11 Exposure scenarios (oral and dermal) used to evaluate model predictions.

Type of Dosing	Oral	Dermal	Dermal
Number of Doses	1	1	2
Dose (mg/kg)	0.152	3.44	6.89
Volume of Applied Dose (mL)	N/A	20	40
Surface Area Exposed (%)	N/A	80	90

3. Model Purpose

In this case study, a Margin of Internal Exposure (MoIE) has been estimated for phenoxyethanol using a PBK model to estimate blood concentrations following exposures to phenoxyethanol in humans that could be compared with concentrations that do not elicit cellular responses *in vitro*. A MoIE differs from a traditional margin of exposure (MoE) in that it is calculated as the ratio of a measure of internal exposure, such as blood concentration or target-tissue dose, rather than comparing external exposure concentration or ingested doses (Bessems *et al*. 2017). The use of a PBK model reduces the uncertainty in the risk assessment by incorporating chemical-specific information on the uptake, distribution, metabolism, and excretion of the chemical (Clewell *et al*. 2008). This strategy is aligned with the US EPA's next generation blueprint for toxicology, which seeks to characterize whether a chemical acts via defined biological pathways/targets or if it may induce cellular changes by a non-specific mechanism (Thomas *et al*., 2019).

4. Methods and Materials

The model structure was developed and parameterized without the use of animal data (Figure 13). As such, it is a simplified version of the Troutman model. Namely, there is no

lung compartment for PhE, and the PAA model includes only liver, kidney, and a rest of body compartment (Figure 13). *In vitro* data were used where available (i.e., hepatic clearance and skin permeation), rather than calibration based on animal data, and *in silico* prediction of other parameters (i.e., partition coefficients) was employed to assign parameter values. Intrinsic clearance data from these studies were scaled using *in vitro* to *in vivo* scaling (Yoon *et al*. 2012) to estimate the hepatic clearance used in the PBPK model.

Model predictions were verified through comparison with the available human data. Howes *et al*. (1991) reported time course urinary excretion of PAA following oral and dermal exposures. Predictions were visually compared with these data to evaluate the adequacy of the model.

There were several major assumptions made in the development of the model. All compartments in the model are flow limited. Metabolic conversion of PhE to PAA is considered to be a linear process occurring in the liver. Dermal metabolism was considered negligible due to rapid permeation through the skin and the relatively small conversion rate determined *in vitro* compared to hepatic clearance. A typical equation for tissue mass balance under these assumptions is:

$$\frac{dA}{dt} = Q \times (Ca - C/P) \; - \; Cl \times Fu \times \frac{C}{P}$$

where *A* is the amount in a tissue, *Q* is the blood flow to the tissue, *Ca* is the arterial plasma concentration, *C* is the tissue concentration, *P* is the tissue:plasma partition coefficient, *Cl* is the clearance rate, and *Fu* is the fraction unbound in plasma.

Urinary excretion of PAA is assumed to be due to glomerular filtration and the fraction of compound that is unbound in the plasma:

$$\frac{dU}{dt} = C_{PAA} \times Fu_{PAA} \times Cl_U$$

where *U* is the amount of PAA in urine, C_{PAA} is the concentration of PAA in plasma, Fu_{PAA} is the fraction of PAA unbound in plasma, and Cl_U is the clearance rate to urine.

Oral absorption is modelled as a first-order absorption process, moving ingested PhE from the gut and into the liver via the portal vein:

$$\frac{dAbs}{dt} = Ka \times A_G$$

where *Abs* is the amount absorbed from the gut, *Ka* is the first-order oral absorption rate constant, and A_G is the amount in the gut.

Dermal absorption is modelled following the approach used by Troutman *et al*. (2015). A skin surface compartment is incorporated to house the applied dose in terms of the volume and surface area, and a single skin compartment. Transfer to the systemic circulation occurs

in the skin compartment. Dermal absorption is driven by a permeability coefficient for uptake from the surface into the skin (units of cm/hr), the exposure area and volume of application, the amount of phenoxyethanol applied, duration of application, and the fraction absorbed. The flux through the skin is driven by a permeability coefficient, which is multiplied by chemical concentration on the surface of the skin:

$$\frac{dAbs_{skin}}{dt} = Kp \times \frac{SA_{dose}}{V_{dose}} \times \mathrm{A_{surface}}$$

$$\frac{dA_{skin}}{dt} = Q_{skin} \times (Ca - C_{skin}/P_{skin}) + \frac{dAbs_{skin}}{dt}$$

where Abs_{skin} is the amount absorbed into the exposed skin from the surface, Kp is the permeability coefficient, SA_{dose} is the surface area dosed, V_{dose} is the volume dosed, $A_{surface}$ is the amount on the skin surface, A_{skin} is the amount in the exposed skin, Q_{skin} is the blood flow to the exposed skin, Ca is the arterial plasma concentration, C_{skin} is the concentration in the exposed skin, and P_{skin} is the skin:plasma partition coefficient. The permeability coefficient was determined from *in vitro* experiments and adjusted based on the Howes *et al*. (1991) data by Troutman *et al*. (2015).

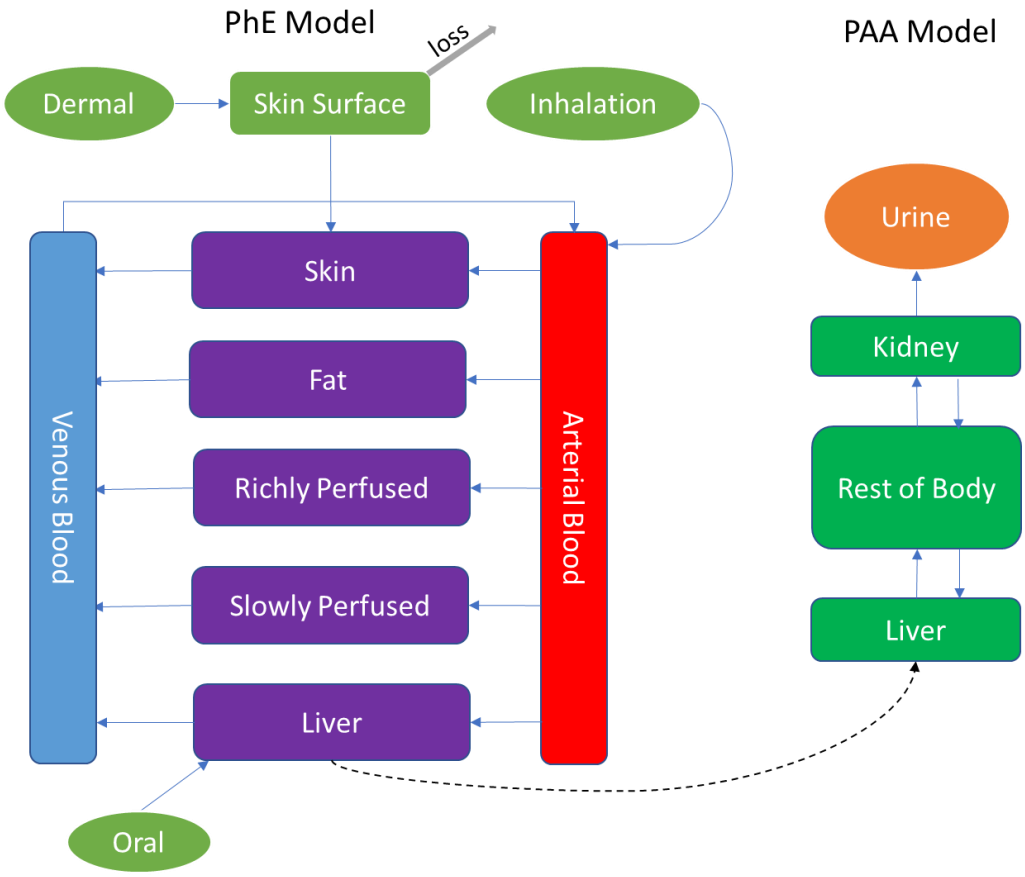

Figure 13 PBK model schematic for PhE and PAA. The PhE model has 5, perfusion-limited tissue compartments including skin, fat, liver, and lumped richly and slowly perfused tissues. PhE exposure is modelled via oral, dermal, and inhalation routes. Loss from the skin surface due to evaporation or transfer to clothing is included, competing with the dermal absorption rate. The PAA metabolite is generated in the liver, and modelled as a 3-compartment model including kidney, liver, and a rest of body compartment with elimination via urinary excretion.

The physiological parameters (tissue volumes and blood flows, ventilation rate, protein contents) and sources are shown in Table 12, and chemical-specific parameter values are shown in Table 13. The majority of the tissue volumes and blood flows are set to values published by Troutman *et al*. (2015). The value of slowly perfused tissues was a combination of slowly perfused and muscle flows. Volume of distribution for the metabolite PAA was set to total body water following Campbell *et al.* (2015). The model published by Livingston and Lee (2001) was used to calculate body surface area based on body weight. Tissue:blood partition coefficients (PC) were predicted by Troutman *et al.* (2015) using the ADME Workbench (v1.2.6.1). Richly perfused tissues were set to equal liver:blood partition (PRPT = PLIV) while slowly perfused were set to skin:blood partition (PSPT = PSk).

Table 12 Human PBK physiological parameter values for phenoxyethanol. Source for values is Troutman *et al*. (2015) unless otherwise specified. Tissue volumes reported are from the reference man (ICRP, 1975), and tissue blood flows from Bartels *et al*. (2012).

Parameter	Units	Symbol	Value
Body mass	kg	BW	60
Blood Flows (Fraction of Cardiac Output) [a]			
Alveolar Ventilation	$L/h/kg^{0.75}$	QCC	15
Cardiac Output	$L/h/kg^{0.75}$	QPC	15
Liver	1	QLIVC	0.2589
Fat	1	QFATC	0.0464
Skin	1	QSkC	0.0536
Slowly Perfused	1	QSPTC	0.1639
Volumes (fraction of BW) [b]			
Liver	1	VLIVC	0.0257
Fat	1	VFATC	0.2142
Skin	1	VSkC	0.0371
Richly Perfused	1	VRPTC	0.0633
Blood	1	VBLDC	0.079
Hepatocellularity [c]	millions of hepatocytes per gram liver	hpgl	99

a Richly perfused blood flow = 100% QC minus liver, fat, skin, and slowly perfused; Slowly perfused blood flow = slow plus muscle from Troutman *et al*. (2015)
b Richly perfused tissue volume = sum of the gut, richly perfused, gut lumen, kidney, and lung from Troutman *et al*. (2015); Slowly perfused tissue volume = 0.85% of BW minus liver, fat, skin, blood and richly perfused tissue volumes
c Barter *et al*. (2007)

Table 13 Chemical-specific PBK parameters.

Parameter	Units	Symbol	Value	Source

Parameter	Units	Symbol	Value	Source
Molecular weight PhE	g/mole	MW	138.17	(1)
Molecular weight PAA	g/mole	MW	152.15	(1)
Partition Coefficients				
Arterial blood	1	PBA	300815	(2)
Fat	1	PFAT	0.660	(2)
Liver	1	PLIV	0.771	(2)
Skin	1	PSk	1.122	(2)
Rich	1	PRPT	PLIV	Set to Liver Value
Slow	1	PSPT	PSk	Set to Skin Value
Liver (PAA)	1	PLivPAA	0.68	(2)
Kidney (PAA)	1	PKidPAA	3.5	(2)
Protein Binding[a]				
Fraction unbound in blood (PhE)	1	FUPLS	0.42-1	(2)
Fraction unbound in plasma (PAA)	1	FUPLS_PAA	0.14-1	(2)
Oral absorption				
GI -> liver	1/h	Ka	5	Default
Dermal penetration	cm/h	Kp	0.0025	(3) fitted
Dermal loss	cm/h	Kloss	0.0025	(3) fitted
Metabolism				
Hepatocyte clearance	µL/min/million cells	CL_Hep_invitro	25.3	(4)
PAA Urinary Clearance	$L/h/kg^{3/4}$	CLUCPAA	0.3	Set to GFR

[a] Protein binding was set to the value reported by Troutman *et al*. (2015), and also set to 1 for unrestricted clearance simulation.

(1) PubChem
(2) Troutman *et al*., 2015
(3) Roper *et al*., 1997
(4) Cosmetics Europe

To assess the relative effect of different model parameters (P) on the predicted output (O), a local sensitivity analysis was conducted. The sensitivity analysis function in Berkeley Madonna was used to estimate the relative change in output in response to a given change of input parameter value, $\Delta O/\Delta P$ (Beck *et al*., 1977). A ΔP of 0.1% was used to calculate the sensitivity coefficient (SC). The resulting $\Delta O/\Delta P$ were then normalized in order to facilitate comparison across input parameters using the following equation.

$$\text{Sensitivity coefficient} = SC = (\Delta O/\Delta P) \times P/O$$

Analysis was conducted to examine the variability in model predictions of internal dose metrics resulting from variability in key input parameters identified by the sensitivity analysis. Parameters varied included those found to have normalized sensitivity coefficients greater than 0.1. Table 14 shows the parameter variability distributions. Most parameters describing physiology (e.g., tissue blood flows and volumes) were assigned normal distributions, while body weight, partition coefficients, urinary clearance, and dermal absorption/evaporation rate constants were described with lognormal distributions. Except for intrinsic hepatic clearance, parameter variation was described with a coefficient of variation (CV), with values either taken from Clewell *et al*. (1999) or set to a default of 30%. For hepatic clearance, a CV of 41% from Ito *et al*. (2014) was used to represent populations with no polymorphism of enzyme.

Table 14 Distributions used for variability analysis.

Parameter	Units	Distribution	Natural Center	Mean	CV	SD	LB	UB	CV Source
Kp	cm/h	lognormal	0.0025	-6.035	0.3	0.29	0.0013	0.0043	Default 30%
Kloss	cm/h	lognormal	0.0025	-6.035	0.3	0.29	0.0013	0.0043	Default 30%
BW	kg	lognormal	60	4.06	0.26	0.26	35	97	Default 30%
PSk	unitless	lognormal	1.122	0.072	0.3	0.29	0.60	1.9	Clewell *et al*., 1999
Pliv	unitless	lognormal	0.77	-0.304	0.3	0.29	0.41	1.3	Clewell *et al*., 1999
CLUCPAA	$L/h/kg^{3/4}$	lognormal	0.3	-1.25	0.3	0.29	0.16	0.52	Default 30%
CL_h_invitro	uL/min/million	normal		25.3	0.41	10	5.3	45.3	Ito *et al*., 2014
Hpgl	million cells per g liver	normal		99	0.3	30	40	158	Default 30%
FUPLS_PAA	unitless	normal		0.21	0.3	0.063	0.084	0.34	Default 30%
FUPLS	unitless	normal		0.56	0.3	0.17	0.22	0.90	Default 30%
QCC	$L/h/kg^{3/4}$	normal		15	0.22	3.3	8.4	22	Clewell *et al*., 1999
QLivC	unitless	normal		0.2589	0.32	0.083	0.093	0.42	Clewell *et al*., 1999
QSkC	unitless	normal		0.0536	0.3	0.016	0.021	0.086	Clewell *et al*., 1999
QSPTC	unitless	normal		0.1639	0.3	0.049	0.066	0.26	Clewell *et al*., 1999
VSkC	unitless	normal		0.0371	0.16	0.0059	0.025	0.049	Clewell *et al*., 1999
VLivC	unitless	normal		0.0257	0.3	0.0077	0.010	0.041	Default 30%
VBldC	unitless	normal		0.074	0.3	0.022	0.030	0.12	Default 30%
VRPTC	unitless	normal		0.0633	0.3	0.019	0.025	0.10	Clewell *et al*., 1999
VdC	L/kg	normal		0.7	0.3	0.21	0.28	1.1	Default 30%

.

5. Modelling Results

Oral and dermal exposure scenarios were used to test the developed model. The scenarios are listed in Table 15. The model provided an acceptable comparator with the existing data (Figures 14-16). The consumer exposure scenario for PhE in cosmetics was estimated assuming whole body application of lotion applied twice daily by a 60 kg human. The assumed volume of lotion application (3.91 mL) and resulting dose (0.616 mg/kg body weight) was taken from Troutman *et al*. (2015). The resulting simulation of this consumer use scenario is shown in Figure 17.

Table 15 Exposure scenarios used to evaluate the model, and to simulate the cosmetic use scenario.

Type of Dosing	Oral	Dermal	Dermal	Body Lotion
Number of Doses per Day	1[b]	1[b]	1[b]	2
Number of Days	1[b]	3[b]	2[a,b]	2
Dose (mg/kg)	0.18[b]	3.4[b]	6.9[b]	0.616
Volume of Applied Dose (mL)	N/A	20[b] mL	40[b] mL	3.91 mL
Body Surface Area (cm^2)	N/A	21000[c] cm^2	21000[c] cm^2	15670 [c] cm^2
Surface Area Exposed (%)	N/A	80[b]	90[b]	100
Total Area Exposed (cm^2)	N/A	16800 cm^2	18900 cm^2	15670 cm^2
Body Weight (kg)	70	70	70	60

a. Dosing started on day two
b. Howes, 1991
c. Troutman *et al*., 2015, total surface area minus head for a 60 kg female

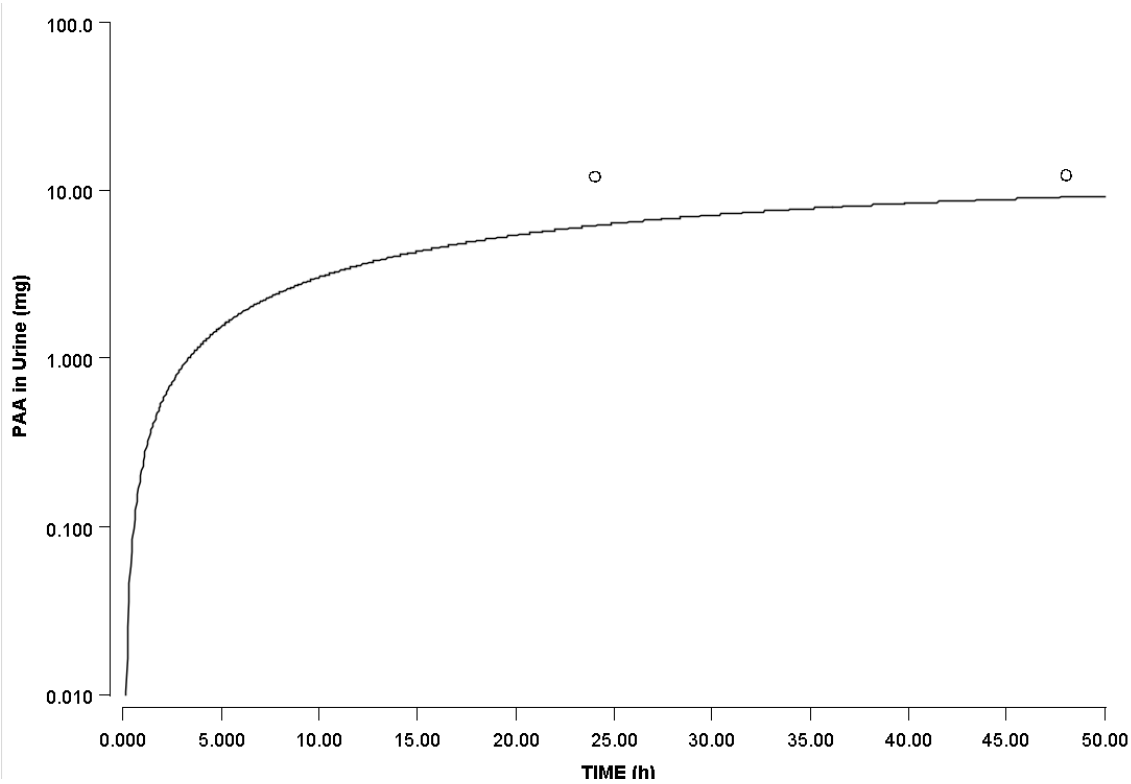

Figure 14 Circles = data from Howes (1991), line = simulation. Urinary PAA following oral exposure to 0.152 mg/kg PhE.

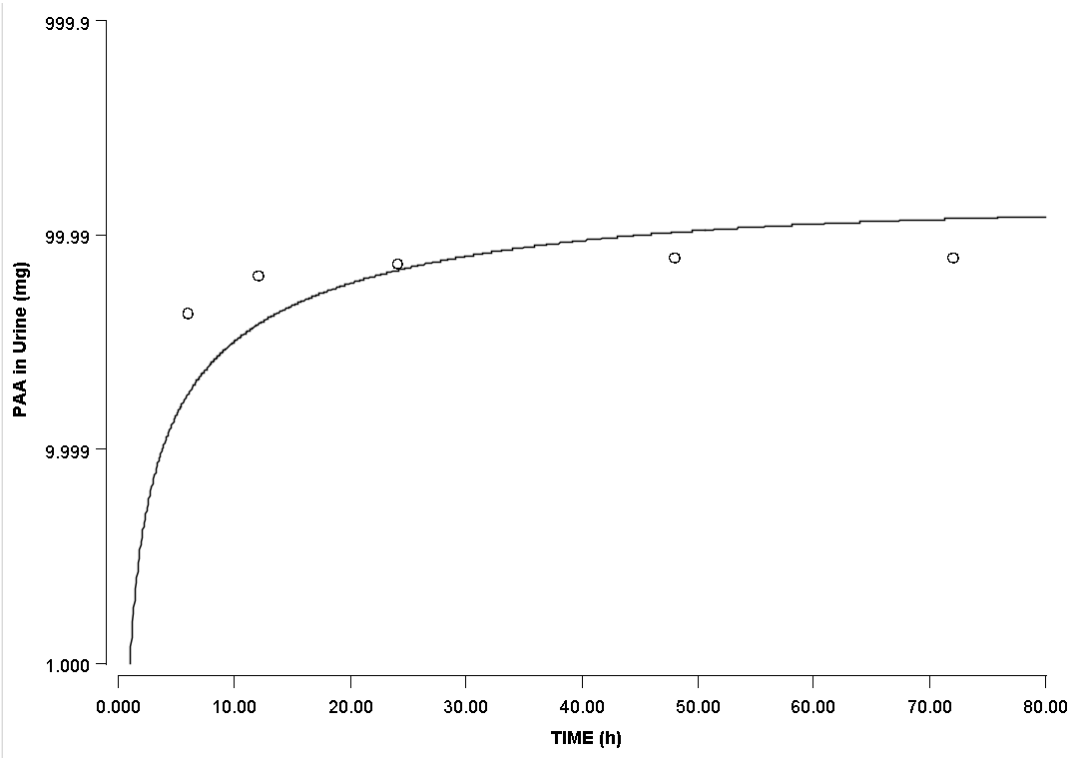

Figure 15 Circles = data from Howes (1991), line = simulation. Urinary PAA following a single dermal application of 3.44 mg/kg PhE.

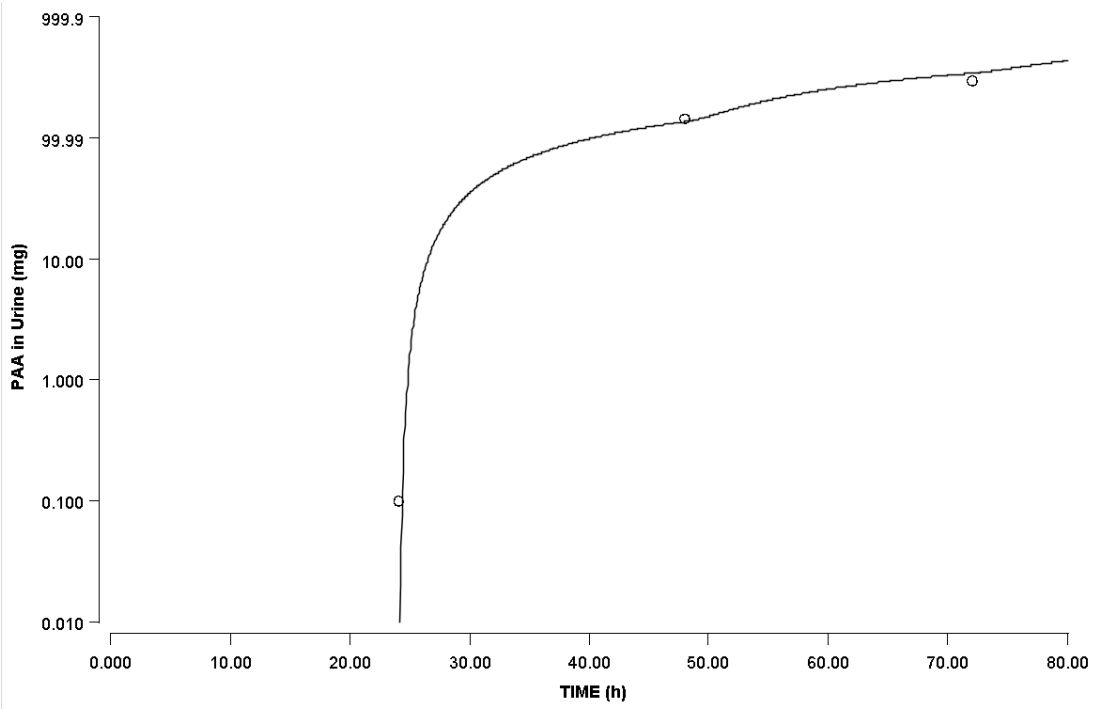

Figure 16 Circles = data from Howes (1991), line = simulation. Urinary PAA following dermal applications of 6.89 mg/kg PhE at 24 and 48 hours.

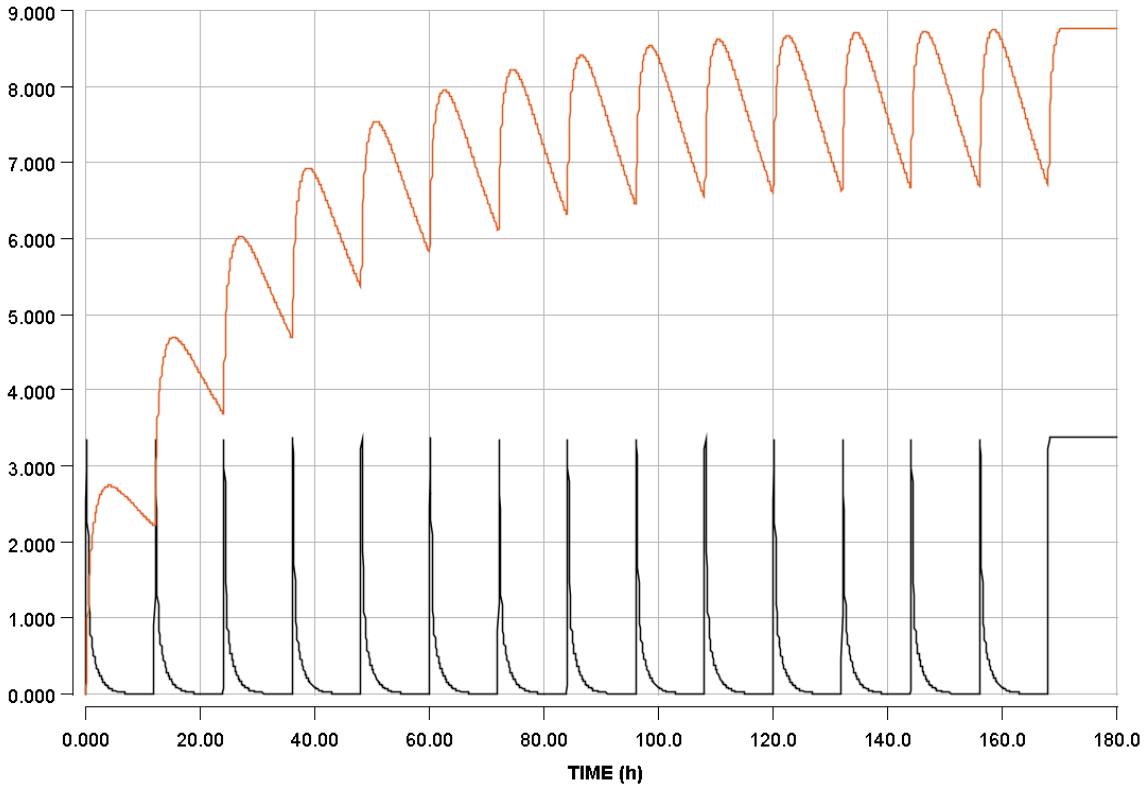

Figure 17 . Time-course concentration and C_{max} for PhE (black) and PAA (red) following cosmetic exposure scenario (see Table 5).

The result of the sensitivity analysis is shown in Tables 16-19. Sensitivity of model predictions of C_{max} and AUC of PhE and PAA in blood, and PAA in kidney were evaluated. Parameters with sensitivity coefficients greater than 0.1 or less than -0.1 for each dose metric are shown. A positive value indicates an increase in the outcome with a given increase in the parameter. While, a negative value indicates a decrease in outcome given an increase in the parameter. These most influential parameters were selected for variability analysis.

Table 16 Sensitivity coefficients (SC) for PhE C_{max} in blood.

Parameter	SC
FUPLS	-0.12
CLint	-0.12
hpgl	-0.12
Kp	0.58
PSk	-0.57
VSkC	-0.53
QSkC	0.46
Kloss	-0.42
VLivC	-0.12
QLivC	-0.21
QSPTC	-0.26
SADose	0.16
AppliedVol	-0.16
Pliv	-0.13
VBldC	-0.12
VRPTC	-0.11

Table 17 Sensitivity coefficients for PhE AUC in blood.

Parameter	SC
Kp	0.50
Kloss	-0.50
QLivC	-0.61
QCC	-0.61
FUPLS	-0.39
CLint	-0.39
hpgl	-0.39
VLivC	-0.39
BW	0.15

Table 18 Sensitivity coefficients for PAA C_{max} and AUC in blood.

Parameter	Cmax	AUC
CLUCPAA	-0.82	-0.91
FUPLS_PAA	-0.82	-0.91
Kp	0.50	0.50
Kloss	-0.50	-0.50
VdC	-0.18	
BW	0.23	0.26

Table 19 Sensitivity coefficients for PAA C_{max} and AUC in kidney.

Parameter	Cmax	AUC
FUPLS_PAA	-0.92	-1.0
Kp	0.50	0.50
Kloss	-0.50	-0.50
CLUCPAA	-0.92	-1.0
VdC	-0.10	
PKidPAA	1.0	1.0

The results of the variability analysis are shown in Tables 20. As expected from the smaller sensitivity coefficient for intrinsic hepatic clearance from the sensitivity analysis, only the AUC of PhE is noticeably affected by the polymorphism in ADH3. The contribution of all parameter variability is somewhat greater for the AUC for PhE, though it is similar to other dose metrics. The ratio of the 95th to 5th percentiles is less than about 5 for all dose metrics. The ratio of the 95th to the 5th percentile ranges from approximately 3 (C_{max} for PhE) to 5 (AUC for PhE).

Table 20 Summarized results of the variability analysis. Dose metrics for PhE and PAA in blood, and PAA in kidney.

	Blood Phenoxyethanol		Blood PAA		Kidney PAA	
	C_{max}	AUC_{24}	C_{max}	AUC_{24}	C_{max}	AUC_{24}
	µM	µmol*h/L	µM	µmol*h/L	µM	µmol*h/L
Mean	3.7	7.3	10.5	230	36	789
SD	1.4	4.2	4.9	115	17	401
5th %ile	1.8	3.3	4.5	93	15	312
95th %ile	6.2	15	20	453	69	1569

6. Model Code

; 2-phenoxyethanol (PhE) PBPK model for Cosmetics Europe case study

; Developed by Eric Hack, John Troutman, Alina Efremenko, and Harvey Clewell

; 5 compartment PBPK model

; Liver, Fat, Skin, Slowly Perfused and Rapidly Perfused Tissues (and gas exchange)

{

Instructions for running the model simulations

Cosmetic exposure scenario:

Set Sim = 1, OR

DDOSE = 0.616, drepeat = 12, SADose = 15670, AppliedVol = 3.91, BW = 60

Note the model may need to run for several days (ca. 8-10 days) for PAA to reach pseudo-equilibrium

Howes subject A dermal exposure data

Set Sim = 2, OR

DDose = 3.44, drepeat > Stoptime, SADose = 16800, AppliedVol = 20, BW = 70

Howes subject D repeated dermal exposure data

Set Sim = 3, OR

DDose = 6.89, dstart = 24, drepeat = 24, SADose = 18900, AppliedVol = 40, BW = 70

```
Howes oral exposure data
Set Sim = 4, OR
ODose = 0.152, BW = 70
}

;----------------------------------------------------------------------------------------------------------
; Solver settings
METHOD STIFF

STARTTIME = 0
STOPTIME = 24
DTOUT = 0.01
DTMAX = 0.01

;----------------------------------------------------------------------------------------------------------
; Parameters to set simulation scenario
; See comments below for parameter descriptions
; Sim = 1 --> Cosmetic, 2 --> Howes A, 3 --> Howes D, 4 --> Howes Oral
Sim = 1             ; Scenario identifier, default to Cosmetic use scenario
DDose = IF (Sim=1) THEN 0.616 ELSE IF (Sim=2) THEN 3.44 ELSE IF (Sim=3) THEN
6.89 ELSE IF (Sim=4) THEN 0 ELSE 0
drepeat = IF (Sim=1) THEN 12 ELSE IF (Sim=2) THEN (StopTime+1) ELSE IF (Sim=3)
THEN 24 ELSE IF (Sim=4) THEN 1e6 ELSE 1e6
dstart = IF (Sim=3) THEN 24 ELSE 0
muSADose = IF (Sim=1) THEN 15670 ELSE IF (Sim=2) THEN 16800 ELSE IF (Sim=3)
THEN 18900 ELSE IF (Sim=4) THEN 16800 ELSE 16800
muAppliedVol = IF (Sim=1) THEN 3.91 ELSE IF (Sim=2) THEN 20 ELSE IF (Sim=3)
THEN 40 ELSE IF (Sim=4) THEN 1 ELSE 1
ODose = IF (Sim=4) THEN 0.152 ELSE 0
BW0 = IF (Sim=1) THEN 60 ELSE 70
```

```
;-------------------------------------------------------------------------------------------------------------
---------------------------------

; Monte Carlo simulation parameters

MCrun = 1       ; dummy count parameter for batch runs

Vary = 0        ; set to 0 to fix all parameters except clearance at their nominal values

Poly = 0; set to 1 to use polymorphic distributions for CLint, 0 for nominal CLint value


;-------------------------------------------------------------------------------------------------------------
---------------------------------

; Define parameter means


; Fraction PhE unbound in plasma

; 0.56 is mean of QSAR predicted values (ChemSilico v1.6.1 (fup = 0.71), ACD/Percepta
v14.0.0 (fup = 0.37) and ADMET Predictor v6.5.0013 (fup = 0.59))

; Fraction PAA unbound in plasma

; mean of QSAR predicted values (ChemSilico v1.6.1 (fup = 0.31), ACD/Percepta v14.0.0
(fup = 0.17) and ADMET Predictor v6.5.0013 (fup = 0.14))


Kp0 = 0.0025

Kloss0 = 0.0025

;BW0 = 60

PSk0 = 1.122

PLIV0 = 0.77

PKidPAA0 = 3.5

CLUCPAA0 = 0.31                 ; urinary clearance rate constant
(L/h/kg^3/4), either set to GFR or fitted to Howes data (depending on excretion model)

muLnKp = LOGN(Kp0) - 1/2*LsdKp**2               ; dermal penetration rate (cm/h)

muLnKloss = LOGN(Kloss0) - 1/2*LsdKloss**2      ; loss rate, evaporation or
transfer to clothing, fitted to in vivo data by Troutman (cm/h)

muLnBW = LOGN(BW0) - 1/2*LsdBW**2               ; body mass (kg)

muLnPSk = LOGN(PSk0) - 1/2*LsdPSk**2    ; skin:blood PC

muLnPLIV = LOGN(PLIV0) - 1/2*LsdPLIV**2 ; liver:blood PC

muLnPKidPAA = LOGN(PKidPAA0) - 1/2*LsdPKidPAA**2    ; kidney:blood PC

muLnCLUCPAA = LOGN(CLUCPAA0) - 1/2*LsdCLUCPAA**2    ; Urinary
clearance of PAA (L/h/(kg bw)^0.75, set to human GFR (Campbell et al)

muCL0 = 25.3            ; uL/min/million, hepatic instrinsic clearance measured
(Pharmacelcus)
```

```
muhpgl = 99             ; million hepatocytes per gram liver (Barter et al., 2007)
;muSADose = 16800       ; surface area exposed (cm**2)
;muAppliedVol = 1       ; volume of PhE applied (cm**3) Note: need to account for % of
PhE in product
muQCC = 15.0            ; cardiac output L/h/kg^(3/4)
muQLivC = 0.2589        ; fractional blood flow to liver
muQSkC = 0.0536         ; fractional blood flow to skin (human value from Troutman)
muQSPTC = 0.0300 + 0.1339     ; fractional blood flow to slowly perfused tissues (slow +
muscle in Troutman et al.)
muVSkC = 0.0371         ; fractional volume of skin
muVBLDC = 0.074         ; fractional volume of blood
muVRPTC = 0.0633        ; fractional volume of rishly perfused tissues
muVLIVC = 0.0257        ; fractional volume of liver
muFUPLS_PAA = 0.21 ; Free fraction of PAA in plasma.  Troutman used 21%.
 SHOULD THIS BE LOGNORMAL?
muFUPLS = 0.56          ; Free fraction of PhE in plasma.  Troutman used 56%.
 SHOULD THIS BE LOGNORMAL?
muVdC = 0.7             ; L/kg BW, set to total body water following Campbell et al (2015)
paraben model



;-------------------------------------------------------------------------------------------------------
---------------------------------
; Define variability (CVs)
cvCL0_0 = 0.41                ; Default of 0.3 for rate constants (CLint is handled
differently so that different CV's can be set in the parameter window)
cvFUPLS_0 = 0.3               ; Default 0.3 for rate constants (FUPLS is handled
differently so that different CV's can be set in the parameter window)
cvKp = 0.3*Vary                     ; Default of 0.3 for rate constants
cvKloss = 0.3*Vary            ; Default of 0.3 for rate constants
cvBW = 0.3*Vary               ; Default of 0.3
cvPSk = 0.3*Vary              ; Clewell et al., 1999 slowly perfused CV
cvPLIV = 0.3*Vary             ; Clewell et al., 1999
cvPKidPAA = 0.3*Vary          ; Clewell et al., 1999
cvCLUCPAA = 0.3*Vary          ; defaulting to prevalent CV for kinetic
parameters in Clewell et al., 1999
cvCL0 = cvCL0_0*Vary          ; set to cvCL0_0
```

```
cvhpgl = 0.3*Vary               ; Default of 0.3
cvSADose = 0.0*Vary             ; Fixed dosing scenario
cvAppliedVol = 0.0*Vary                 ; Fixed dosing scenario
cvQCC = 0.22*Vary               ; Clewell et al., 1999
cvQLivC = 0.32*Vary             ; Clewell et al., 1999
cvQSkC = 0.3*Vary               ; Clewell et al., 1999 slowly perfused CV
cvQSPTC = 0.3*Vary              ; Clewell et al., 1999
cvVSkC = 0.3*Vary               ; default 30% in absence of data
cvVBLDC = 0.3*Vary              ; default 30% in absence of data
cvVRPTC = 0.3*Vary              ; default 30% in absence of data
cvVLIVC = 0.3*Vary              ; default 30% in absence of data
cvFUPLS_PAA = 0.3*Vary          ; defaulting to prevalent CV for kinetic parameters in
Clewell et al., 1999
cvFUPLS = cvFUPLS_0*Vary        ; defaulting to prevalent CV for kinetic parameters in
Clewell et al., 1999
cvVdC = 0.3*Vary                ; defaulting to prevalent CV for volumes in Clewell et al.,
1999


;-------------------------------------------------------------------------------------------------------
---------------------------------
; Compute standard deviation and bounds
nsd = 2             ; number of SDs for lower and upper bounds

; Log-scale SDs for lognormally distributed parameters
LsdKp = sqrt( LOGN( 1 + cvKp**2 ) )
LsdKloss = sqrt( LOGN( 1 + cvKloss**2 ) )
LsdBW = sqrt( LOGN( 1 + cvBW**2 ) )
LsdPSk = sqrt( LOGN( 1 + cvPSk**2 ) )
LsdPLIV = sqrt( LOGN( 1 + cvPLIV**2 ) )
LsdPKidPAA = sqrt( LOGN( 1 + cvPKidPAA**2 ) )
LsdCLUCPAA = sqrt( LOGN( 1 + cvCLUCPAA**2 ) )
sdCL0 = muCL0*cvCL0
sdhpgl = muhpgl*cvhpgl
sdSADose = muSADose*cvSADose
```

```
sdAppliedVol = muAppliedVol*cvAppliedVol
sdQCC = muQCC*cvQCC
sdQLivC = muQLivC*cvQLivC
sdQSkC = muQSkC*cvQSkC
sdQSPTC = muQSPTC*cvQSPTC
sdVSkC = muVSkC*cvVSkC
sdVBLDC = muVBLDC*cvVBLDC
sdVRPTC = muVRPTC*cvVRPTC
sdVLIVC = muVLIVC*cvVLIVC
sdFUPLS_PAA = muFUPLS_PAA*cvFUPLS_PAA
sdFUPLS = muFUPLS*cvFUPLS
sdVdC = muVdC*cvVdC

;-----------------------------------------------------------------------------------------------------------
; Lower bounds
loLnKp = muLnKp - nsd*LsdKp
loLnKloss = muLnKloss - nsd*LsdKloss
loLnBW = muLnBW - nsd*LsdBW
loLnPSk = muLnPSk - nsd*LsdPSk
loLnPLIV = muLnPLIV - nsd*LsdPLIV
loLnPKidPAA = muLnPKidPAA - nsd*LsdPKidPAA
loLnCLUCPAA = muLnCLUCPAA - nsd*LsdCLUCPAA
loCL0 = max(0, muCL0 - nsd*sdCL0)
lohpgl = max(0, muhpgl - nsd*sdhpgl)
loSADose = max(0, muSADose - nsd*sdSADose)
loAppliedVol = max(0, muAppliedVol - nsd*sdAppliedVol)
loQCC = max(0, muQCC - nsd*sdQCC)
loQLivC = max(0, muQLivC - nsd*sdQLivC)
loQSkC = max(0, muQSkC - nsd*sdQSkC)
loQSPTC = max(0, muQSPTC - nsd*sdQSPTC)
loVSkC = max(0, muVSkC - nsd*sdVSkC)
loVBLDC = max(0, muVBLDC - nsd*sdVBLDC)
loVRPTC = max(0, muVRPTC - nsd*sdVRPTC)
```

```
loVLIVC = max(0, muVLIVC - nsd*sdVLIVC)
loFUPLS_PAA = max(0, muFUPLS_PAA - nsd*sdFUPLS_PAA)
loFUPLS = max(0, muFUPLS - nsd*sdFUPLS)
loVdC = max(0, muVdC - nsd*sdVdC)

;-------------------------------------------------------------------------------------------------------------
---------------------------------
; Upper bounds
hiLnKp = muLnKp + nsd*LsdKp
hiLnKloss = muLnKloss + nsd*LsdKloss
hiLnBW = muLnBW + nsd*LsdBW
hiLnPSk = min( 1, muLnPSk + nsd*LsdPSk )          ; 1 is a hard upper bound
hiLnPLIV = min( 1, muLnPLIV + nsd*LsdPLIV )          ; 1 is a hard upper bound
hiLnPKidPAA = muLnPKidPAA + nsd*LsdPKidPAA
hiLnCLUCPAA = muLnCLUCPAA + nsd*LsdCLUCPAA
hiCL0 = muCL0 + nsd*sdCL0
hihpgl = muhpgl + nsd*sdhpgl
hiSADose = SA                                     ; max is total surface area (cm2)
hiAppliedVol = muAppliedVol + nsd*sdAppliedVol
hiQCC = muQCC + nsd*sdQCC
hiQLivC = muQLivC + nsd*sdQLivC
hiQSkC = muQSkC + nsd*sdQSkC
hiQSPTC = muQSPTC + nsd*sdQSPTC
hiVSkC = muVSkC + nsd*sdVSkC
hiVBLDC = muVBLDC + nsd*sdVBLDC
hiVRPTC = muVRPTC + nsd*sdVRPTC
hiVLIVC = muVLIVC + nsd*sdVLIVC
hiFUPLS_PAA = min( 1, muFUPLS_PAA + nsd*sdFUPLS_PAA)
hiFUPLS = min(1, muFUPLS + nsd*sdFUPLS)
hiVdC = muVdC + nsd*sdVdC


;-------------------------------------------------------------------------------------------------------------
---------------------------------
; Sample distributions
```

; Modeled as state variables that do not change so that only the initial value changes for each iteration

init LnKp = max(loLnKp, min(NORMAL(muLnKp, LsdKp), hiLnKp))

init LnKloss = max(loLnKloss, min(NORMAL(muLnKloss, LsdKloss), hiLnKloss))

init LnBW =max(loLnBW, min(NORMAL(muLnBW, LsdBW), hiLnBW))

init LnPSk = max(loLnPSk, min(NORMAL(muLnPSk, LsdPSk), hiLnPSk))

init LnPLIV = max(loLnPLIV, min(NORMAL(muLnPLIV, LsdPLIV), hiLnPLIV))

init LnPKidPAA = max(loLnPKidPAA, min(NORMAL(muLnPKidPAA, LsdPKidPAA), hiLnPKidPAA))

init LnCLUCPAA = max(loLnCLUCPAA, min(NORMAL(muLnCLUCPAA, LsdCLUCPAA), hiLnCLUCPAA))

init CL0 = max(loCL0, min(NORMAL(muCL0, sdCL0), hiCL0))

init hpgl = max(lohpgl, min(NORMAL(muhpgl, sdhpgl), hihpgl))

init SADose = max(loSADose, min(NORMAL(muSADose, sdSADose), hiSADose))

init AppliedVol = max(loAppliedVol, min(NORMAL(muAppliedVol, sdAppliedVol), hiAppliedVol))

init QCC = max(loQCC, min(NORMAL(muQCC, sdQCC), hiQCC))

init QLivC = max(loQLivC, min(NORMAL(muQLivC, sdQLivC), hiQLivC))

init QSkC = max(loQSkC, min(NORMAL(muQSkC, sdQSkC), hiQSkC))

init QSPTC = max(loQSPTC, min(NORMAL(muQSPTC, sdQSPTC), hiQSPTC))

init VSkC = max(loVSkC, min(NORMAL(muVSkC, sdVSkC), hiVSkC))

init VBLDC = max(loVBLDC, min(NORMAL(muVBLDC, sdVBLDC), hiVBLDC))

init VRPTC = max(loVRPTC, min(NORMAL(muVRPTC, sdVRPTC), hiVRPTC))

init VLIVC = max(loVLIVC, min(NORMAL(muVLIVC, sdVLIVC), hiVLIVC))

init FUPLS_PAA = max(loFUPLS_PAA, min(NORMAL(muFUPLS_PAA, sdFUPLS_PAA), hiFUPLS_PAA))

init FUPLS = max(loFUPLS, min(NORMAL(muFUPLS, sdFUPLS), hiFUPLS))

init VdC = max(loVdC, min(NORMAL(muVdC, sdVdC), hiVdC))

;----------

; set rates of change to 0

LnKp' = 0

LnKloss' = 0

lnBW' = 0

```
LnPSk' = 0
LnPLIV' = 0
LnPKidPAA' = 0
LnCLUCPAA' = 0
CL0' = 0
hpgl' = 0
SADose' = 0
AppliedVol' = 0
QCC' = 0
QLivC' = 0
QSkC' = 0
QSPTC' = 0
VSkC' = 0
VBLDC' = 0
VRPTC' = 0
VLIVC' = 0
FUPLS_PAA' = 0
FUPLS' = 0
VdC' = 0

;-------------------------------------------------------------------------------------------------------------
---------------------------------
; Take antilogs of lognormally distributed parameters
Kp = exp(LnKp)
Kloss = exp(LnKloss)
BW = exp(LnBW)
PSk = exp(LnPSk)
PLIV = exp(LnPLIV)
PKidPAA = exp(LnPKidPAA)
CLUCPAA = exp(LnCLUCPAA)



;-------------------------------------------------------------------------------------------------------------
---------------------------------
; Polymorphic Clearance Distributions
```

```
;-----------------------------------------------------------------------------------------------------------
---------------------------------
; ADH3 clearance
; Simulate 2 distributions with means 2-fold apart, average of the 2 means is 25.3 (the measured value).
; Each distribution is normal and spans about an order of magnitude.

CL1' = 0
CL2' = 0
CL3' = 0            ; not used, but retained as space for 3rd population

init CL1 = max( min( normal(34, 13.9), 61.2 ), 6.8 )        ; ADH3*1 (wild type) in European population
init CL2 = max( min( normal(17, 7.14), 31 ), 3 )            ; ADH3*2 (polymorphic) in European population
init CL3 = CL0              ; not used

;-----------------------------------------------------------------------------------------------------------
---------------------------------
; Prevalence of allellic forms of ADH3
P1 = 0.556          ; ADH3*1 (wild type) in European population
P2 = 0.444          ; ADH3*2 (polymorphic) in European population
P3 = 1              ; not used, P1 and P2 add up to 1.

;-----------------------------------------------------------------------------------------------------------
---------------------------------
; Choose a subpopulation and record (0 if Poly set to 0)
init P0 = random(0, 1)
P0' = 0
Pop = IF (P0 >= Poly) THEN 0 ELSE IF (P0 <= P1) THEN (1) ELSE IF (P0 <= P1+P2) THEN (2) ELSE (3)

;-----------------------------------------------------------------------------------------------------------
---------------------------------
; Set the clearance for the selected population (CL0 if Poly set to 0)
```

CL_Hep_invitro = IF (P0 >= Poly) THEN CL0 ELSE IF (P0 <= P1) THEN (CL1) ELSE IF (P0 <= P1+P2) THEN (CL2) ELSE (CL3)

;----------

; Chemical Parameters

; PhE

MW = 138.17 ; Molecular Weight (g/mole)

logp = 1.16 ; Octanol-Water Partition Coefficient (predicted using EpiSuite or ACD/Percepta by Troutman)

; Phenoxyacetic acid metabolite (PAA)

MW_PAA = 152.15 ; Molecular Weight (g/mole)

;----------

; Dosing Parameters

; Oral dosing

;ODOSE =0.0 ; bolus oral dose (mg/kg BW)

OD = ODOSE*1000*BW/MW ; (umole)

ODSwitch = IF ODOSE >0 then 1.0 else 0.0 ; boolean dose switch

; Inhalation

CONC = 0.0 ; Initial concentration (ppm)

CI = CONC/24.45 ; (uM)

TCHNG = 6.0 ; length of exposure (h)

; Dermal

; Calculate Total Area of Skin (cm^2), Livingston and Lee (2001)

SA = (0.1173*(BW)**0.6466) * 10**4 ; total body surface area, cm2 (the 10**4 converts m2 to cm2)

;DDOSE = 0.0 ; mg/kg dermal dose applied

;dstart = 0 ; time of first dermal dose (hr)

;drepeat = 9e9 ; repeat interval for dermal doses (hr)

```
DD = DDOSE*1000*BW/MW   ; daily dose (umoles) Note: repeated if drepeat is set


;-----------------------------------------------------------------------------------------------------------
---------------------------------
;GI absorption
Ka = 5                          ; 1st order absorption rate, GI to liver (1/h)

;-----------------------------------------------------------------------------------------------------------
---------------------------------
;Urinary Excretion of PAA
CLUPAA = CLUCPAA * BW**0.75     ; urine excretion of PAA (L/hr)
VOLUC = 22                      ; Urine production rate, (ml/kg/day, human)
ICRP 1975
VOLU = (VOLUC*BW)/24/1000               ; Volume of urine per hour (L/h)

;-----------------------------------------------------------------------------------------------------------
---------------------------------
; TISSUE VOLUMES (fraction of BW)
VFATC = 0.2142                  ; fat
VSPTC = 0.85 - VLIVC - VFATC - VSkC - VBLDC - VRPTC   ; slowly perfused tissue
HCT = 0.0                       ; Hematocrit (volume fraction of RBC in whole
blood)
VKidC = 0.0044          ; L/kg BW, Troutman et al., 2015

;-----------------------------------------------------------------------------------------------------------
---------------------------------
; FLOWS (fraction of QC)
QPC = 15.0                              ; alveolar ventilation rate L/hr/kg^(3/4)
QFATC = 0.0464                          ; fat
QRPTC = 1- QLIVC - QFATC - QSkC - QSPTC; richly perfused tissues
QFlag = IF (QRPTC < 0) THEN 1 ELSE 0            ; flag if invalid blood flows are
sampled
QKidC = 0.1800                          ; kidney, Troutman et al., 2015

;-----------------------------------------------------------------------------------------------------------
---------------------------------
```

```
; PARTITION PREDICTIONS
; PC QSAR in PLETHEM, same as IndusChemFate model (Jongeneelen and ten Berge)
PBA = 267300
PFAT = 13.5
PRPT = PLIV
PSPT = PSk

PLivPAA = 0.680                    ; Liver:blood, Troutman et al., 2015
PKidPAA = 3.5                      ; Kidney:blood, Troutman et al., 2015

;-------------------------------------------------------------------------------------------------------------
; Allometric scaling of tissue volumes (L or kg)
VLIV = VLIVC * BW                  ; liver
VFAT = VFATC * BW                  ; fat
VSk = VSkC * BW                    ; skin
VBLD = VBLDC * BW                  ; blood
VPLS = VBLD*(1-HCT)                ; plasma
VRPT = VRPTC * BW                  ; rapidly perfused
VSPT = VSPTC * BW                  ; slowly perfused
VBal = BW*0.85 - VLIV - VFAT - VSk - VBLD - VRPT - VSPT   ; volume balance (should be zero)

; Volume of distribution for PAA metabolite (L or kg)
VKid = VKidC*BW
Vd = (VdC - VLivC - VKidC)*BW

;-------------------------------------------------------------------------------------------------------------
; Allometric scaling of tissue blood flows (L/h)
QC = QCC *(1-HCT)*BW**0.75         ; cardiac output
QLIV = QLIVC * QC                  ; liver
QFAT = QFATC * QC                  ; fat
QSk = QSkC * QC                    ; skin
QRPT = QRPTC * QC                  ;rapidly perfused tissue
```

```
QSPT = QSPTC * QC                                   ; slowly perfused tissue
QBal = QC - QLIV - QFAT - QSk - QRPT - QSPT         ; flow balance (should be zero)

QKid = QKidC*QC                                     ; kidney for PAA

; Alveolar Ventilation (L/hr)
QP = QPC*BW**0.75

;-------------------------------------------------------------------------------------------------------------
; Extrapolation of in vitro hepatic clearance to in vivo

; In-vitro clearance (CL) for non-saturable metabolism
CL_Mic_invitro = 0                  ; microsomes, uL/min/mg microsomal protein
CL_Cyt_invitro =  0                 ; cytosol, uL/min/mg cytosolic protein

; In-vitro Vmax and KM for saturable metabolism
Vmax_Mic_invitro = 0                ; maximal rate in microsomes, umol/min/mg microsomal protein
Vmax_Cyt_invitro = 0                ; maximal rate in cytosol, umol/min/mg cytosolic protein
Vmax_Hep_invitro = 0                ; maximal rate in hepatocytes, umol/min/10^6 hepatocytes
KM = 1                              ; Michaelis Menten affinity constant (umole/L)

; Skin clearance (non-saturable metabolism)
CL_PMF_invitro = 0                  ; post mitochondrial fraction, uL/min/mg protein, 0.00096 uL/min/mgp in rat skin from Roper

; HEPATIC PROTEIN ABUNDANCE
mppgl = 39.99                       ; mg Microsomal Protein per gram liver
cppgl = 80.7                        ; mg Cytosolic Protein per gram liver
pppgsk = 11                         ; mg PMF protein per gram skin (McCracken et al 1993, male Wistar rat, no human data)

; Non Saturable Metabolism
CL_Mic_invivo = CL_Mic_invitro * (10^-6) * 60 * mppgl * 1000        ; L/h/kg Liver
```

```
CL_Cyt_invivo = CL_Cyt_invitro * (10^-6) * 60 * cppgl * 1000  ; L/h/kg Liver
CL_Hep_invivo = CL_Hep_invitro * (10^-6) * 60 * hpgl * 1000  ; L/h/kg Liver
CL_PE_invivo= CL_Mic_invivo+CL_Cyt_invivo + CL_Hep_invivo       ; L/h/kg Liver
CLSk_invivo = CL_PMF_invitro * (10^-6) * 60 * pppgsk * 1000; L/h/kg Skin

; Saturable Metabolism
Vmax_Mic_invivo = Vmax_Mic_invitro * 60 * mppgl * 1000              ;       umol/h/kg
Liver
Vmax_Cyt_invivo = Vmax_Cyt_invitro * 60 * cppgl * 1000              ;       umol/h/kg
Liver
Vmax_Hep_invivo = Vmax_Hep_invitro*60*hpgl*1000           ; umol/h/kg Liver
Vmax_PE_invivo = Vmax_Mic_invivo + Vmax_Cyt_invivo +Vmax_Hep_invivo;

; Scale Metabolism by liver and skin volume
CL_PE = CL_PE_invivo* VLIV                  ; L/h
Vmax_PE = Vmax_PE_invivo*VLIV               ; umol/h
CLSk = CLSk_invivo*VSk                      ; Clearance in skin (L/h)


;================================================================
================
; Tissue compartment dynamic equations


;----------------------------------------------------------------------------------------------------
---------------------------------
; 2-PhE (flow limited for all tissues)

;----------------------------------------------------------------------------------------------------
---------------------------------
; Arterial Blood
APLS' = QC * (CV - CPLS) + QP * (CI - CX)    ; amount in (venous, inhaled) - out
(arterial, exhaled) (umole/h)
init APLS = 0
CPLS = APLS/VPLS              ; concentration (umole/L)
CPLS_MG= CPLS *MW /1000  ; mg/L
```

```
AUC_CPLS' = CPLS                ; area under the curve (umole*h/L)
init AUC_CPLS = 0
AUC_CPLS_MG = AUC_CPLS*MW/1000
CX = CPLS/PBA                   ; exhaled concentration (umole/L)
AI' = QP * CI                   ; amount inhaled (umole)
init AI = 0.0
AX' = QP*CX                     ; amount exhaled (umole)
init AX = 0.0

;-------------------------------------------------------------------------------------------------------------
---------------------------------

; Venous Blood
CV = (QRPT*CVR + QSPT*CVS + QLIV*CVL + QFAT*CVF + QSk*CVSk) / QC
 ; mixed venous blood concentration (umole/L)

;-------------------------------------------------------------------------------------------------------------
---------------------------------

; Gut
AG' = -KA*AG                    ; rate of removal from lumen (umole/h)
init AG = OD*ODSwitch                   ; initial bolus amount (umole)
AABS' = KA*AG                   ; rate of absorption of oral dose into gut tissue (umole/h)
init AABS = 0

;-------------------------------------------------------------------------------------------------------------
---------------------------------

; LIVER
AL' = QLIV*CPLS - QLIV*CVL + AABS' - AMET1' - AMET2' ; amount (arterial in +
gut in - out - metabolism) (umole/h)
init AL  = 0.0
CL  = AL / VLIV                                                 ; concentration
(umole/L)
CVL = CL/PLIV                                                   ; concentration
leaving (umole/L)

; Linear Metabolism
AMET1' =CL_PE * (CL*FUPLS) / PLIV                               ;umole/h
```

```
init AMET1 = 0

; Saturable Metabolism
AMET2' = (Vmax_PE * (CL * FUPLS) / PLIV) / ( (CL / PLIV) + KM)    ; umole/h
init AMET2 = 0

;-------------------------------------------------------------------------------------------------------------
; Fat
AF' = QFAT*CPLS - QFAT*CVF                    ; umole/h
init AF  = 0.0
CF  = AF / VFAT                          ; umole/L
CVF = CF/PFAT                            ; umole/L

;-------------------------------------------------------------------------------------------------------------
; Rapidly Perfused
AR' = QRPT*CPLS - QRPT*CVR                    ; umole/h
init AR  = 0.0
CR  = AR / VRPT                          ; umole/L
CVR = CR/PRPT                            ; umole/L

;-------------------------------------------------------------------------------------------------------------
; Slowly Perfused
AS' = QSPT*CPLS - QSPT*CVS                    ; umole/h
init AS  = 0.0
CS  = AS / VSPT                          ; umole/L
CVS = CS/PSPT                            ; umole/L

;-------------------------------------------------------------------------------------------------------------
; Skin
ASk' = QSk*(CPLS - CVSk) + ASkAbs' - ASkMet'      ; change in amount in skin (umole/h)
init ASk = 0.0
```

```
ASkAbs' = Kp*(SADose/AppliedVol)*ASurf                ; rate absorbed from skin surface (umole/h)
init ASkAbs = 0.0
ASkLost' = KLoss*(SADose/AppliedVol)*ASurf            ; rate lost from skin surface (umole/h)
init ASkLost = 0.0
ASkMet' = CLSk*CVSk                                   ; rate of skin metabolism (umole/h)
init ASkMet = 0.0

tApply = 0.1                                          ; application duration (h)
RADDose = (TIME >= DStart) * (MOD(TIME, DRepeat) <= tApply) * DD/tApply ; application rate, duration tApply, repeat @ DRepeat
ADDose' = RADDose                                     ; application rate (umole/h)
init ADDose = 0
ASurf2' = RADDose - ASkAbs' - ASkLost'
init ASurf2 = 0

ApplDose' = pulse(DD, DStart, DRepeat)
init ApplDose = 0
ASurf' =ApplDose' - ASkAbs' - ASkLost'                ; change in amount on skin surface, applied - absorbed - lost (umole/h)
;ASurf' =RADDose - ASkAbs' - ASkLost'                 ; change in amount on skin surface, applied - absorbed - lost (umole/h)
init ASurf = 0
CSk = ASk/VSk                                         ; concentration (umole/L)
CVSk = CSk/PSk                                        ; concentration leaving (umole/L)
ASkMG = ASk*MW/1000                                   ; amount (mg)

;-------------------------------------------------------------------------------------------------------------
; PAA METABOLITE
; Three-compartment model (liver, kidney, and rest of body) with production in liver from PhE metabolism and renal clearance in kidney
```

```
;-------------------------------------------------------------------------------------------------------------
---------------------------------

; Liver

ALivPAA' = AMET1' + AMET2' + QLiv*(CPAA - CVLivPAA) ; umole/hr PAA produced, entering from blood, leaving in venous blood

init ALivPAA = 0.0                                  ; umole

CLivPAA = ALivPAA/VLiv                              ; umole/L

CVLivPAA = CLivPAA/PLivPAA


;-------------------------------------------------------------------------------------------------------------
---------------------------------

; Kidney

AKidPAA' = QKid*(CPAA - CVKidPAA) - RUPAA     ; umole/hr PAA entering from blood, leaving in venous blood, minus excretion

init AKidPAA = 0.0

CKidPAA = AKidPAA/VKid

CVKidPAA = CKidPAA/PKidPAA


;-------------------------------------------------------------------------------------------------------------
---------------------------------

; Rest of body

APAA' = ASkMet' - QLiv*(CPAA - CVLivPAA) - QKid*(CPAA - CVKidPAA) ; umole/hr PAA produced in skin plus distribution to/from liver and kidney

init APAA = 0.0                                 ; umole

CPAA = APAA/Vd                                  ; umole/L PAA in rest of body

CPAA_MG = CPAA/1000.0*MW_PAA                    ; mg/L


;-------------------------------------------------------------------------------------------------------------
---------------------------------

; Areas under curves

AUCPAA' = CPAA                                  ; area under rest if body concentration curve (umole-h/L)

init AUCPAA = 0.0                               ; umole*h/L

AUCPAA_MG = AUCPAA/1000.0*MW_PAA  ; mg*h/L

AUCPAALiv' = CLivPAA                                ; umole-h/L

init AUCPAALiv = 0

AUCPAAKid' = CKidPAA                            ; umol-h/L
```

```
init AUCPAAKid = 0

;-------------------------------------------------------------------------------------------------------------
; Excretion
; GFR-based excretion in modified Corley kidney in Troutman PhE-PAA model
RUPAA = CPAA*fuPls_PAA*CLUPAA                ; umole/h, where CLUPAA is the GFR
; Excretion from kidney, venous blood equilibration
;RUPAA = CLUPAA*CVKidPAA                     ; umole/h PAA excreted in urine
; Excretion from kidney tissue
;RUPAA = CLUPAA*CKidPAA                      ; umole/h
UPAA' = RUPAA                          ; umole PAA in urine
Init UPAA = 0.0
CUPAA = RUPAA/VOLU                     ; umole/L PAA conc in urine
UPAA_MG = UPAA/1000.0*MW_PAA           ; mg PAA excreted in urine

;-------------------------------------------------------------------------------------------------------------
; Calculate Cmax
init Cmax = 0
lastdose = STOPTIME - MOD(STOPTIME-1e-6, drepeat)          ; the 1e-6 is to handle cases where the modulus is 0 (which gives zero dose)
Cmax' = IF (time < lastdose) THEN (APLS'/VPLS) ELSE Max(APLS'/VPLS,0)
init CmaxPAA = 0
CmaxPAA' = IF (time < lastdose) THEN (APAA'/Vd) ELSE Max(APAA'/Vd,0)
CmaxPAAVKid' = IF (time < lastdose) THEN (AKidPAA'/VKid/PKidPAA) ELSE Max(AKidPAA'/VKid/PKidPAA,0)
init CmaxPAAVKid = 0
CmaxPAAKid' = IF (time < lastdose) THEN (AKidPAA'/VKid) ELSE Max(AKidPAA'/VKid,0)
init CmaxPAAKid = 0

;-------------------------------------------------------------------------------------------------------------
; Calculate last 24-hr AUC
```

```
init AUC24 = 0
init AUCLiv24 = 0
AUC24' = IF (STOPTIME - time < 24) THEN (CPLS) ELSE 0
AUCLiv24' = IF (STOPTIME - time < 24) THEN (CL) ELSE 0

init AUCPAA24 = 0
init AUCPAALiv24 = 0
init AUCPAAKid24 = 0
init AUCPAAVKid24 = 0
AUCPAA24' = IF (STOPTIME - time < 24) THEN (CPAA) ELSE 0
AUCPAALiv24' = IF (STOPTIME - time < 24) THEN (CLivPAA) ELSE 0
AUCPAAKid24' = IF (STOPTIME - time < 24) THEN (CKidPAA) ELSE 0
AUCPAAVKid24' = IF (STOPTIME - time < 24) THEN (CVKidPAA) ELSE 0
AUCPAAVKid_24_mghpL = AUCPAAVKid24*MW_PAA/1000          ; mg-h/L

;-------------------------------------------------------------------------------------------------------------
; MASS BALANCE

;-------------------------------------------------------------------------------------------------------------
; PhE
; Amount in body (umole)
TMASSb =  AL + AS + AR + AF + APLS + ASk
; Amount eliminated (umole)
TMASSe= AMET1 + AMET2 + ASkMet + AX
; Dosed Amount (umole)
TMASSd = AABS + AI + ASkAbs
; Mass balance equation (umole)
MASSBAL = (TMASSd - TMASSb - TMASSe)

;-------------------------------------------------------------------------------------------------------------
; PAA
; Amount in body (umole)
```

```
TMASSb_PAA =  APAA + ALivPAA + AKidPAA
; Amount eliminated (umole)
TMASSe_PAA = UPAA
; Amount formed (umole)
TMASSf_PAA = AMET1 + AMET2 + ASkMet
; Mass balance equation (umole)
MASSBAL_PAA = (TMASSf_PAA - TMASSb_PAA - TMASSe_PAA)
```

Annex II. Differentially Expressed Genes

Please refer to the separate publication for full Annex II
ENV/JM/HA(2021)2/ANN1

Annex III. Gene Level BMD Results

Please refer to the separate publication for full Annex III
ENV/JM/HA(2021)2/ANN1

Annex IV. Pathway Level BMD Results

Please refer to the separate publication for full Annex IV
ENV/JM/HA(2021)2/ANN1

Annex V. *In vitro* AUCs in HepaRG 340000 cell per well

Please refer to the separate publication for full Annex V
ENV/JM/HA(2021)2/ANN1

Annex VI. *In vitro* AUCs in HepG2 30000 cell per well

Please refer to the separate publication for full Annex VI
ENV/JM/HA(2021)2/ANN1

Annex VII. *In vitro* AUCs in HepG2 51000 cell per well

Please refer to the separate publication for full Annex VII
ENV/JM/HA(2021)2/ANN1

Annex VIII. *In vitro* AUCs in MCF7 51000 cell per well

Please refer to the separate publication for full Annex VIII
ENV/JM/HA(2021)2/ANN1